Summer 2014

# Thermoelectric ELISA for quantification of 8OHdG in a microfluidic device

Gergana Nestorova

# THERMOELECTRIC ELISA FOR QUANTIFICATION OF 8OHDG

# IN A MICROFLUIDIC DEVICE

by

Gergana Nestorova, B.S., M.S.

A Dissertation Presented in Partial Fulfillment
of the Requirements of the Degree
Doctor of Philosophy

COLLEGE OF APPLIED AND NATURAL SCIENCES
LOUISIANA TECH UNIVERSITY

August 2014

ProQuest Number: 10644140
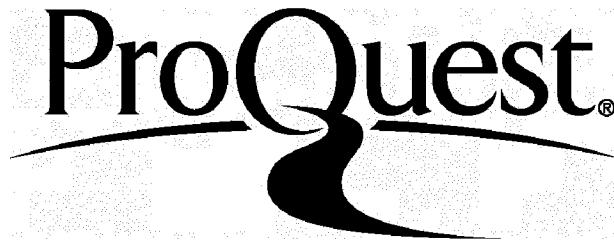
ProQuest 10644140

# LOUISIANA TECH UNIVERSITY

## THE GRADUATE SCHOOL

05/23/2014
_____
Date

We hereby recommend that the dissertation prepared under our supervision

by **Gergana G. Nestorova**
_____

entitled _____

**Thermoelectric ELISA for quantification of 8OHdG in a microfluidic device**
_____

_____

_____

be accepted in partial fulfillment of the requirements for the Degree of

**Doctor of Philosophy**
_____

_____
Supervisor of Dissertation Research
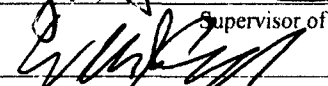
_____
Head of Department

Biological Sciences
_____
Department

Recommendation concurred in:

_____

_____
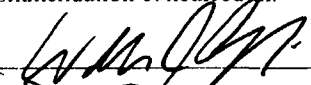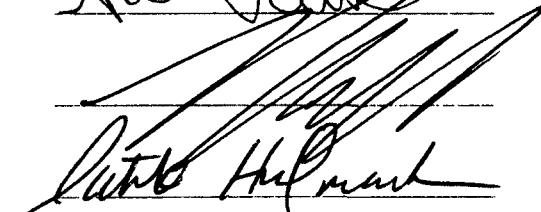
_____    Advisory Committee

_____

**Approved:**
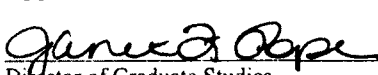
_____
Director of Graduate Studies

_____
Dean of the College

**Approved:**
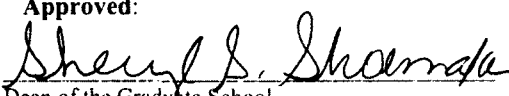
_____
Dean of the Graduate School

GS Form 13a
(6/07)
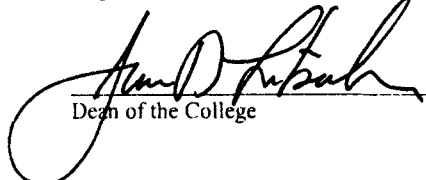
# ABSTRACT

This research demonstrates the feasibility of a novel method for performing thermoelectric enzyme-linked immunosorbent assay (ELISA) in a microfluidic device. The feasibility of the thermoelectric ELISA is demonstrated by measuring the concentration of 8-hydroxy 2-deoxyguanosine (8OHdG) in urine samples from amyloid precursor protein (APP) transgenic mice. The detection method is based on formation of a complex between 8OHdG and anti-8OHdG capture antibody conjugated to biotin. The complex is immobilized over the measuring junctions of a thermopile via biotin streptavidin interaction. The concentration of the analyte is determined by using enzyme linked secondary IgG antibody specific to the primary one. The concentration of 8OHdG is determined by the initiation of an enzymatic reaction between glucose and glucose oxidase that is conjugated to the secondary IgG antibody. The heat released by the reaction of glucose and glucose oxidase is measured using an antimony-bismuth thermopile integrated in a microfluidic device. The amount of heat detected by the sensor is inversely proportional to the concentration of 8OHdG. A standard calibration curve using known concentrations of synthetic 8OHdG is generated and used to determine the concentration of the oxidized guanine in mouse urine samples.

# APPROVAL FOR SCHOLARLY DISSEMINATION

The author grants to the Prescott Memorial Library of Louisiana Tech University

the right to reproduce, by appropriate methods, upon request, any or all portions of this

Dissertation. It is understood that "proper request" consists of the agreement, on the part

of the requesting party, that said reproduction is for his personal use and that subsequent

reproduction will not occur without written approval of the author of this Dissertation.

Further, any portions of the Dissertation used in books, papers, and other works must be

appropriately referenced to this Dissertation.

Finally, the author of this Dissertation reserves the right to publish freely, in the

literature, at any time, any or all portions of this Dissertation.

Author _Gergana Nestorova_

Date _07/22/2014_

# DEDICATION

This work is dedicated to my supportive husband, Dr. Dentcho Genov, and my wonderful children-Alexander and Gabriela.

# TABLE OF CONTENTS

# LIST OF FIGURES

# LIST OF TABLES

# ACKNOWLEDGMENTS

# CHAPTER 1

# INTRODUCTION

## 1.1 Goal

The goal of this dissertation research was to develop a novel, thermoelectric method for performing enzyme-linked immunosorbent assay (ELISA) in a microfluidic device. The technology was used to accurately quantify the concentration of urinary levels of 8-hydroxydeoxyguanosine (8OHdG) in amyloid precursor protein (APP) transgenic mice. It is a novel, rapid, easy-to-use, inexpensive and accurate method for detection and quantification of urinary levels of 8-hydroxydeoxyguanosine (8OHdG). The thermoelectric ELISA is based on the binding of 8OHdG to a capture primary antibody. The concentration of the analyte is determined using glucose oxidase conjugated secondary antibody. The analysis of urinary 8OHdG is performed in a microfluidic device with integrated thin-film antimony-bismuth thermopiles that can detect the heat released by the reaction of a substrate (glucose) with an enzyme (glucose oxidase). Measuring the heat of the enzymatic reaction provides a simplified method for performing ELISA since it eliminates expensive fluorescent and luminescent detectors.

## 1.2 Rationale

The feasibility of thermoelectric ELISA depends on whether the oxidation of glucose in the presence of glucose oxidase generates sufficient amount of heat that can be

detected by the thermopile. In addition, the application of this method for quantification

of urinary levels of 8OHdG depends on whether the thermopile is sensitive enough to

respond accurately when different concentrations of enzyme are used to react with the

same amount of glucose. Exothermic heat for glucose oxidation in the presence of

glucose has been previously measured using antimony-bismuth thermopiles. The

exothermic heat that is generated is estimated to be -79kJ mol$^{-1}$. Glucose was detected

thermoelectrically in both water and blood flowing under laminar flow conditions

(Guilbeau, Towe and Muehlbauer 1987). The chemical reaction for oxidation of glucose

in the presence of glucose oxidase is:

$$Glucose + O_2 + H_2O \xrightarrow{Glucose\ Oxidase} Gluconic\ Acid + H_2O_2 + 79kJ\ mol \quad (1)$$

Tangutooru *et al.* (2012) confirmed the microfluidic system has the sensitivity to

detect the enthalpy of the reaction between glucose and glucose oxidase using a thin film

antimony-bismuth thermopile. The enzyme was immobilized on the lower channel wall

of the device over the measuring junctions of the thermopile using a layer-by-layer

technique (Tangutooru, *et al.* 2012).

## 1.3     Significance

Reactive oxygen species cause oxidative damage to the DNA molecule leading to

a cellular oxidative stress. Nuclear oxidative damage is implicated in a number of age-

related diseases such as cancer and Alzheimer's disease. 8OHdG is one of the most

sensitive biomarkers for oxidative stress and can be detected in serum, urine and/or DNA

isolated from cells and tissues in humans and animals. Usually the damaged DNA is

enzymatically repaired and 8OHdG is excreted in the urine. The levels of 8OHdG in

urine are accepted as a biomarker for "whole body" oxidative DNA damage. The

presence of 8OHdG in the urine represents the amount of repaired oxidized guanine and increased levels of 8OHdG are indicative of increased oxidative stress in general. The excreted 8OHdG in the urine is not subject to further metabolism and the samples do not require any enzymatic digestion prior to performing analysis (Weiss and Lunte 2000). Since guanine has the lowest oxidative potential when compared to other DNA bases it forms the most abundant marker of oxidative stress. It is a widely studied biomarker of oxidative stress due to its implications in CG to AT transverson (Zhang, *et al.* 2013). The most common methods for detection of 8OHdG in urine samples include enzyme-linked immunosorbent assay (ELISA), mass spectroscopy (MS), high performance liquid chromatography (HPLC), and capillary electrophoresis. The current methods for 8OHdG analysis are too expensive for widespread use. There is a need for novel technology that could provide a more cost effective way to quantify 8OHdG in urinary samples. The thermoelectric ELISA evaluated in this study could provide an affordable method for widespread detection of levels of cellular oxidative stress. In addition, this technology could have applications in a number of other areas such as pathogen detection, quantification of biomarkers and cytokines, and methylations analysis of DNA and RNA.

## 1.4    Hypothesis

The concentration of the analyte is inversely proportional to the magnitude of the signal detected by the thermoelectric sensor. When the concentration of 8OHdG in the biological sample increases, competitive binding between the analyte and the secondary antibody decreases the efficiency of binding between the primary and the IgG enzyme linked antibody. In addition, 8OHdG physically obstructs the active enzyme sites and decreases the efficiency of the enzymatic reaction.

# CHAPTER 2

# INTRODUCTION

## 2.1 Molecular Structure of 8OHdG

One of the major types of DNA damage by free radicals is 8-hydroxy-2-
deoxyguanosine (8OHdG). Free radicals are molecules with one or more unpaired
electrons in the outer shell. Reactive oxygen species (ROS) can be formed in an organism
under the influence of environmental factors such as X-rays, smoking, and other
carcinogens (Wu, *et al.* 2004). An excessive generation of oxidants creates an imbalance
between ROS production and antioxidant defense and the biological system enters into a
state of oxidative stress. When oxidative stress is present, ROS can cause oxidative
damage to lipids, proteins, and DNA. Under conditions of oxidative stress, the DNA
molecule is constantly damaged and then repaired (Halliwell 2007). Guanine is the base
that is mostly prone to oxidation. When oxidation occurs, a hydroxyl group is added to
the 8th position of the guanine molecule and the oxidized product, 8OHdG, is the most
common form of ROS induced lesion of the DNA molecule (**Figure 2-1**) (Wu, *et al.*
2004).
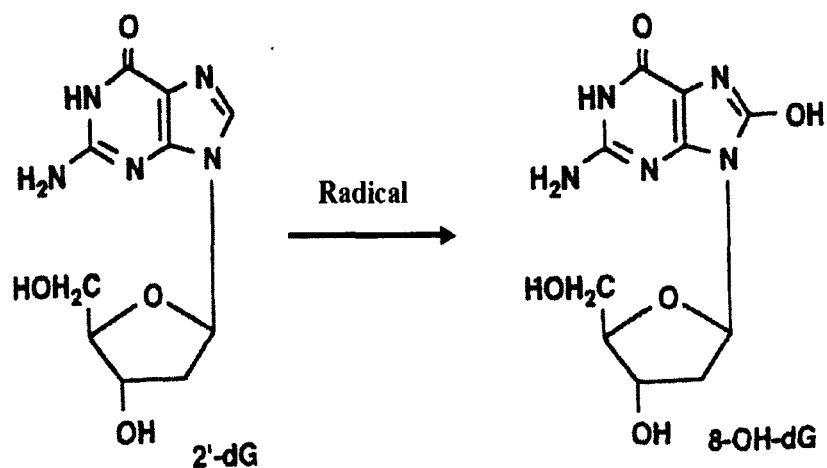
**Figure 2-1:** Chemical structure of 8OHdG (Kasai , *et al.* 1986).

2.1.1    *Pathway to Modification*

Reactive oxygen species can lead to the generation of different base adducts and the most common one is 8OHdG. Due to the low oxidation potential of guanine relative to the other DNA bases it is easily oxidized. An attack on C8 of the guanine leads to the formation of guanine C8-OH adduct radical that can form either 2,6 –diamino-4-hydroxy-5-formamidopyrimidine (FapyGua) or oxidation of the guanine radical to form 8OHdG **(Figure 2-2)**. The formation of either FapyGua or 8OHdG depends on the oxygen tension. FapyGua is formed under reduced oxygen tension, while 8OHdG is formed when the oxygen tension is higher (Lovell and Markersbery 2007).
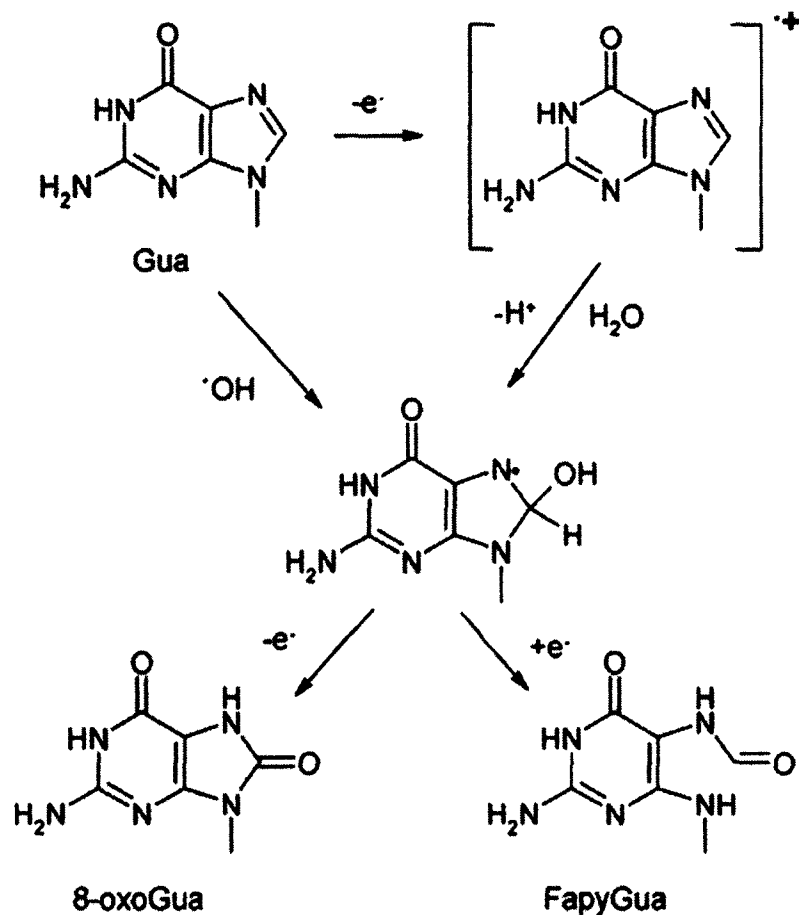
**Figure 2-2:** Reaction pathway for hydroxyl radical attack of guanine to form 8-
hydroxyguanine and 2, 6-diamino-4-hydroxy-5-formamidopyrimidine
(Cadet *et al*, 2009).

Oxidized DNA and RNA undergo repair and the oxidized nucleotides and bases

are excreted in the urine without further modification; thus the excretion of repair

products in urine represent the average rate of damage to the whole body. Oxidized

products of the DNA repair mechanisms excreted in the urine include 8OHdG, 8-

hydroxyguanine (oxidized base), and analogues of 8OHdG derived from RNA (**Figure 2-
3**). Weimann *et al*. estimated using high-performance liquid chromatography-electrospray

tandem mass spectroscopy (HPLC MS/MS) that the total exertion of modified guanine

species was 211 nmol in a 24 hour period. The oxidized base accounted for 64%, the

ribonucleoside for 23%, and the deoxynucleoside for 13%, indicating a significant rate of

RNA oxidation (Weimann, Belling and Poulsen 2002). Urinary 8OHdG and the free base

8-OH-Gua are produced in two pathways: from oxidized guanine nucleotides formed in

the nucleotide pool and after damage repair in the replicated DNA strand. When oxidized

dGTP is formed in the nucleotide pool, MTH1 nucleotide sanitization enzyme removes

the pyrophosphate and 8-OH-dGMP is digested by a 5'(3')-nucleotidase, then the

modified base is removed from the cell and excreted in the urine (Kasai, Kawai and Yun-

shan 2008). To repair damage to the nucleic acid molecule as a result of oxidative stress,

multiple repair systems have evolved that include base excision repair, nucleotide

excision repair, and mismatch repair. Oxidative lesions that are not repaired can cause

CG to AT transversion during DNA replication and as a result alter protein synthesis. The

base excision repair mechanism excises the modified base while the nucleotide excision

repair mechanism removes the damaged nucleotides in fragments up to 30 bases in

length. The two major repair enzymes involved in oxidized guanine repair are 8-

oxoguanine DNA glycosylase 1(OGG1) and mutY homologue (MUTYH). The base

excision repair enzyme OGG1 removes the oxidized guanine base from the DNA by

catalyzing hydrolysis of the N-glycosylic bond that links the damaged base to the sugar

moiety of the DNA molecule. Repair of the formed apurinic site requires incorporation of

a single nucleotide by DNA polymerase, followed by strand ligation by DNA ligase.

MUTYH is a DNA glycosylase that removes adenine that is misincorporated opposite to

the oxidized guanine. MUTYH serves as a backup mechanism where OGG1 has failed to

remove the modified base. Removal of the mismatched adenine base allows for insertion

of the correct cytosine nucleotide and it also gives an opportunity for the OGG1 enzyme

to remove the oxidized guanine base (Loft, *et al.* 2008). In addition to DNA, guanine

oxidized base can be formed in the RNA molecule as a result of direct oxidation of the base or through direct incorporation of the base in RNA from the nucleotide pool. Since RNA is single-stranded and is not protected by proteins, it is more susceptible to oxidative damage when compared to DNA. Human polynucleotide phosphorolase protein (PNP) and human Y-box–binding protein 1(YB-1) recognize and sequester the damaged RNA from the translational machinery (Moreira, *et al.* 2008).



guanine → 8-hydroxyguanine → 8-hydroxyguanosine (RNA) / 8-hydroxydeoxyguanosine (DNA)
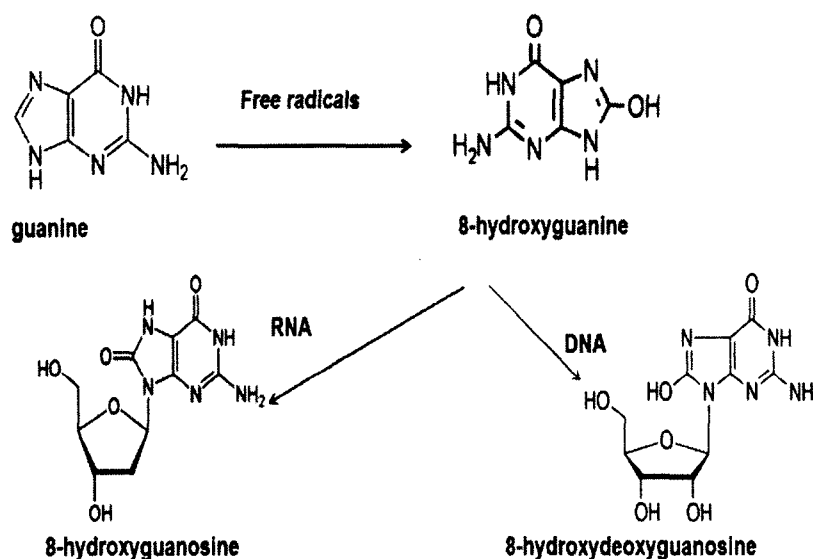
**Figure 2-3:** Oxidized products of DNA and RNA repair.

2.1.2    *8OHdG as a Biomarker of Oxidative Stress and its Role in Disease*

Reactive oxygen species can attack lipids, proteins, and nucleic acids. When nuclear or mitochondrial DNA is damaged, the oxidized base and nucleotide are excised and excreted in the urine. The urinary level of 8OHdG is a biomarker of generalized oxidative stress and is linked to a number of aging associated degenerative diseases such as cancer, diabetes, and atherosclerosis. 8OHdG levels can be measured in specific tissues. While the excretion of 8OHdG in the urine represents the average rate of damage

in the body, the levels of oxidized guanine bases in nuclear DNA is an indicator of oxidative stress in this particular tissue and it reflects the balance between damage and repair in the cells (Wu, *et al. 2004*).

Oxidative damage to nuclear DNA is an important factor in mutagenesis and carcinogenesis. An oxidized base that is not repaired can pair with A and G residues and as a result increase the frequency of a spontaneous GC to TA transversion mutation that is involved in carcinogenesis. Oxidative damage not repaired by the enzyme repair mechanisms contributes significantly to the in vivo rate of mutation (Klungland, *et al.* 1999). Significantly higher levels of 8OHdG were measured using ELISA in the urine of patients with bladder and prostate cancer when compared to a control group. The levels of oxidized species in patients with bladder cancer were 70.5ng mg$^{-1}$ creatine, while patients with prostate cancer had levels of 58.8ng mg$^{-1}$ creatine, and healthy individuals had 36.1ng mg$^{-1}$ creatine (Chioua, *et al.* 2003). Higher levels of 8OHdG were measured in the urine of patients with small cell lung carcinoma when compared to a control group (Erholaa, *et al.* 1997). Loft *et al.* (2006) found a correlation between the levels of urinary excretion of 8OHdG and the risk for lung cancer. The analyses were performed on urine samples using HPLC with electrochemical detection. The excretion of 8OHdG was higher in the smokers group and the incidence rate ratio of lung cancer was significantly associated with excretion of 8OHdG, confirming that oxidative damage is an important biomarker for lung cancer risk (Loft, *et al.* 2006).

Chronic inflammation, such as rheumatoid arthritis and diabetes, could lead to continuous reactive oxygen species generation and to accumulation of 8OHdG in mitochondrial and nuclear DNA. Oxidative stress plays a major role in the pathogenesis

of both types of diabetes mellitus (I and II) and is a major contributor to subsequent

diabetic complications. Higher levels of 8OHdG were also measured in the serum of

diabetic patients. Serum 8OHdG was significantly increased in diabetic patients

($24.90\pm6.29$ ng mL$^{-1}$) compared with age-matched normal subjects ($5.86\pm1.82$ ng mL$^{-1}$,

P<0.01). The levels of 8OHdG were significantly increased in patients with diabetic

nephropathy when compared with diabetic patients without vascular complications

($26.89\pm6.44$ng mL$^{-1}$ vs $23.14\pm5.59$ng mL$^{-1}$, P<0.05) (Pan, *et al.* 2007).

Oxidative DNA damage is implicated in aging and neurodegenerative diseases

such as Alzheimer's disease. The brain is very susceptible to oxidative damage due to its

high oxygen consumption rate and energy demand, and relatively limited antioxidant

capacity. It is estimated that 2% of the oxygen consumed by the cells is converted to

ROS. Elevated levels of 8OHdG were measured in patients with late-stage Alzheimer's

disease using gas spectroscopy with mass spectroscopy. The results were compared with

the levels of 8OHdG in an age matched control group. The samples were obtained from

short postmortem interval autopsies. The levels of 8OHdG were significantly elevated in

the Alzheimer's patients when compared to the control group (Lovell and Markersbery

2007). Another study confirmed that the levels of 8OHdG in intact DNA to free 8OHdG

in ventricular cerebrospinal fluid from Alzheimer's disease (AD) patients removed at

autopsy were elevated in Alzheimer's disease subjects. Levels of the modified base were

determined using gas chromatography/mass spectrometry with selective ion labeling.

The ratio of the oxidized guanine was increased 1.08 times in intact DNA when

compared to free oxidized guanine, indicating increased cellular levels of oxidative stress

and decreased repair capacity (Lovell and Markesbery 2001). Higher levels of oxidized

poly (A) mRNA were measured in postmortem brain analysis from AD patients using

Northwestern blotting with anti-8OHG antibody. These results suggest the role of RNA

oxidative damage in AD neurological damage (Moreira, *et al.* 2008).

### 2.2 Methods for Detection and Quantification of 8OHdG

Oxidative modified DNA can be quantified to determine the extent of DNA

damage due to oxidative stress. To quantify 8OHdG in tissue samples, enzymatic

digestion using enzymes such as endonuclease and glycosylase has to be performed to

cleave the oxidized product and release it into a solution before it can be quantified. This

step is not necessary when the level of oxidized guanine is measured in the urine,

simplifying the analysis of 8OHdG in urinary samples (Wu, *et al.* 2004).

Several analytical methods are used to measure levels of 8OHdG in the urine.

These include ELISA, capillary electrophoresis with various detectors, such as UV,

electrochemical (ED), amperometric (AP) and laser induced fluorescence (LIF), high

performance liquid chromatography (HPLC), and mass spectrometry with gas

chromatography (MS/GS). Each method has different limits of detection (LOD) (**Table 2-1**).

**Table 2-1:** Analytical methods for 8OHdG detection

| Approach | LOD | Disadvantages | Reference |
|---|---|---|---|
| CE-ED | 50nM | SPE purification | (Weiss and Lunte 2000) |
| CE-AP | 20nM | SPE purification | (Mei, *et al.* 2003) |
| CE-LIF | 0.18fmol | High deviation | (Zhang, *et al.* 2013) |
| CE-UV | 17μM | Low sensitivity | (Kvasnicováa, *et al.* 2003) |
| HPLC-ED | 80nM | Complex purification | (Rebelo, Piedade and Oliveira-Brett 2004) |
| MS/GS | 2.5nM | High background noise | (Lin, *et al.* 2004) |
| HPLC-MS/MS | 0.5nM | High cost | (Weimann, Belling and Poulsen 2002) |
| ELISA | 2nM | Cross reactivity of the antibody | (Yin, *et al.* 1995) |

2.2.1 *ELISA*

ELISA is the most common method for quantification of 8OHdG in urine

samples. This immunoassay is based on the use of antibody to detect the concentration of

antigen in a sample. Quantification of 8OHdG is usually performed in a competitive

ELISA form. Competitive ELISA is based on the principle that the amount of antigen in the biological sample is inversely proportional to the concentration of the detection antibody. This method involves reaction of the sample containing an unknown concentration of the analyte (8OHdG) with an unlabeled primary antibody. During the incubation the antigen in the sample competes with the antigen coated on the plate to bind to capture antibody. A higher concentration of 8OHdG in the sample leads to lower concentration of bound anti-8OHdG antibody to the surface of the plate. The concentration of the bound antibody to the surface of the plate is determined using enzyme labeled secondary antibody that reacts with a specific substrate to produce a fluorescent signal (Yin, *et al.* 1995).

Shimoi *et al.*, (2002) compared the HPLC-EC method with an ELISA test to determine the levels of 8OHdG in human urine samples. ELISA and HPLC-EC had a good correlation when the urine samples were purified via HPLC. The ELISA method overestimated the concentration of 8OHdG by two fold when the urine samples were not HPLC purified. It is believed that this is caused by cross reaction of the primary antibody with another structurally related compound (Shimoi, *et al.* 2002).

The advantage of using ELISA is the simplicity of the assay when compared to more complex technologies such as HPLC, CE, and MS. The method can have potential applications using numerous matrices such as urine, serum, cell culture medium or plasma. In addition, the costs associated with obtaining the equipment, processing and running the samples are much lower when compared to other methods. In addition both anti 8OHdG polyclonal and monoclonal antibodies are commercially available. The disadvantage is that the samples have to be purified to obtain accurate measurements of

the concentration of 8OHdG in the urine. Since this method overestimates the amount of 8OHdG, using ELISA is appropriate for comparative monitoring studies. HPLC purification is required to determine the absolute value of 8OHdG since the antibody usually recognizes additional oxidized guanine compounds such as oxidized guanine base, and oxidized ribonucleotide (Shimoi, *et al.* 2002). In addition, urea is the most abundant compound of the urine. Commercially available monoclonal antibody N45.1 cross reacts with urea, a compound that shares similar –NH-CO-N- structure with oxidized guanine (Songa, *et al.* 2009).

### 2.2.2 *Capillary Electrophoresis*

Capillary electrophoresis (CE) technology involves separation of the analyte based on the size to charge ratio and provides higher separation efficiency in a complex biological matrix as compared to liquid chromatography methods. CE with various detectors, such as UV, electrochemical, amperometric and laser induced fluorescence (LIF) were used to measure the concentration of 8OHdG in urine samples. Analyzing a urine sample with CE-ED requires a solid phase extraction (SPE) step to clean up and pre-concentrate the urine sample. CE with electrochemical detection provides lower limits of detection of the analytes when compared to other CE detection methods such as LIF. The limit of detection of 8OHdG in urine samples using CE-ED was 50nM and the signal to noise ratio was 3. The disadvantage of this method is the requirement for an additional SPE with a C18 columns step prior to 8OHdG quantification, which adds complexity to the sample preparation. In addition, this technology requires an end-column de-coupler to reduce the effect of the high electric field (Weiss and Lunte 2000).

Levels of urinary 8OHdG were measured using capillary electrophoresis with simple end column amperometric detection. The sensitivity of 8OHdG detection was improved using a focusing technique of dynamic pH junction and the limits of 8OHdG detection were 20nM. 8OHdG contains a phenolic hydroxyl group in its structure so it becomes partially ionized at pH greater than 7. Optimal focusing of 8OHdG was observed at pH 8.15. The major disadvantage of this method is that it requires SPE purification with C18/OH columns prior to the analysis (Mei, *et al*. 2003)

CE with laser induced detection (LIF) provides even higher separation efficiency, a lower limit of detection and simplicity. The limits of detection of 8OHdG using CE-LIF were 0.18fmol. This technique involves the use of specific primary antibody to detect 8OHdG followed by conjugation to a secondary fluorescently labeled detection antibody. Fluorescently labeled 8OHdG was resolved by a capillary electrophoretic system using a fluorescent detector. The standard deviation was 11.32% for the migration time and 5.52% for the peak area. The advantages of using this method are high separation efficiency, excellent selectivity, simplicity and low limit of detection. In addition, this technology does not require sample purification and concentration. The disadvantage of this technology is high cost of maintaining and operating the instrument and relatively high standard deviation between measurements (Zhang, *et al*. 2013).

Another method to quantify the levels of 8OHdG in untreated urine samples involves using CE with UV detection. Since the samples are not treated and pre-concentrated the limits of detection are higher when compared to other CE methods. The limits of detection of 8OHdG were estimated to be $17\mu M$. This method uses untreated urine samples, which simplifies the procedure and shortens the time of analysis.

However, this technology suffers from lower sensitivity and as a result is only applicable to samples with higher concentrations of 8OHdG (Kvasnicováa, *et al.* 2003).

2.2.3     *Mass Spectrometry*

Another analytical technique for 8OHdG quantification is mass spectrometry coupled with HPLC or gas chromatography (GS). GS/MS technology requires that acidic or enzymatic hydrolysis must be performed on the sample prior to the analysis to liberate the bases from the DNA backbone. While acidic hydrolysis liberates both modified and unmodified bases, enzymatic digestion removes only modified bases from the sample. Since GS can be performed only on volatile compounds the bases have to be converted into volatile derivatives using either trimethylsilyl (TMS) or terbobutyldimethylsilyl (TBDMS) groups (Ravant 2005). GS/MS technology can be applied using a single step sample clean up that can be used for large-scale studies. An isotopically labeled 8OHdG analog was added to the sample as an internal standard. Samples were eluted through a SPE and derivatized. GS/MS was performed using selective ion monitoring. The limits of detection of this method were 2.5nM. The advantages of this method are sensitivity and a simplified sample cleaning procedure (Lin, *et al.* 2004). One of the major disadvantages of this method is that the sample has to be derivatized prior to analysis, creating additional artificial oxidation products that interfere with the analysis by increasing the background noise. In addition, an artificial DNA oxidation to the normal bases occurs during the silylation step that artificially increases the level of measured analyte several orders of magnitude. In addition, this method requires an isotope labeled internal standard for precise measurements which is not commercially available (Kasai 2003). Both HPLC

and MS are very sensitive techniques. The application of these methods in a clinical

setting is limited by high cost, complex sample purification steps, and low throughput.

High-performance liquid chromatography-electrospray tandem mass spectroscopy

(HPLC-MS/MS) combines the advantages of the HPLC and MS technologies. This

method was successfully used to quantify and discriminate all types of 8-hydroxylated

guanine modifications in the urine such as oxidized base, ribonucleoside,

deoxyribonucleoside, and the non-oxidized base in a single run. The limit of detection of

the nucleobase was 2nM, while for the nucleoside 0.5nM. The advantage of this

technology is that it requires only a small sample volume; no pretreatment and

purification step; and all modified forms of guanine can be measured in a single run.

Compared to the HPLC-ED this method is much more versatile and specific. HPLC-

MS/MS does not require a derivatization step, eliminating the possibility of artificial

DNA oxidation. The disadvantage is the cost of the equipment and the high level of

technical expertise required to operate the instrument, which makes it inaccessible to

many laboratories (Weimann, Belling and Poulsen 2002).

2.2.4    *HPLC*

One of the most common separation methods for quantification of 8OHdG is

HPLC with electrochemical detection. This method is based on the fact that the oxidized

purine has a redox potential below the potential of the normal nucleoside. The

electrochemical detector can specifically oxidize the modified guanine base and the

liberated electrons are detected. The sensitivity of this detection method is based on the

fact that unmodified nucleosides are not oxidized at the specific potential that is used

(Ravant 2005). This method involves HPLC isocratic elution with amperometric

detection on a glassy carbon electrode. The detection limit of this method was 80nM. It

provides better limits of detection and better selectivity and can also be used to measure

several oxidized products at the same time. The disadvantage of using this method is that

the equipment for HPLC is expensive to run and maintain and a significant amount of

organic solvent is required. It also requires complicated and time consuming purification

steps using solid phase extraction procedures (Rebelo, Piedade and Oliveira-Brett 2004).

A disadvantage of this technology is that the timing of the 8OHdG elution fraction was

inconsistent since it is affected by minor changes in solvent composition, temperature,

and the column and pump conditions (Kasai 2003). Another criticism of ELISA

technology is that it overestimates the concentration of 8OHdG in the urine samples. This

is most likely caused by cross reactivity of the urine sample towards additional

compounds in the urine and detection of 8OHdG and its analogues such as the modified

base and the modified form derived from RNA. To overcome these issues, a monoclonal

antibody specific for 8OHdG (N45.1) was characterized and applied in quantitative

immunohistochemistry. N45.1 recognizes both the modified base and deoxyribose

structure of 8OHdG. This monoclonal antibody did not cross-react with the original four

deoxyribonucleosides, other DNA base-modified products such as 8-hydroxy-2'-

deoxyadenosine and O6-methyl-2'-deoxyguanosine, or urine components such as uric

acid, creatine, and creatinine (Toyokuni, *et al.* 1997).

## 2.3    Thermoelectricity and Thermopiles

Thermoelectric current is produced when a temperature gradient is applied to a

closed circuit composed of two dissimilar conductors. The pairs of conductors are called

thermocouples and it converts thermal energy to electrical energy. The magnitude of the

electrical current depends on the temperature difference between the two junctions. The thermoelectric behavior of a material is influenced by the temperature, composition of the materials, stress and other variables. The thermoelectric effect is based on the principles of modern electron theory. The free electrons inside the metal behave like a gas and their densities differ among different metals. When two different metals are placed in contact, the metal at the junctions become oppositely charged when they are maintained at different temperatures. The difference in charge produces a potential difference across the junction (Pollock 1985).

Thermocouples are created by joining two different metals together such that two junctions are formed, each of which can be exposed to different temperatures. When two or more thermocouples are connected in the series they form a thermopile. One of the junctions of the thermopile is usually designated as the measuring (or active) junction and the other is designated as the reference junction. If the measuring junction is maintained at a temperature that is different from the reference junction, an electrical potential called the Seebeck Voltage can be measured between the two junctions. The magnitude of the Seebeck voltage is proportional to the temperature difference between the junctions and the Seebeck coefficient (thermoelectric power) of the selected metal pair, S12, as shown by **Eq. 2-1**

$$V_{12} = S_{12} (T_1 - T_2).$$ **Eq. 2-1**

If bulk antimony and bismuth are selected as the two metals, the Seebeck coefficient is 119 $\mu$V $^\circ$K$^{-1}$. The magnitude of the Seebeck voltage of thin-film

thermopiles also depends upon the number of thermocouple junction pairs that are connected in series, N, as shown by **Eq. 2-2**

$$V_T = N S_{12} (T_1 - T_2).$$                    **Eq. 2-2**

Extremely small amounts of heat can be measured by positioning the measuring junctions in close proximity to the heat source. The reference junctions should be located away from the heat source, although close enough to possess the same baseline thermal signature as the measuring junctions. The Seebeck coefficient depends on the composition of the material and on the working temperature. The voltage output of the thermocouple depends on the temperature difference between the measuring and reference junctions. The output of the thermopile is the sum of the outputs of each thermocouple (Xie, *et al.* 1994).

## 2.4    Layer-by-layer Self-assembly

Layer-By-layer (LbL) electrostatic adsorption is a widely used procedure for proteins, enzymes, and nanoparticles immobilization. LbL assembly is based on the alternate adsorption of oppositely charged ions on the substrate. The technique is based on charge neutralization and charge re-saturation upon the adsorption of oppositely charged ions on the substrates (**Figure 2-4**) (Lvov, Ariga and Ondaa, *et al.* 1999). Strong ionic, electrostatic and hydrogen bonds hold the oppositely charged species to form uniform and stable films. These molecularly organized films are easily prepared, have high strength and are similar to those produced in highly expensive and sophisticated methods used for metals and semiconductors. Charge re-saturation occurs during polyion adsorption resulting in the terminal charge for each polyion layer adsorbed. There is no

restriction for the choice of polyelectrolytes. Films in the range of 5-1000 nm can be

obtained by knowing the composition of polyelectrolytes.
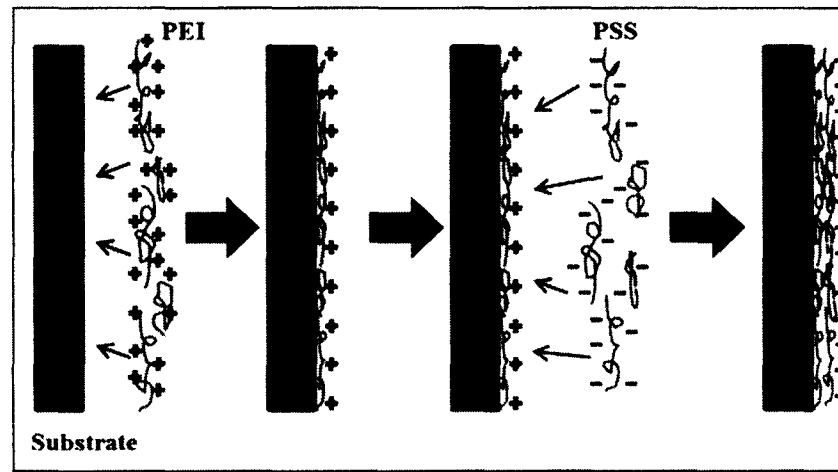


**Figure 2-4:** General adsorption procedure of polyelectrolyte (Lvov, *et al.* 1995)

Lvov *et al.* (1999) described the standard procedure for layer-by-layer self-

assembly and the effects of sample preparation, layer-by-layer adsorption conditions and

polyion concentration. For assembly of protein or enzyme multilayers, alternate

adsorption with polyions is necessary. These polyions act as "electrostatic glue" to hold

proteins or enzymes. The most common polyions (**Figure 2-5**) used in LbL assembly

include poly (styrene sulphonate) (PSS), poly (vinyl sulphate) (PVS) and poly (acrylic

acid) (PAcr), dextran sulfate, and sodium alginate. Polycations include poly

(ethylenimine) (PEI), poly (dimethyl diallyl ammonium chloride) (PDDA), poly

(allylaminehydrochloride) (PAH), and polylysine and chitosan (Lvov and Möhwald

2000).

poly(acrylic acid), PAA     poly(dimethyldiallylammonium chloride), PDDA

poly(styrenesulfonate) sodium salt, PSS     Branched poly(ethyleneimine), PEI-b
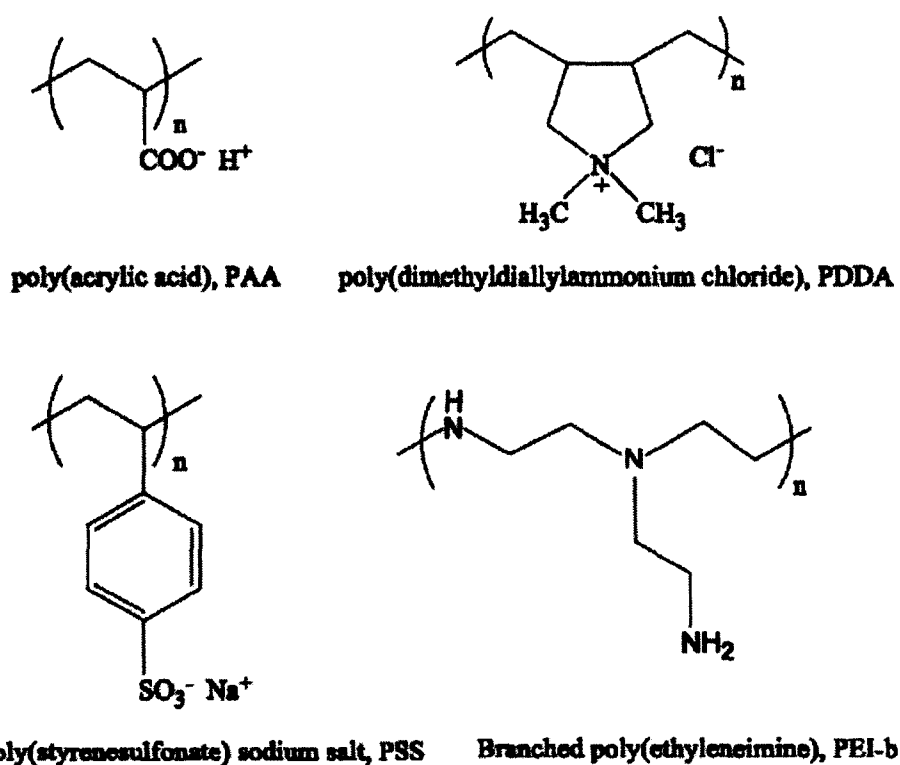
**Figure 2-5:** Structure of polyions.

## 2.5    Microfluidics and Calorimetry

Microfluidic devices have at least one channel with dimension less than 1mm.

Microfluidic devices provide the advantage of having reduced sample volume, less

expensive manufacturing, and the possibility for integration of several devices in more

complex instruments to develop more compact and portable systems.

### 2.5.1    *Fundamentals of Microfluidics*

An important parameter that is used to characterize fluid flow in a microfluidic

system is the Reynolds number. It is a dimensionless number that measures the ratio of

inertial to viscous forces in the liquid. The inertial forces are proportional to flow

diameter, velocity and fluid density. For tube flow, when the Reynolds number is less

than 2100 (**Eq.2-3**), the particles move in laminar flow, i.e., in paths parallel to the overall flow direction without mixing

$$Re = \frac{\rho VL}{\mu} = \frac{VL}{v}.$$

**Eq. 2-3**

V is the mean velocity of the fluid (m s$^{-1}$), L is the linear dimension (m), $\mu$ is the viscosity of the fluid (Pa s$^{-1}$), v is the kinematic viscosity (m$^2$ s$^{-1}$), and $\rho$ is the density of the fluid (kg m$^{-3}$) (Bruus 2006).

The chemical reagents are transported in the microfluidic device via the motion of fluids. The motion of fluids inside the channel could be constrained by the boundaries and geometry of the channel or it could be efficiently controlled by flow focusing. Hydrodynamic focusing of fluids is achieved when the sample flow from inlet 2 is constrained laterally within the center of the channel by the flow of inlet 1 channel. The width of the focused stream can be controlled by adjusting the relative flow rates of inlet 1 and inlet 2 (Lee, *et al.* 2006).

## 2.5.2    *Microfluidic Calorimeters*

Microfluidic calorimeters detect the exothermic heat released during a chemical reaction and can be used to characterize a variety of chemical processes that do not require labeling of the analyte. Microfluidic calorimeters have the advantages of fast response and low application cost, combined with the capability of analyzing a small quantity of sample. They also provide the opportunity for portability and possible parallel processing. Calorimetry is an excellent tool for analysis of a broad spectrum of biochemical reactions. Thermopiles are widely used as sensors in microfluidic calorimetry for detection of biochemical reactions because they have a high-common mode thermal noise rejection ratio and are well suited for miniaturization. The output of

the calorimeter depends on the flow rate, the concentration of the reactants as well as where the reaction occurs with respect to the hot junction of the thermopile (Zhang and Tadigadapa 2004).

Usually, the measurement of small temperature changes using thermopiles requires control of the thermopile reference junction temperature and the ambient temperature to accurately differentiate the thermal signals from the noise. To achieve this, heaters are usually used to control the temperature of the reference junction. The high signal resolution of the calorimeter is achieved by placing the system inside a thermostat that has excellent temperature stability (less than 100 $\mu K$). High power sensitivity and a small time constant are achieved by fabricating silicon microfluidic calorimeters. The heat power sensitivity of a silicon chip calorimeter using Sb/Bi thermopiles is 4-7 V $W^{-1}$. The heat power sensitivity depends on the thermal conductivity of the liquid and the height of the chamber. Although it has many advantages such as excellent sensitivity and resolution, fabrication of silicon microfluidic calorimeters with temperature control elements increases the cost, complexity and the size of the system and limits its widespread application (Lerchner et al., 2006).

Kopparthy et al., (2012) developed a thermoelectric sensor for detection of a biochemical reaction without the need to control the external thermal environment using heat sources or thermostats to control the ambient temperature. The device consists of a 100 $\mu M$ deep flow channel created using xurography and Bi/Sb thermopiles attached to the bottom of the device. The thermopile has a Seebeck coefficient of 7 $\mu V$ $mK^{-1}$ and excellent rejection of common mode thermal signals. The combination of hydrodynamically focused flow with a novel thermopile design eliminated the need for

external temperature control. The sensitivity of the device was estimated to be $0.045VsJ^{-1}$

(Kopparthy, *et al.* 2012).

2.5.3      *Application of Microfluidic Calorimeters*

Calorimeters with integrated thermopiles are used to detect a variety of chemical

reactions that produce a detectable amount of exothermic heat. A microfluidic

calorimeter with p-type polysilicon/gold thermopiles was used to measure the heat of

enzymatic reactions involving glucose oxidase, catalase, urea and glucose. A sensitivity

of $53.5\mu V\ M^{-1}$ for glucose, $26.5\mu V\ M^{-1}$ for hydrogen peroxide, and $17\mu V\ M^{-1}$ for urea

was obtained (Zhang and Tadigadapa 2004). A calorimetric sensor with an integrated

thin-film thermopile was developed to measure the enzymatic enthalpy of glucose

oxidation in either phosphate buffer solution or in blood. To test the sensor in a

physiological environment, the thermopile was implanted in a cardiovascular shunt of an

anesthetized dog and glucose measurements were obtained. This technology had the

potential for clinical application for measuring levels of blood glucose. The thermopile

consisted of 50 thermocouples of antimony and bismuth metal that were attached to the

tip of a catheter. The response time of the sensor was very fast, less than 6 s, and it had a

stable baseline level and enhanced signal to noise ratio. The sensor response to glucose

had the same sensitivity both in phosphate buffer and in blood. The average sensitivity to

glucose measured in the blood stream was $33-47nV\ mg^{-1}$ (Muehlbauer, *et al.* 1990). A

microbiosensor with integrated thermopiles fabricated on a quartz chip was developed to

measure the exothermic heat produced by oxidation of glucose oxidase. The thermopiles

were manufactured by doping boron in polysilicon together with aluminum and provided

an output of $2mV\ K^{-1}$. The linear range of detection of glucose was 2 to 25mM of glucose

with a standard deviation of 5% (Xie, *et al.* 1994). A microfluidic calorimeter was used

to measure the temperature change during glucose oxidation in the presence of glucose

oxidase. An antimony-bismuth thermopile with a high common mode rejection ratio was

used to measure the heat released by the oxidation of glucose. The enzyme was

assembled over the lower channel of the device using layer-by-layer self-assembly. The

glucose oxidase was adsorbed to the glass coverslip by alternate electrostatic adsorption

of polyelectrolytes and enzyme. The limit of detection of the device was $1.0mg \ dL^{-1}$ of

glucose (2.8nmol of glucose) (Tangutooru, *et al.* 2012).

## 2.6    Enzyme-Linked Immunosorbent Assay (ELISA)

ELISA is an analytical technique in which the concentration of antigen, antibody

or analyte is determined by enzymatic activity measurements. It is based on the

application of enzymes as labels for antigens, analytes and antibodies and subsequent

detection of an enzymatic reaction using luminescent detectors.

2.6.1    *Fundamentals of ELISA*

ELISA technology is used for accurate quantification of the amount of antigen or

antibody in clinical samples. There are three main methods for performing ELISA: direct

ELISA, indirect ELISA, and sandwiched ELISA.

In direct ELISA the antigen is attached to the surface of a multiwall plate by

adsorption. Enzyme labeled antibody specific to the antigen is added to the well plate and

after an incubation period and a subsequent wash step, a substrate specific for the enzyme

is added to the well plate and the color change of the solution in the well plate is read by

a luminescent reader. This type of immunoassay format is the simplest form of ELISA.

Indirect ELISA follows the same basic procedure as direct ELISA: binding of antigen to the solid substrate and reaction with unlabeled antigen (**Figure 2-6**). However, the concentration of the antigen is estimated using a reaction with a secondary enzyme conjugated antibody. The secondary antibody is produced against the immunoglobulin of species in which the detection antibodies are produced. This allows for great flexibility in use of anti-species conjugates and the sample can be tested for a specific antigen using a single anti-species conjugate. The disadvantage of indirect ELISA is the wide degree of non-specific binding in individual samples that increases variability in assay results.
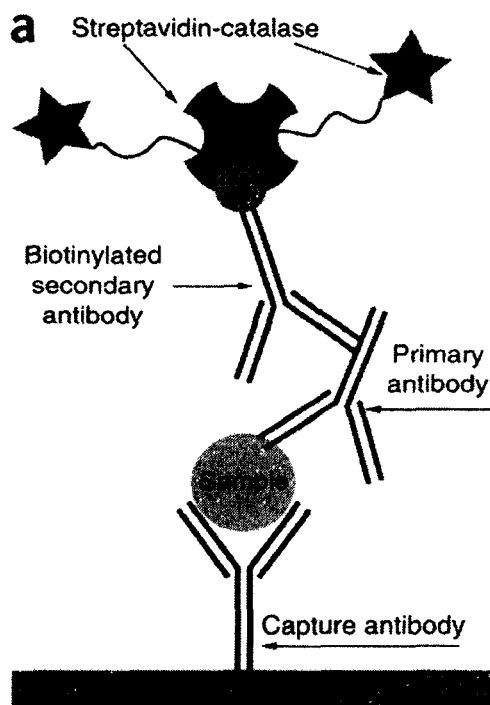
**Figure 2-6:** Principle of indirect ELISA (Rica and Stevens 2013).

Sandwiched ELISA can be divided into two groups: direct and indirect. In direct sandwiched ELISA, the primary antibody is attached to the surface and binds the antigen. The trapped antigen is detected by another antibody that is conjugated to an enzyme. The limitation of this method is the limited specificity of this antibody set. The antigens must

also have two antigenic (epitope) sites since both the capture and the detection antibody have to bind. This limits the application of this method to relatively large antigenic complexes.

Indirect sandwich ELISA is similar to direct sandwich ELISA in the sense that a primary antibody, antigen, and secondary antibody are used. In contrast to direct sandwich ELISA, the secondary antibody is not conjugated to an enzyme. After incubation and a wash step, the complex is detected by adding anti-species enzyme conjugated detection antibody (Crowther 2000).

### 2.6.2    *Applications of ELISA*

ELISA is a method used to detect proteins and antibodies in serum, urine, and plasma samples. Its applications include measuring the serum antibody concentration in a number of viral tests, e.g., (HIV, Malaria test, west Nile virus), home pregnancy testing, and in the food industry for the detection of allergens such as milk and peanuts. ELISA is also used in toxicology for rapid screening for certain classes of drugs.

ELISA can be used to detect both viral proteins as well as antibodies to viruses. It is a highly sensitive assay that can detect proteins at the picomolar to nanomolar range $(10^{-12}$ to $10^{-9}$ moles per liter). It is the mainstay for the diagnosis of infections by many different viruses, including HIV-1, HTLV-1, adenovirus, and cytomegalovirus. The HIV test is based on the detection of serum antibodies to HIV envelope antigen. The ELISA test is based on adsorption of HIV envelope antigens to a concanavalin A coated solid support. If antibodies against HIV are present in the serum, they are captured by the surface immobilized antigen and detected by peroxidase conjugated antibody (Robinson *et al.*, 1990). ELISA technology was also used for detection of IgG and IgM antibodies to

West Nile virus in human sera. The antibodies were captured by west Nile virus antigen adsorbed to a surface substrate. The captured IgG and IgM antibodies were quantified by using alkaline-phosphatase conjugated anti-human IgG and IgM antibodies (Feinstein, *et al.* 1985).

The ELISA method is the basic technology behind home pregnancy testing. The immunoassay measures the level of beta-human chorionic gonadotropin (beta-hCH) in blood and urine that is produced after implantation using a sandwich ELISA method. Unique combinations of two monoclonal antibodies that are specific for hCG are used to detect the levels of the antigen. A monoclonal antibody that is specific to hCG is coated to the surface of the well and the urine and/or blood specimen is allowed to react with it. Detection of the antigen is achieved with a penicillinase enzyme conjugated secondary antibody that binds to a different epitope site of hCG. The detection antibody develops a blue color upon reaction with a substrate (Joshi, *et al.* 1981).

ELISA is a sensitive technique used for detection of trace amounts of allergens such as peanuts and mold in processed food. Since peanuts are a major source of allergens, to minimize the risk of cross contamination it is important to develop an approach for detection of these trace amounts. Sandwich ELISA using two specific antibodies against the peanut protein is used to detect low amounts of the protein in the food sample. Secondary antibody conjugated to a horse-radish peroxidase enzyme is used to confirm the presence of the protein (Stephan and Vieths 2004).

2.6.3      *Antigen-Antibody Interaction Detection using Thermistors (TELISA)*

The most widely used method for detection of antibody-antigen interactions is the enzyme-linked immunosorbent assay (ELISA). In ELISA, the enzyme is linked to the

antibody, antigen, or other reference sample of interest and after the coupling reaction a

spectrophotometer based assay for enzymatic activity is carried out to determine the

concentration of the analyte of interest. Mattiason *et al.* (1977) developed a novel method

for analysis and detection of compounds in biological fluids using antibody-antigen

interactions detected by an enzyme thermistor. The technology was used to quantify the

concentration of human serum albumin in biological samples. The principle of the assay

was based on competitive ELISA. Anti-human serum albumin was immobilized on a

solid matrix packed inside a glass column. A known amount of human serum albumin

catalase aggregate was mixed with a biological sample containing a known amount of

human serum albumin. The mix was reacted with immobilized antibodies that resulted in

a competitive binding of the mix of antigens and the antibody. To quantify the

concentration of albumin in the biological samples, hydrogen peroxide, a substrate for

catalase, was introduced in the system and the heat of the reaction was recorded using a

thermistor. The limit of detection of this method is $10^{-10}$M and the reported standard

variation was 0.9%. The advantage of this method is that it can be applied using a number

of enzymes since the method is based on detection of the enthalpy of the reaction

(Mattiasson, *et al.* 1977). A number of different enzymes were used to test the

performance of the thermistor based ELISA. These include penicillinase, tyrosinase,

invertase, and glucose oxidase. The metabolites detected include Penicillin G, phenol,

tyrosine, sucrose and glucose. The concentration range of glucose detection was $5 \times 10^{-4}$

$- 5 \times 10^{-5}$ M, while for sucrose it was $10^{-3} - 5 \times 10^{-2}$. The lower sensitivity of the sucrose

detection was most likely caused by lower specific activity of the albumin-conjugated

proteins (Mattiasson 1977).

## 2.7 Heat and Mass Transfer

2.7.1 _Enthalpy of Glucose Oxidation by Glucose Oxidase_

Glucose is oxidized in the presence of glucose oxidase. The product of the enzymatic reaction is gluconic acid and the substrate is β-D-Glucose. The enzyme utilizes molecular oxygen as an electron acceptor to produce hydrogen peroxide. The chemical reaction of glucose oxidation in the presence of glucose oxidase is:

$$Glucose + O_2 + H_2O \xrightarrow{Glucose\ Oxidase} Gluconic\ Acid + H_2O_2 + 79kJ\ mol$$
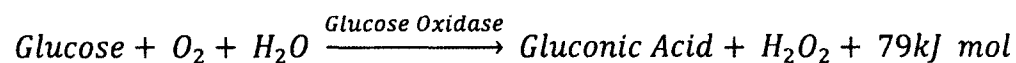
The enzymatic reaction proceeds in two steps: reductive and oxidative half reactions. In the reductive step, glucose oxidase catalyzes the oxidation of β-D-Glucose to gluconic acid. In the oxidative step, the reduced enzyme is oxidized by oxygen to produce hydrogen peroxide. In a subsequent reaction, the hydrogen peroxide could be cleaved by catalase to produce water and oxygen.

The above reaction is exothermic and the heat produced for one mole of glucose consumed is 79 kJ. In the presence of catalase, hydrogen peroxide forms oxygen and water. The catalase reaction is also exothermic and generates 100 kJ heat. The reaction equation is:

$$H_2O_2 \xrightarrow{catalyse} \frac{1}{2}O_2 + H_2O + 100\ kJ.$$
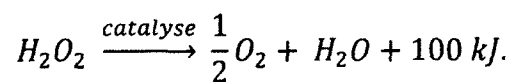
The optimal pH for the enzymatic reaction is 4-7. The Michaelis constant (Km) and the maximal limiting rate velocity (Vmax) of glucose oxidase from _A. niger_ are 33mM and 458 U mg$^{-1}$ respectively (Bankar, Bule and Singhal, 2009).

2.7.2 _Fundamentals of Heat and Mass Transfer_

Heat transfer is a physical process that is associated with the transit of energy due to a temperature difference in a medium. There are three different modes of heat transfer:

conduction, convection and thermal radiation. Conduction refers to heat transfer across a stationary gradient that can be solid or fluid. Convection refers to heat transfer that occurs between a solid surface and a moving fluid that are at different temperatures. Thermal radiation refers to the net radiation heat exchange between two surfaces at different temperatures when there is no intervening medium (Incropera and Dewitt 2008).

The physical mechanism that governs conduction is the transfer of energy between the atoms or molecules of the interacting materials. The conductive heat transfer process can be quantified using Fourier's law. The heat flux, q (W m$^{-2}$), is the heat transfer rate per unit area that is perpendicular to the direction of transfer. The heat flux is directly proportional to the temperature gradient and the thermal conductivity, k (W mK$^{-1}$) of the material, and inversely proportional to the thickness (L) of the material (**Eq.2-4**):

$$q = k\frac{\Delta T}{L}.$$ **Eq.2-4**

The convection heat transfer mode is due to the random molecular motion of particles and the macroscopic motion of the fluids. There are two types of convection heat transfer according to the flow: forced and natural convection. Forced convection is a flow caused by an external source, while natural convection is caused by buoyancy forces. The rate equation (**Eq.2-5**), that describes the convective heat flux is Newton's law of cooling. The convective heat flux, q (W/m), is proportional to the temperature difference between the surface and the fluid ($\Delta T$) and the convective heat transfer coefficient, h (W/m$^2$K)

$$q = h\Delta T.$$ **Eq.2-5**

The physical mechanisms that underline radiation are changes to electron configuration of the matter emitting the energy. The matter can be solids, liquids or gasses. The thermal radiation heat transfer does not require a medium, because the energy is transported via electromagnetic waves. The heat flux (E) that is emitted by a surface is proportional to the emissivity of the surface ($\varepsilon$), Stefan-Boltzmann constant ($\delta$), and the temperature of the surface (**Eq.2-6**)

$$E = \varepsilon \delta T^4.$$    **Eq.2-6**

Thermal resistance is the ability of a material or system to resist the flow of heat. The thermal resistance for conduction (**Eq.2-7**), R (K W$^{-1}$), is directly proportional to the thickness of the material (L), and inversely proportional to the thermal conductivity of the material (k) and the surface area (A)

$$R = \frac{L}{kA}.$$    **Eq.2-7**

The thermal resistance for convection (**Eq.2-8**) is inversely proportional to the convective heat transfer coefficient (h), and to the area (A)

$$R = \frac{1}{hA}.$$    **Eq.2-8**

# CHAPTER 3

# METHODS

## 3.1    Experimental Design

Thermoelectric ELISA for quantification of 8OHdG was performed in a microfluidic device with an integrated antimony-bismuth thin-film thermopile. Quantification of the analyte was achieved using a capture antibody specific to the analyte (8OHdG). The detection of the capture event was recorded using a secondary antibody labeled with glucose oxidase. A fixed concentration of glucose was injected into the fluid flowing within the microfluidic device and the heat of the enzymatic reaction was detected by a thermopile. The heat of the reaction was quantified by measuring the area under the curve of the thermopile response. A standard calibration curve was generated for various concentrations of the 8OHdG. The performance of the system was tested with mouse urine samples containing unknown amounts of 8OHdG obtained from APP transgenic mice that have high levels of oxidative stress.

Thermoelectric detection and quantification of 8OHdG was performed using the microfluidic device with integrated thin-film thermopile shown in **Figure 3-1**.
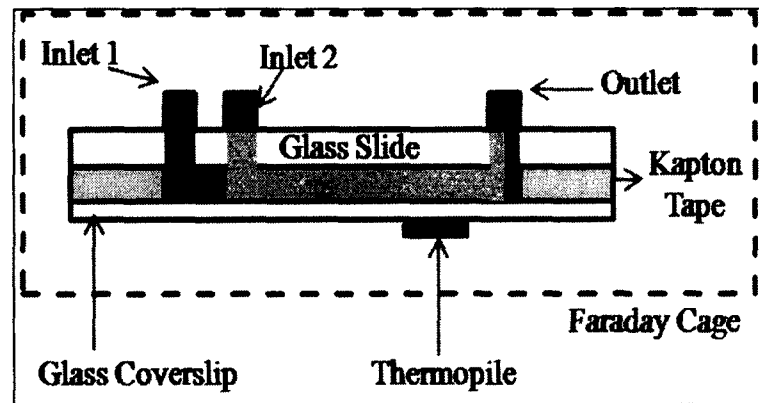
**Figure 3-1:** Microfluidic device with integrated thermopiles (Tangutooru, *et al.* 2012).

The microfluidic device consists of two, 1/16 inch outer diameter inlet ports

(Upchurch Scientific, Oak Harbor, WA) attached over holes drilled into a glass

microscope slide (Electron Microscopy Sciences, Hatfield, PA); a flow channel; a

rectangular region where the 8OHdG/primary antibody/secondary antibody complex is

immobilized to the inner surface of a streptavidin coated glass coverslip within the

measuring junctions of the thermopile; an antimony-bismuth, thin-film thermopile that is

attached to the external surface of the coverslip; and a channel outlet port (Upchurch

Scientific, Oak Harbor). The flow channel is formed using xurography, a polymer/glass

fabrication technique employing 100μM thick polyimide tape coated on each side with

silicone adhesive (Bartholomeusz, Boutte, Andrade 2005). During operation, phosphate-

citrate buffer solution (Sigma-Aldrich, St. Louis, MO) is independently introduced into

the two inlet ports. The flow rates through the two inlets are adjusted such that the flow

through Inlet 1 hydrodynamically focuses the fluid entering the device via Inlet 2. By

adjusting the ratio of the flows through the two inlets, the fluid introduced through Inlet 2

flows down the centerline of the device over the immobilized 8OHdG/primary

antibody/secondary antibody complex and the measuring junctions of the thermopile. The

fluid introduced through Inlet 1 flows only over the reference junctions of the thermopile. Laminar flow prevents the two fluid streams from mixing (Lee, *et al*. 2006). Thermal events common to both the reference and measuring junctions are rejected by the thermopile. This eliminates the need for careful control of the ambient and reference junction temperatures. To quantify the concentration of 8OHdG, a sample containing phosphate-citrate buffer and D-glucose (100mg dL$^{-1}$) (Sigma Aldrich, St. Louis, MO) was introduced as a bolus into the inlet 2 flow stream. When the glucose reached the antibody/glucose oxidase complex, heat was released if glucose was oxidized by the glucose oxidase enzyme conjugated to the IgG antibody. As a result, the temperature of the coverslip under the antibody/antigen complex increased relative to the temperature of the coverslip not coated with glucose oxidase conjugated secondary antibody. The temperature change was detected by the measuring junctions of the thermopile but not by the reference junctions.

### 3.2    Two-dimensional Unsteady State Mathematical Model

A mathematical model that simulates the unsteady state dynamics and enzymatic reaction kinetics between glucose and glucose oxidase was developed and solved using Mathcad. The model predicts the output voltage change of a thin-film thermopile attached to the lower channel wall of the device. The model assumes that the solution is well mixed, the mass flow rate and the physical properties of the materials and the solution are constant, the system is insulated and is operated under adiabatic conditions. Other assumptions that are included in the model are homogeneous heat generation and negligible radial and axial mass diffusion.

An energy balance was performed for the fluid flowing within the channel, the channel walls adjacent to the reaction zone and the thermopile support. The general form of the energy balance equation was given by the following equation:

*Rate of accumulation of thermal energy within the system = the net rate at which thermal energy enters the system as a result of bulk fluid flow + net rate at which thermal energy enters the system via conduction and/or convection + volumetric rate of thermal energy generation by the enzymatic reaction.*

The model assumes the enzymatic reaction occurs within the volume of the fluid flowing between the upper and lower channel walls. The upper channel wall of the microfluidic device is fabricated using 1.0 mm thick glass while the lower channel wall is 150 micron thick glass cover slip. The thermopile is fabricated on 125 micron thick Kapton® tape and protected with acrylic tape (**Figure 3-2**).
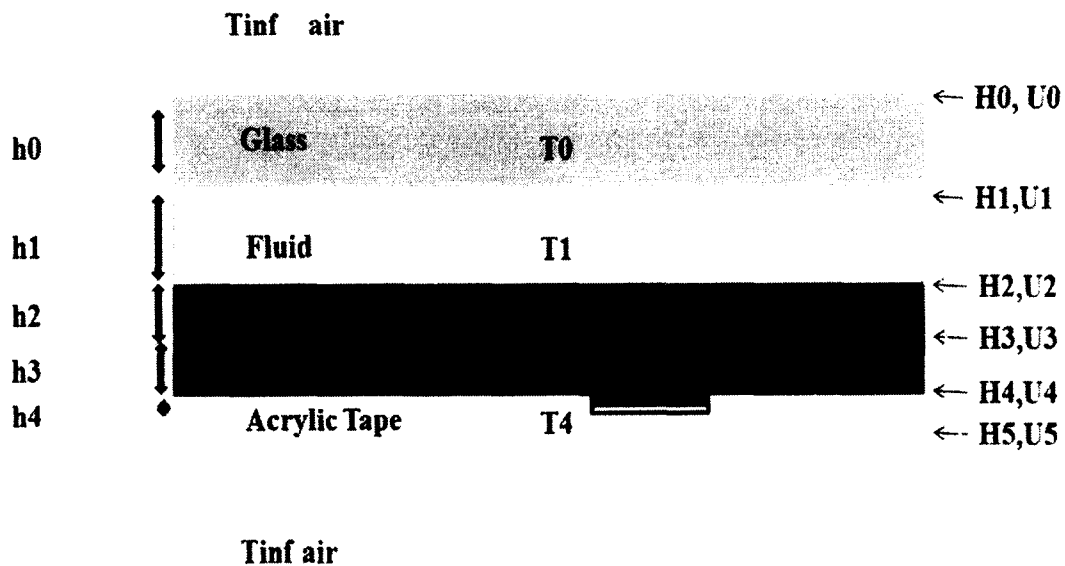
**Figure 3-2:** Side view schematic of microfluidic system

Four ordinary differential equations predict the change of the temperature of the fluid in the reaction zone, the two walls of the microfluidic channel above and below the reaction zone, and the Kapton thermopile film in contact with the measuring and the reference junctions of the thermopile. The equations were solved using the Radau numerical integration method for stiff systems using Mathcad. The thermopile output as a function of time was calculated by multiplying the theoretical thermopile sensitivity and the predicted variation in wall temperature assuming a 60 junction antimony-bismuth thin-film thermopile with a theoretical sensitivity of $7.14\mu V$ $mK^{-1}$.

The wetted perimeter of the channel was calculated using the following equation (**Eq.3-1**):

$$D_h = \frac{2wh1}{w+h1},$$

Eq.3-1

where h1 is the height of the microfluidic device channel and w is the width of the reaction zone.

The thermal convection coefficient assuming the properties of pure water was calculated using the following equation (**Eq.3-2**):

$$H_1 = 7.54\frac{k_{water}}{D_h},$$

Eq.3-2

where 7.54 is Nusselt number for fully developed laminar flow in a rectangular flow channel and the ratio of width to height of the channel is infinity.

T0, T1, T2, T3, and T4 are the temperatures in the middle of each layer of the system, while h0, h1, h2, h3, and h4 are the thicknesses of each layer. $U_0$, $U_1$, $U_2$, $U_3$, $U_4$ and $U_5$ are the values for the overall heat-transfer coefficients for each layer. The overall

heat transfer coefficients for each layer of the system are presented in **Equations 3-3, 3-4, 3-5, 3-6, 3-7, and 3-8**.

$$U_0 = \frac{1}{\frac{1}{H_0} + \frac{\frac{h_0}{2}}{k_0}} \qquad \textbf{Eq.3-3}$$

$$U_1 = \frac{1}{\frac{1}{H_1} + \frac{\frac{h_0}{2}}{k_0}} \qquad \textbf{Eq.3-4}$$

$$U_2 = \frac{1}{\frac{1}{H_2} + \frac{\frac{h_2}{2}}{k_0}} \qquad \textbf{Eq.3-5}$$

$$U_3 = \frac{1}{\frac{\frac{h_3}{2}}{k_2} + \frac{\frac{h_2}{2}}{k_0}} \qquad \textbf{Eq.3-6}$$

$$U_4 = \frac{1}{\frac{\frac{h_3}{2}}{k_2} + \frac{\frac{h_4}{2}}{k_4}} \qquad \textbf{Eq.3-7}$$

$$U_5 = \frac{1}{\frac{1}{H_5} + \frac{\frac{h_4}{2}}{k_4}} \qquad \textbf{Eq.3-8}$$

The area within the measuring junctions of the thermopile where the enzymatic reaction occurs is labeled as $A_s$. The heat of the reaction was calculated to be $1.22\mu J$ $sec^{-1}$, the duration of the reaction was 120 seconds and the flow rate was $25\mu L$ $min^{-1}$.

Five differential equations were developed and solved using Mathcad (**Eq.3-9 to 3-13**)

Glass Equation:

$$\rho_0 c_0 V_0 \left(\frac{d}{dt}T_0(t)\right) = U_1 A_s\big(T_1(t) - T_0(t)\big) - U_0 A_s\big(T_0(t) - T_{inf}\big) \qquad \textbf{Eq.3-9}$$

Fluid equation:

$$\rho_3 c_3 V_1 \left(\frac{d}{dt}T_1(t)\right) = U_2 A_s\big(T_2(t) - T_0(Tt)\big) + Q\rho_3 c_3 - U_1 A_s\big(T_1(t) - T_0(t)\big) \qquad \textbf{Eq.3-10}$$

Cover Slip Equation:

$$\rho_0 c_0 V_0 \left( \frac{d}{dt} T_2(t) \right) = surf\_heat(t) - U_{12} A_s \big( T_2(t) - T_1(t) \big) - U_3 A_s \, (T_2(t) - T_3(t)) \quad \textbf{Eq.3-11}$$

Kapton® Tape Equation:

$$\rho_2 c_2 V_3 \left( \frac{d}{dt} T_3(t) \right) = U_3 A_s \big( T_2(t) - T_3(t) \big) - U_4 A_s \, (T_3(t) - T_4(t)) \quad \textbf{Eq.3-12}$$

Acrylic Tape Equation:

$$\rho_4 c_4 V_4 \left( \frac{d}{dt} T_4(t) \right) = U_4 A_s \big( T_3(t) - T_4(t) \big) - U_5 A_s \, (T_4(t) - T_{inf}) \quad \textbf{Eq.3-13}$$

### 3.3 Heat Transfer Simulations using SolidWorks

SolidWorks software was used to perform time-dependent heat transfer analysis in the microfluidic device. The parameters investigated were the location of the reaction zone and the effects of flow rate and duration of the enzymatic reaction on the heat distribution profile within the system and the thermopile output.

SolidWorks simulations were performed using different locations of the heat source within the system. The simulations were performed for 30 seconds duration of the enzymatic reaction. The first set of results was obtained when the heat source was located along the entire length of the microfluidic channel. The reaction zone was 3 mm wide and 20 mm long. The total amount of heat released during the enzymatic reaction depends on the number of enzyme molecules immobilized over the lower channel wall of the microfluidic system that is proportional to the size of the reaction zone. When the reaction zone was located within the measuring junctions of the thermopile, the rate of heat generation was $1.62 \mu W$. When the reaction zone was located along the length of the device, the heat generation rate increased to $5.05 \mu W$. The reaction zone was 3 mm wide and 8 mm long when located over the thermopile and 3 mm wide and 20 mm long when

located along the length of the device. The simulations were performed using flow rates of 100μL min$^{-1}$ and 25μL min$^{-1}$ for inlet 1 and inlet 2, respectively.

The effect of fluid velocity on the thermopile output was investigated using different flow rate ratios for inlet 1 and inlet 2. The flow rate of inlet 2 was kept constant at 25μL min$^{-1}$ while the flow rate of inlet 1 was reduced from 100μL min$^{-1}$ to 50μL min$^{-1}$. The heat source was located within the measuring junctions of the thermopile and the duration of the enzymatic reaction was 120 seconds. The width of the reaction zone depends on the ratio between the flow rates of both inlets. Decreasing the velocity of Inlet 1 affects the dimensions of the reaction zone. The width of the reaction zone decreased from 4mm to 3mm as the flow rate of inlet 1 increased from 50μL min$^{-1}$ to 100μL min$^{-1}$.

SolidWorks heat transfer simulations were performed for 30 seconds and 120 seconds duration of the enzymatic reaction. The reaction zone was located within the measuring junctions of the thermopile and the flow rates of inlet 1 and inlet 2 were 100μL min$^{-1}$ and 25μL min$^{-1}$, respectively.

### 3.4     Thermoelectric System for Performing ELISA

A schematic of the experimental thermoelectric system for 8OHdG quantification is shown in **Figure 3-3**.
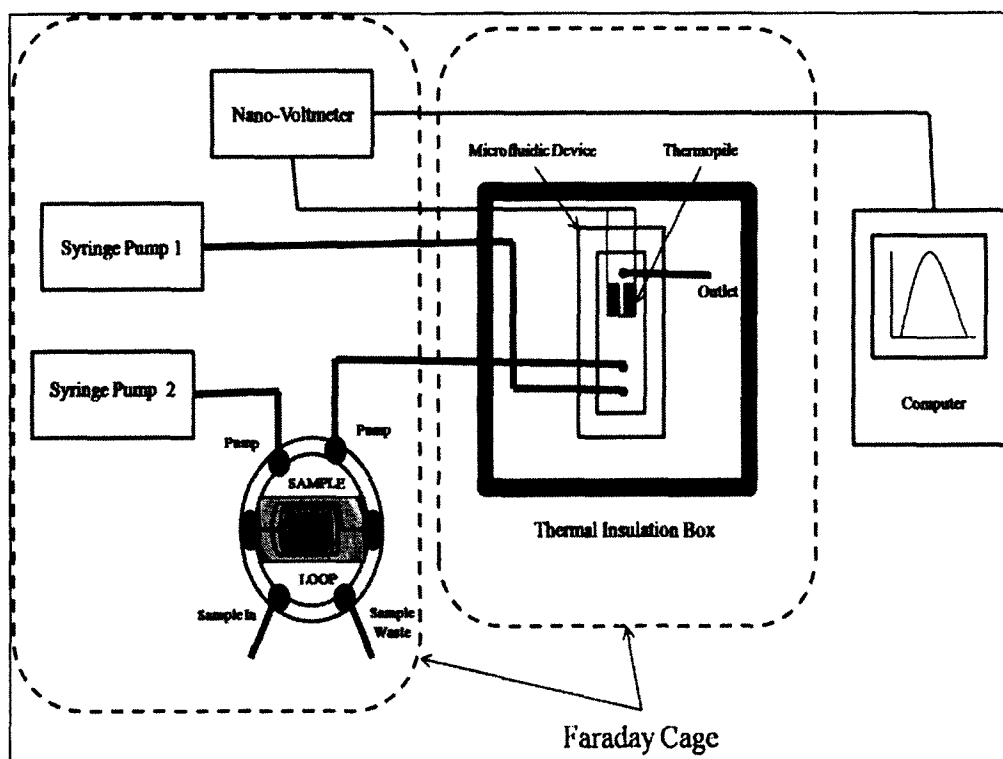
**Figure 3-3:** Schematic diagram of the experimental set-up (Kopparthy, *et al.* 2012).

Two pressure driven Mitos P-Pumps (Dolmite Microfluidics, Charleston, MA)

provided independent injection of phosphate-citrate buffer solutions through 0.01 inch

internal diameter Teflon® tubing (Upchurch Scientific, Oak Harbor, WA) into the inlet

ports of the microfluidic device. A 52μL, 0.01 inch internal diameter sample loop was

loaded with glucose (100mg dL$^{-1}$) in phosphate-citrate buffer. The sample was injected

into the buffer stream being supplied to Inlet 2 using a 6-Port Injection valve, (Model V-

451, Upchurch Scientific, Oak Harbor, WA). A nanovoltmeter (Agilent Technologies,

Santa Clara, CA) was used to measure the thermoelectric e.m.f. of the thermopile. The

output of the nanovoltmeter was recorded and processed using LabView Signal Express

(National Instruments Corporation, Austin, TX).

## 3.5 Thermopile Fabrication

Antimony-bismuth thermopiles with 60 thermocouple junction pairs were
fabricated on 125 μm polyimide supports (**Figure 3-4**) using a Denton model DV-502B
metal evaporation system (Denton Vacuum, Moorestown, NJ).
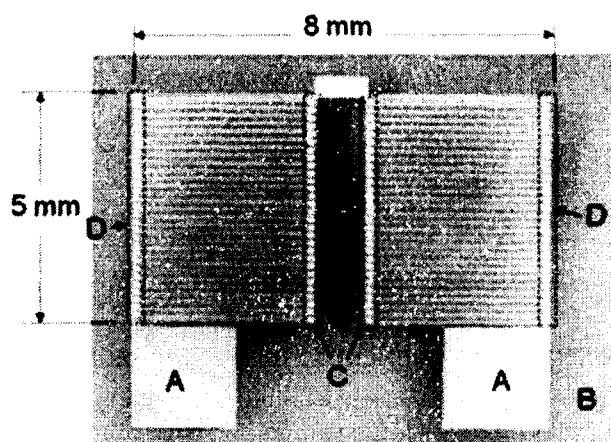


**Figure 3-4:** Antimony-bismuth thermopile with 60 thermocouple junctions (A=contact
pads, B=polyimide support, C=measuring junctions, D=reference
junctions).

Custom designed metal shadow masks containing patterns for creating the
thermopile's thin metal lines were manufactured to our specifications by Town
Technologies Inc. (Town Technologies Inc., Somerville, NJ). A rectangular piece of 125
μM thick polyimide tape (DuPont, Circleville, OH) was placed behind the shadow mask
to create the bismuth line pattern and suspended above the evaporator heat source.
Bismuth metal (Sigma-Aldrich Chemicals, St. Louis, MO) was heated until vaporized,
and the vapors were allowed to condense on the support. The shadow mask containing
the antimony line pattern was carefully aligned to overlap with the bismuth lines at the
thermocouple junctions. The metal evaporation process was repeated using antimony
metal (Sigma-Aldrich Chemicals, St. Louis, MO). Following deposition of the antimony,
the thermopiles were removed from the chamber, tested for electrical continuity, and

protected from physical damage using thin polyimide tape. The thermopiles were attached to the streptavidin-coated coverslip using a small quantity of high-density polysynthetic silver thermal compound (Arctic Silver Inc., Visalia, CA).

### 3.6 Data Collection and Processing

LabView Signal Express software (National Instruments, Austin, TX) was used to store, display and analyze the digital signal. The raw data results were exported to Microsoft Excel and the area under the curve (AUC, $\mu$Vs) was calculated for different 8OHdG concentrations by integrating the area under the voltage versus time profile using the trapezoid rule. The AUC measurements were plotted versus the concentration of 8OHdG and the results were used to generate a standard curve. The results from the standard curve were used to calculate the concentration of 8OHdG in mouse urine samples.

### 3.7 Layer-by-layer Self-assembly

Layer-by-layer self-assembly (LbL) was used to immobilize streptavidin on glass coverslips (Electron Microscopy Sciences, Hatfield, PA). Prior to immobilization, the substrates were cleaned using 2% Micro-90 cleaning solution (Sigma Aldrich, St.Louis, MO). Poly (Ethylene Imine), PEI, (Sigma-Aldrich, Saint Louis, MO) and Poly (Acrylic acid), PAcr, (Sigma Aldrich, Saint Louis MO) were used as polyelectrolytes. PEI (50% w/v in water) and PAcr (35% w/v) were dissolved in distilled water. The pH of both polyelectrolytes was adjusted to 8 by adding NaOH and HCl. The preparation of polyelectrolytes is discussed in Appendix C. A cleaned glass cover slip was immersed in PEI and PAcr alternatively for 15 minutes with intermediate rinsing and drying. The schematic procedure of LbL is shown in **Figure 3-5.** This process was repeated for three

bilayers of PEI/PAcr polyelectrolytes so that a precursor layer was formed. The scheme

that was followed was +/wash/-/wash/+/wash/-/wash/+/wash/-/wash.
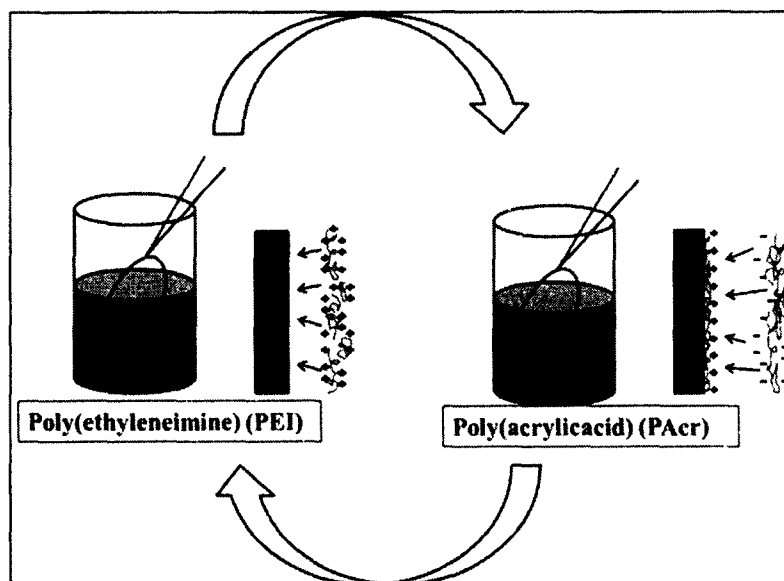


**Figure 3-5:** Layer-by-layer self-assembly procedure (Lvov and Möhwald 2000)

Biotin was attached to the PAcr polyelectrolyte layer via (1-[3-(Dimethyl-

amino) propyl]-3-ethylcarbodiimide hydrochloride (EDC) linkage using a biotin EZ

link kit (Thermo Scientific, Rockford, IL). Amine-PEG-biotin was diluted in EDC

buffer and pipetted onto the PAcr polyelectrolyte layer of the coverslip. The coverslip

was then placed in the humidity chamber (37°C, 90% humidity) for 30 minutes. The

unreacted excess was washed with 10 mM MESb (PH 5.5) for 2 minutes followed by

a wash with 10 mM Tris buffer (pH 7.5) for 2 minutes. Forty micro-liters of

streptavidin solution from the stock solution were pipetted on the biotinylated

polyelectrolyte multilayer. The cover slip was placed in the humidity chamber for 30

minutes and the unreacted excess was washed with 10 mM Tris buffer (Kartalov,

Unger and Quake 2003). The protocol for the preparation of stock biotin and

streptavidin solution is discussed in Appendix C.

## 3.8    Microfluidic Device Fabrication

The microfluidic device was manufactured using xurography. A cutting plotter

(Graphtec America Inc., Santa Ana, CA) was used to form the microfluidic channel

out of 100 µM double sided Kapton® tape (3M, St. Paul, MN). The shape of the

channel was designed using Adobe Illustrator (Adobe, San Jose, CA). The Kapton®

tape was sandwiched between a 25 x 75 mm plain glass microscope slide and a 25 x

75 mm streptavidin-coated coverslip that contained the immobilized antigen/antibody

complex.

## 3.9    Experimental Plan

A series of experiments were performed to optimize the parameters of the

microfluidic device and confirm feasibility of thermoelectric ELISA for detection and

quantification of 8OHdG. The experiments aimed at optimization of the microfluidic

device parameters were performed using glucose oxidase conjugated to biotin (Vector

Laboratories Inc., Burlingame, CA). The enzyme was immobilized over the

measuring junctions of the thermopile via biotin-streptavidin interactions. Glucose

oxidase conjugated to biotin (0.5 mg mL$^{-1}$) was suspended in 50µL phosphate buffer

saline (PBS), loaded over the cover slip and incubated for 30 minutes at 37°C in a

humidity chamber. The effects of several parameters on the output of the thermopile

response were investigated. This included investigating the effects of using a heat sink

under the reference junctions of the sensor, and changing the glucose concentration,

injection sample volume, and flow rates on the output of the thermopile. Several

experiments were performed to study the effect on the thermopile response when

different microfluidic designs were used.

Several different designs of microfluidic channels were fabricated and

evaluated, including hydrodynamically focused, single channel, and three-way split

channel devices. A hydrodynamically focused microfluidic device consists of two

inlets and one outlet. The channel width was 12mm and the channel length was 66mm

(**Figure 3-6**).
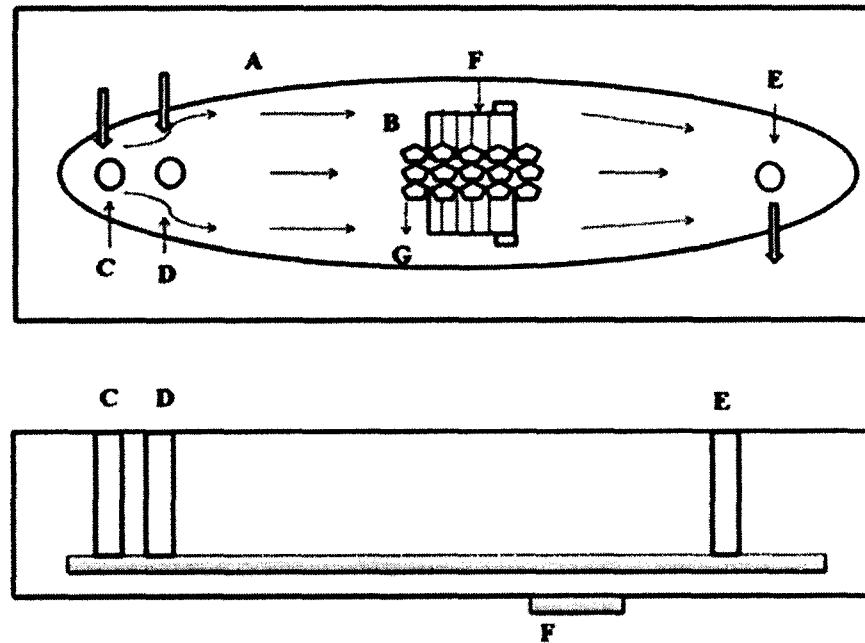


**Figure 3-6:** Schematic showing hydrodynamically focused microfluidic device. (A)
is the flow channel insulation, (B) is the flow channel, (C) is the buffer
solution that hydrodynamically constrains the substrate solution, (D)
solution containing the substrate, (E) is outlet/waste , (F) is
thermopile, (G) is enzyme-conjugated antibody/antigen/ capture
antibody complex.

The single channel device consisted of a single inlet and outlet. The channel

width was 4mm and the channel length was 66mm (**Figure 3-7**).
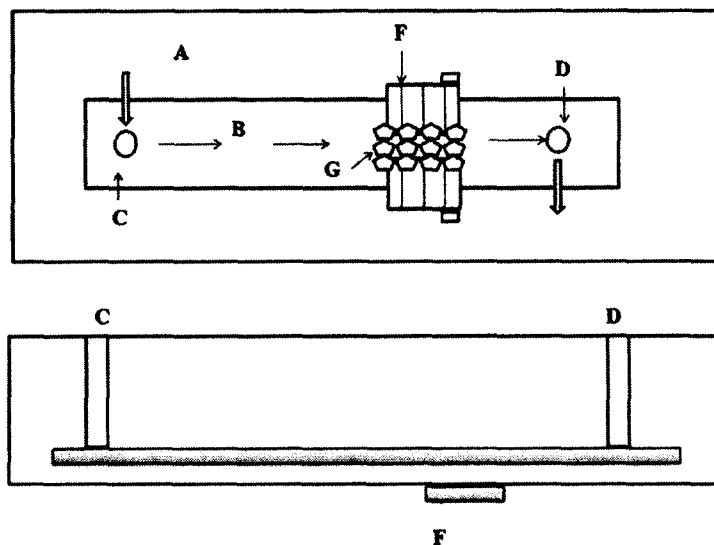
**Figure 3-7:** Schematic showing a single inlet device. (A) is the flow channel insulation, (B) is the flow channel, (C) is the Inlet for introduction of buffer and the substrate solution, (D) is the waste/outlet, (F) is the thermopile, and (G) is the enzyme-conjugated antibody/antigen/ capture antibody complex..

The split channel design consisted of three separate channels that had a width

of 3mm. (**Figure 3-8**).
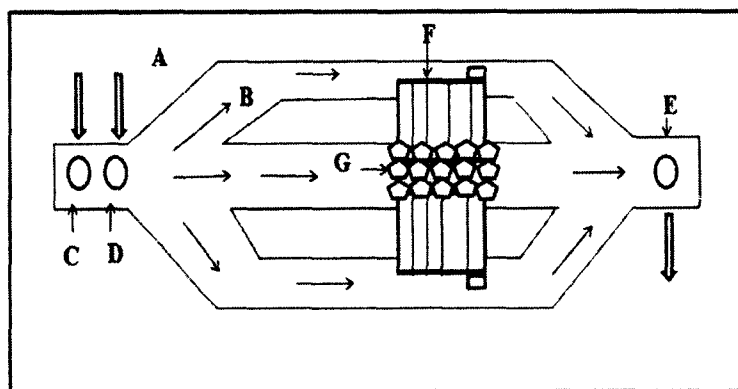


**Figure 3-8:** Schematic showing a three split channel device. (A) is the flow channel insulation, (B) is the flow channel, (C) is the inlet for introduction of buffer, (D) is the inlet for introduction of substrate, (E) is the waster/outlet, (F) is the thermopile, and (G) is the enzyme-conjugated antibody/antigen/capture antibody complex.

A standard calibration curve was generated by performing serial dilution of a

known concentration of the synthetic 8OHdG. Thermoelectric ELISA was used to

quantify the concentration of analyte in APP mouse urine samples.

### 3.10    Standard Calibration Curve Generation

A standard calibration curve was generated for 8OHdG concentration range of

0.0-10µM. The concentration of 8OHdG was quantified using glucose oxidase-linked

IgG antibody. The heat that was released during the enzymatic reaction was inversely

proportional to the concentration of 8OHdG in the biological sample. The data points of

the calibration curve were obtained by performing serial dilutions of 10µM 8OHdG. The

standard calibration curve was created by plotting the values of the area under the curve

(0, 3, 6, and10µM 8OHdG) of the thermopile signal versus the concentration of 8OHdG.

A primary anti-8OHdG polyclonal antibody (20 pmols) conjugated to biotin

(Biossusa, Woburn, MA) was incubated with 2µL of 10µM 8OHdG (Sigma Aldrich, St.

Louis, MO) for 30 minutes on an orbital shaker. A secondary IgG antibody (Abcam,

Cambridge, MA) was conjugated to glucose oxidase using glucose oxidase conjugation

kit (Abcam, Cambridge, MA). The secondary antibody was incubated with the complex

of the primary antibody and the analyte for 30 minutes on an orbital shaker. The primary

antibody/8OHdG/secondary antibody complex was immobilized over the lower channel

wall of the microfluidic device via biotin streptavidin interactions. The immobilization

step was performed for 30 minutes at 37°C in a humidity chamber, followed by a 2

minute wash step with a phosphate citrate buffer. Glucose was introduced in the system

and the heat of the enzymatic reaction was detected and measured by the thermopile.

Anti-8OHdG primary antibody (20pmol) and IgG glucose oxidase conjugated secondary antibody (20pmol) were incubated for 30 minutes on an orbital shaker in the absence of 8OHdG. The primary/secondary antibody complex was immobilized within the measuring junctions of the thermopile and the heat of the enzymatic reaction between glucose and glucose oxidase was measured using a thermopile. The average AUC of the thermopile response was used as the highest point for the standard curve.

### 3.11  8OHdG Quantification in Mouse Urine Samples

Thermoelectric ELISA was used to quantify the concentration of 8OHdG in APP transgenic mice. Twenty pmol of anti-8OHdG primary antibody conjugated to biotin (6.5pmol $\mu L^{-1}$) was incubated with 2$\mu$L of urine sample on an orbital shaker at room temperature for 30 minutes. Twenty $\mu$L IgG antibody conjugated to glucose oxidase was added to the mix and incubated on the orbital shaker for 30 minutes. The antibody/analyte complex was immobilized to a cover slip and incubated for 30 min at 37°C in a humidity chamber. The coverslip was washed with PBS and used for fabrication of the lower channel wall of the microfluidic device.

The concentration of 8OHdG was quantified in three mouse urine samples. For each sample, the injection of the substrate was performed three times and the average area under the curve of the thermoelectric response was used to estimate the concentration of 8OHdG in each sample. Standard deviation and standard error were calculated for each concentration.

# CHAPTER 4

# RESULTS

## 4.1    Microfluidic Device Parameters Optimization

The feasibility of the thermoelectric method for performing ELISA was

confirmed in a series of experiments designed to optimize several operating parameters

that affected the thermopile response. These experiments were performed using glucose

oxidase enzyme conjugated to biotin (Vector Laboratories, Burlingame, CA)

immobilized over the measuring junction of the thermopile via biotin-streptavidin

interaction. The parameters investigated included the type of holder (plastic or

aluminum), the signal recording system (Agilent nanovolt meter or proprietary amplifier),

streptavidin immobilization method (layer-by-layer technology or commercially prepared

coverslips), sample size (13μL or 52μL), the design of the microfluidic channel, glucose

concentration (100mg dL $^{-1}$ and 200mg dL $^{-1}$), flow rates, and the effect of a heat sink on

thermopile response.

### 4.1.1    *Elimination of Nonspecific Noise in the System*

Detection of enzymatic reactions between glucose and glucose oxidase was

evaluated using microfluidic holders made of either plastic or aluminum. The streptavidin

coverslips were commercially prepared by Xenopore Corp (Hawthorne, NJ). Negative

control experiments were performed using streptavidin coverslips without any enzyme

immobilized over the junctions of the thermopile. In these experiments, the injection

51

sample volume was 13µL and the flow rates were 100µL min$^{-1}$ for inlet 1 and 25µL min$^{-1}$

for inlet 2. Phosphate-citrate buffer was used as the buffer flowing through inlet 1 and

inlet 2. Glucose (100mg dL$^{-1}$) was suspended in phosphate-citrate buffer and introduced

in the flow stream. The calculated areas under the curve (AUC, µVs) for each glucose

injection and negative control injections are shown in **Figure 4-1**, **Figure 4-2**, and

**Figure 4-3**.
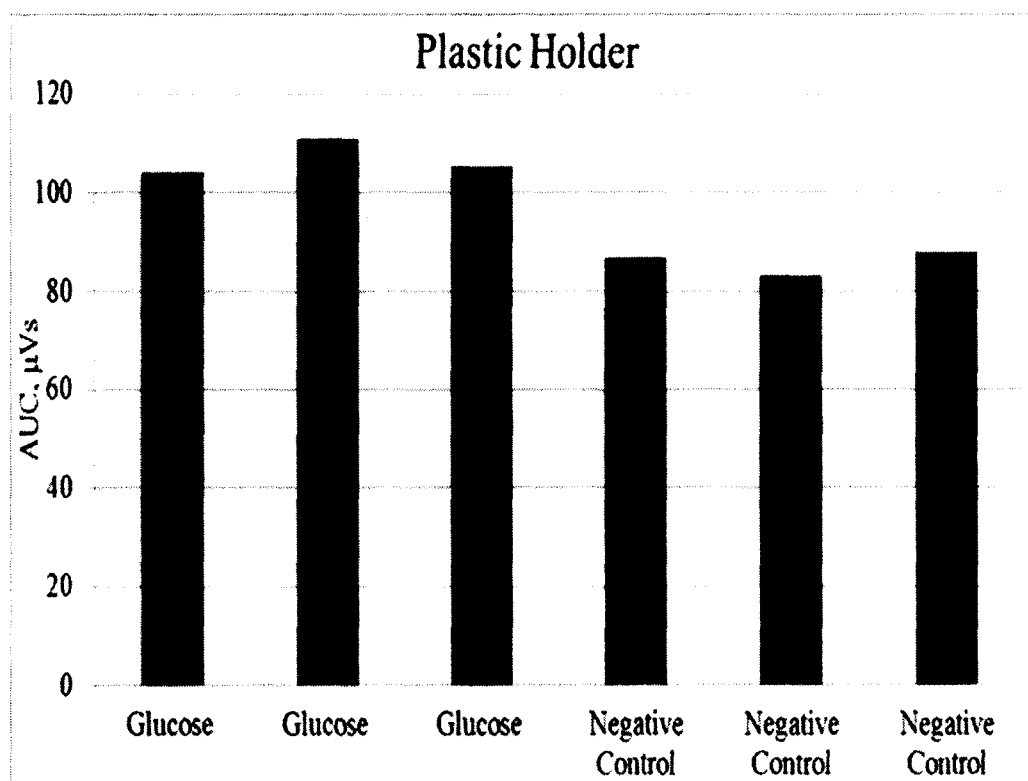


**Figure 4-1:** Peak areas for glucose (100mg dL$^{-1}$) and negative control injections when plastic holder was used.
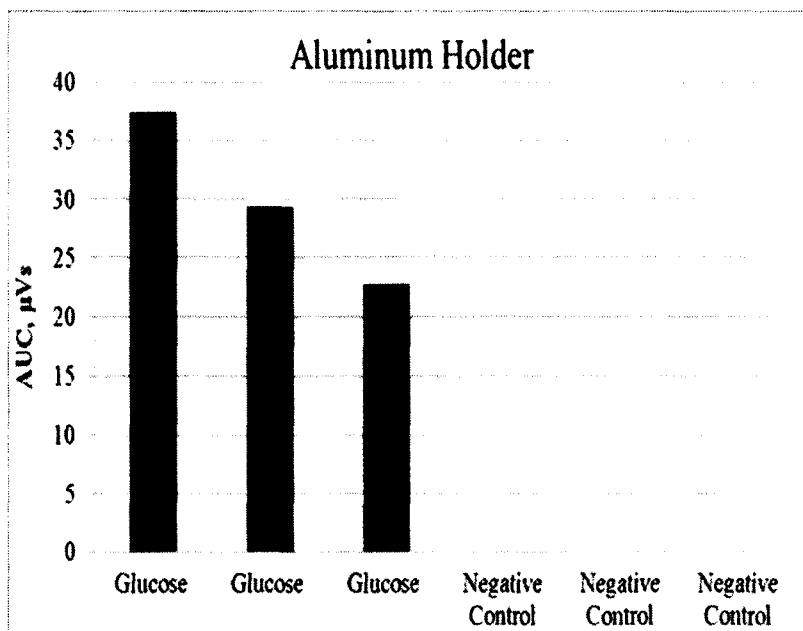
**Figure 4-2:** Peak areas for glucose (100mg dL$^{-1}$) and negative control injections when aluminum holder was used.
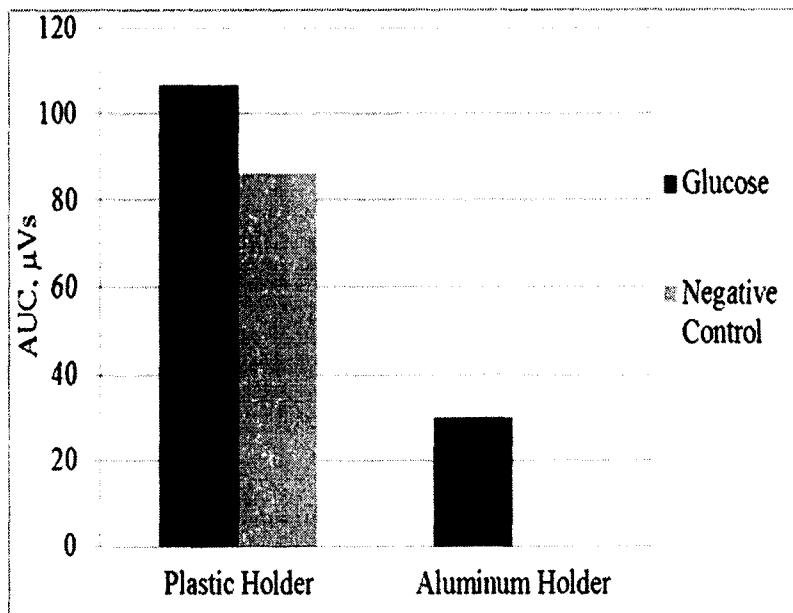


**Figure 4-3:** Average of peak areas for glucose (100mg dL$^{-1}$) and negative control when plastic holder and aluminum holder were used.

The aluminum holder decreased the magnitude of the signal response that was detected and completely eliminated the noise associated with non-specific interactions in the system

### 4.1.2 _Effect of using Nanovolt Meter and Proprietary Amplifier on the Signal_

Glucose oxidation experiments were performed to evaluate the system when an Agilent Nanovolt meter and in-house built amplifier were used to detect the thermoelectric signal. The sampling rate for the Agilent nanovolt meter was 1 sample sec[1]. The amplifier had a sampling rate of 100 samples sec$^{-1}$ and 1000x gain. In these experiments, the sample volume was 13 μL and the flow rates for inlet 1 and inlet 2 were 100μL min$^{-1}$ and 25μL min$^{-1}$ respectively. The streptavidin coverslips were supplied by Xenopore Corporation. The glucose concentration was 100mg dL$^{-1}$. The AUC of the thermoelectric signal when the amplifier and nanovolt meter were used is shown in **Figure 4-4**. The signal response of the thermopile is shown in **Figure 4-5** and **Figure 4-6**.
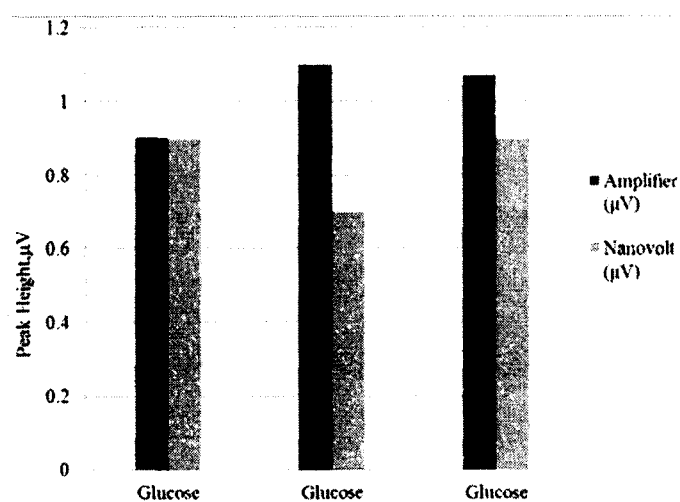


**Figure 4-4:** Peak height for glucose (100mg dL$^{-1}$) when proprietary amplifier and Agilent nanovolt meter were used.
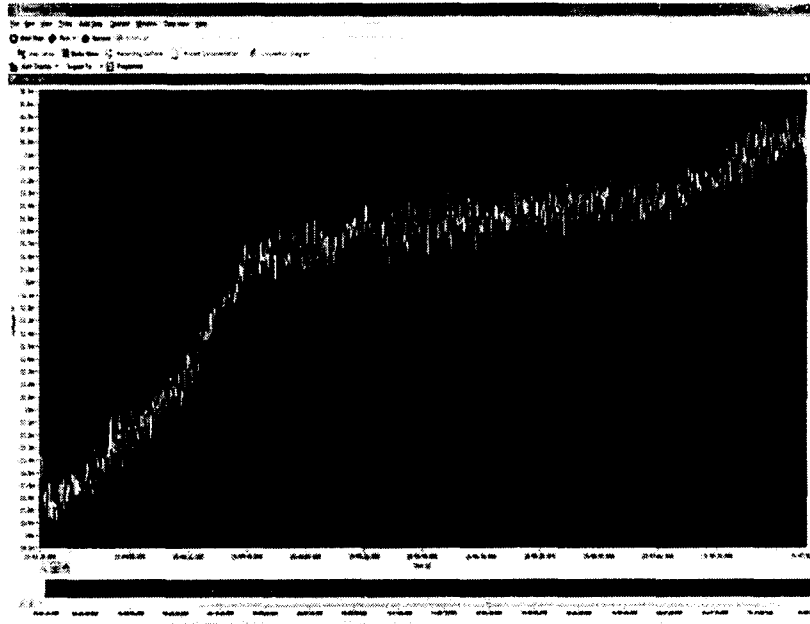
**Figure 4-5:** Signal response when proprietary amplifier was used to measure the thermopile response after glucose injection (100mg dL$^{-1}$).
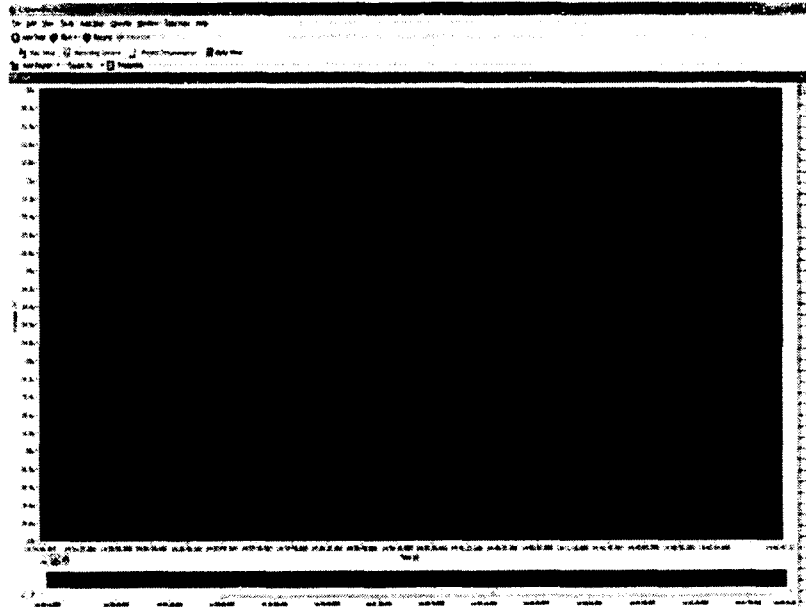


**Figure 4-6:** Signal response when Agilent nanovolt meter was used to measure the thermopile response after glucose injection (100mg dL$^{-1}$).

Data collection using the proprietary amplifier with increased sampling rate

increased the total amount of heat detected by the thermopile. The signal recorded by the

nanovolt meter had a lower level of electrical noise and distinct signal response peak

shape when compared to the amplifier (**Figure 4-5** and **Figure 4-6**).

### 4.1.3    *Effect of Streptavidin Immobilization on Thermopile Response*

To test the effect of streptavidin immobilization on signal response, experiments

were performed using commercially supplied streptavidin coverslips (Xenopore,

Howthorn, NJ) and coverslips coated with streptavidin using layer-by-layer technology.

The flow rates were 100 µL min$^{-1}$ and 25 µL min$^{-1}$ for inlet 1 and inlet 2, respectively,

with an injection sample volume of 13µL. **Figure 4-7** compares the heat generated

(AUC) when two different immobilization methods were used.
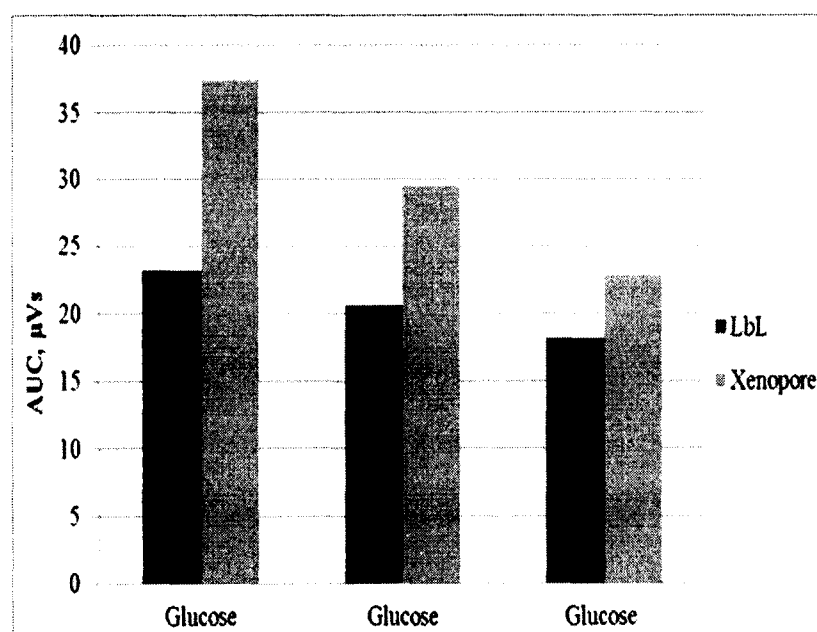


**Figure 4-7:** Peak areas for glucose (100mg dL$^{-1}$) response when different
immobilization methods for streptavidin were used.

The total amount of heat generated in a single injection was reduced when the

streptavidin was immobilized using the layer-by-layer method (**Figure 4 7**). The peak

height (µV) of the signal response when commercially prepared coverslips were used was

also calculated (**Figure 4-8**). The peak height of the signal response when streptavidin

immobilized coverslips using the layer-by-layer method were (**Figure 4-9**) compared to

the peak height when commercially prepared coverslips were used (**Figure 4-8**). The

signal response was 800nV on average when commercially supplied coverslips were

used. The signal decreased to 600nV on average when the layer-by-layer method was

used to immobilize streptavidin.
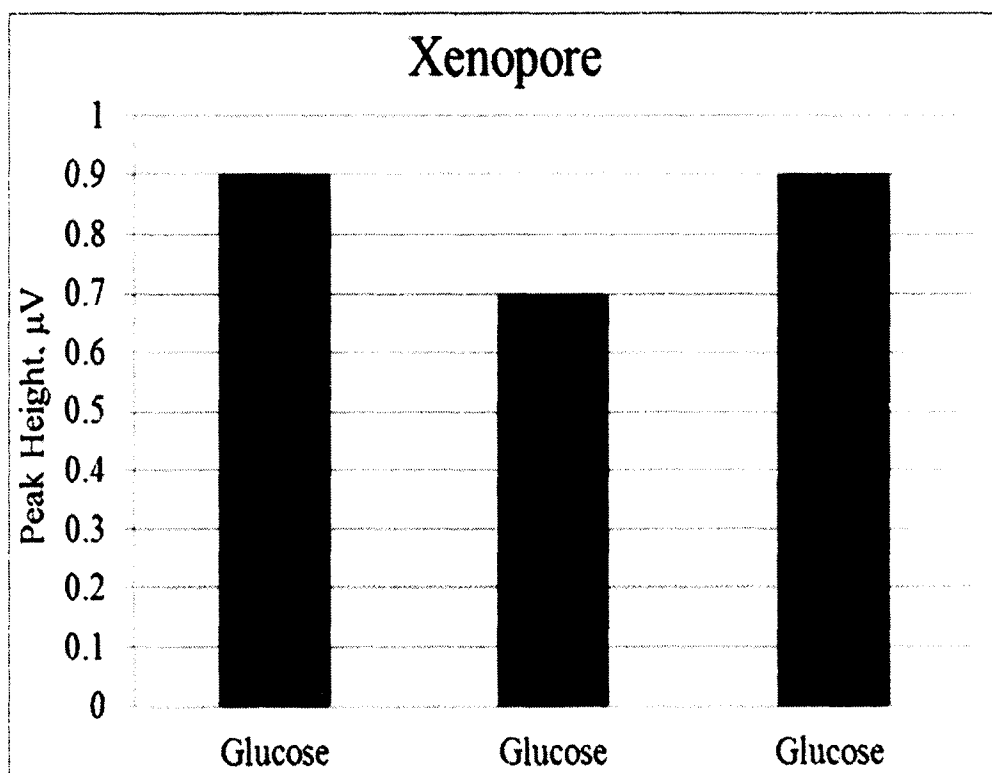


**Figure 4-8:** Peak height for glucose (100mg dL$^{-1}$) response when commercially
supplied streptavidin coated cover slips were used.
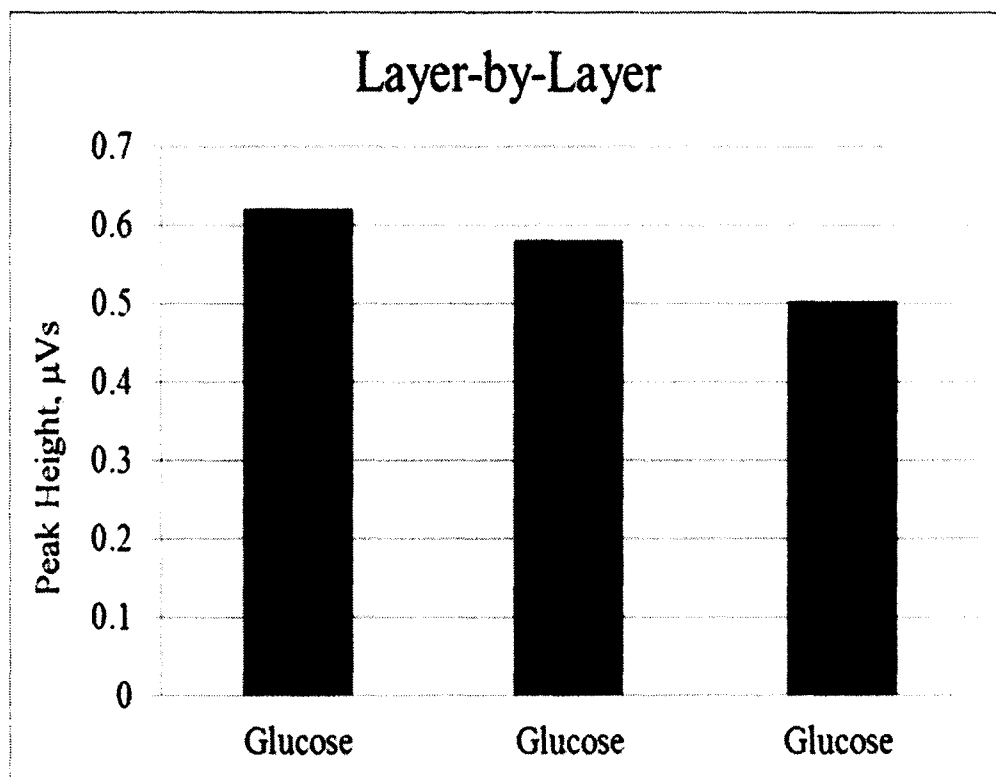
## Layer-by-Layer



**Figure 4-9:** Peak height for glucose (100mg $dL^{-1}$) response when streptavidin was immobilized using layer-by-layer method.

4.1.4    *Effect of Sample Size on Thermopile Response*

To increase the magnitude of the thermopile signal, the volume of the sample size

was increased from 13μL to 52μL. The flow rates used for these experiments were 100μL

$min^{-1}$ and 25μL $min^{-1}$ for inlet 1 and inlet 2, respectively. The streptavidin was

immobilized using the layer-by-layer technique. **Figure 4-10** shows the area under the

curve for the thermopile response when 13μL and 52μL sample loops were used. The

reference junctions of the thermopile were over a heat sink in both experiments.
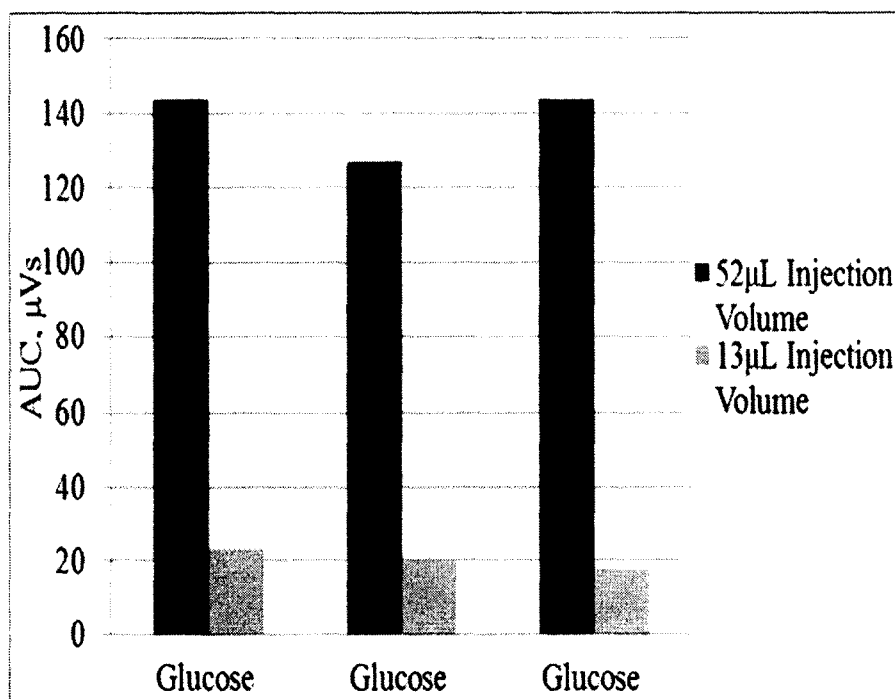
**Figure 4-10:** Peak areas for glucose (100mg dL$^{-1}$) response when sample injection volumes (13μL and 52μL) were used.

Increasing the sample loop volume increased the total amount of heat detected by the thermopile.

4.1.5    *Effect of Flow Rates on the Thermopile Response*

To evaluate the effect of flow rate magnitude and ratio on the thermopile response, several experiments were performed where the flow rate of inlet 2 was reduced from 25μL min$^{-1}$ to 12μL min$^{-1}$ and the ratio of inlet 1/inlet 2 flow rates was changed from 1:2 to 1:4. In this set of experiments streptavidin was immobilized using layer-by-layer technology and 52μL glucose (100mg dL$^{-1}$) was injected. The AUC of the signal response when glucose was injected in a hydrodynamically focused microfluidic device using different flow rate combinations is presented in **Figure 4-11**.
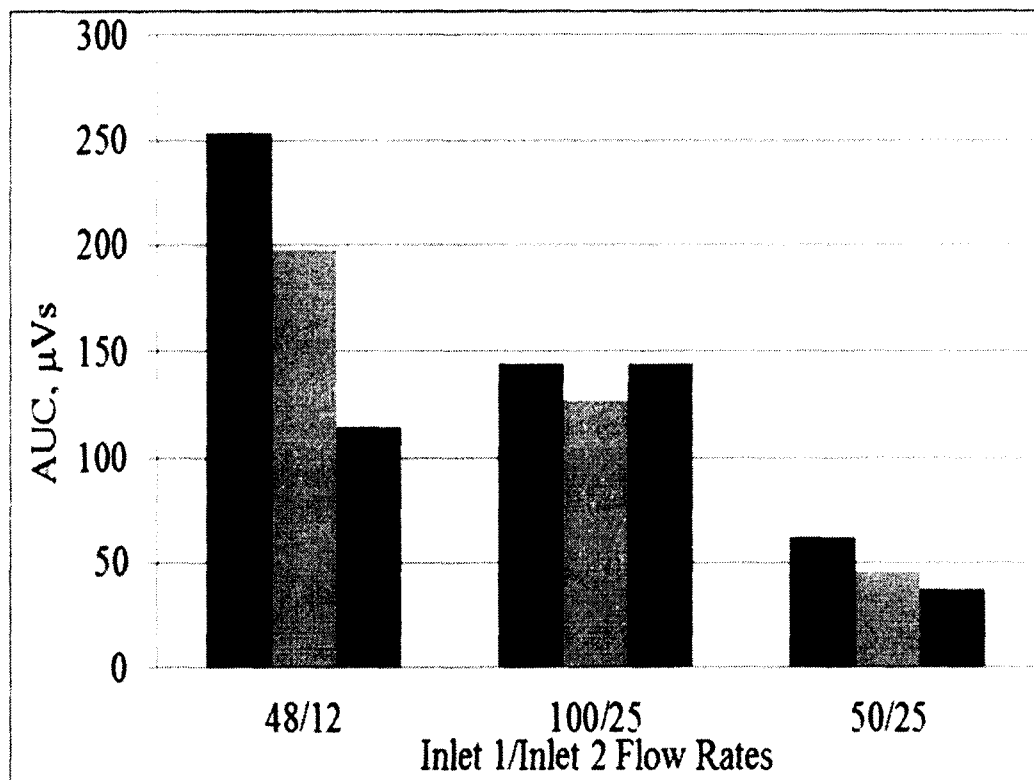
**Figure 4-11:** Signal response after glucose (100mg dL$^{-1}$) injection when different flow rates were used.

The signal response was higher when the flow rate velocity of inlet 2 was reduced from 25μL min$^{-1}$ to 12μL min$^{-1}$ and the flow rates ratio of inlet 1/inlet 2 was reduced from 1:2 to 1:4

4.1.5.1    Effect of Flow Rate Ratio on Thermopile Response

The effect of flow rate ratio of inlet 1 and inlet 2 on the thermopile response was investigated (**Figure 4-12**). It was observed that reducing the ratio of inlet 1/inlet 2 flow rate increases the magnitude of the thermopile signal as measured by area under the curve.
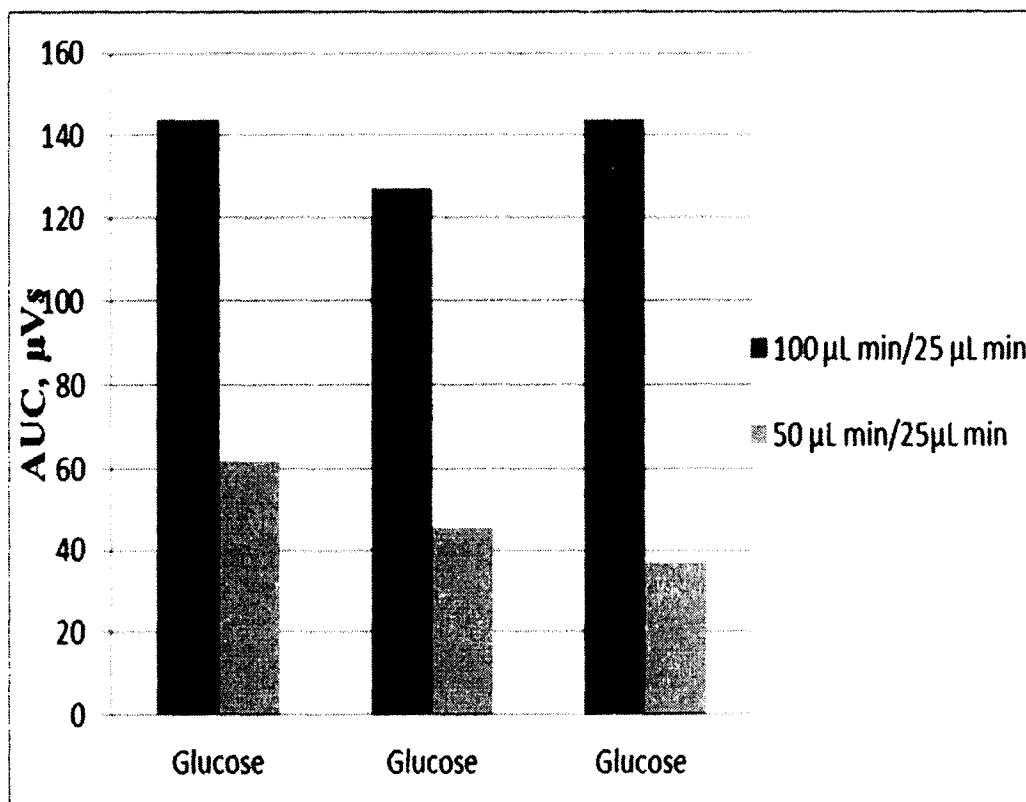
**Figure 4-12:** Peak areas after glucose (100mg dL$^{-1}$) injection when different flow rate ratio was used.

### 4.1.5.2    Effect of Reducing Flow Rate on Thermopile Response

To evaluate the effect of inlet 2 flow rate velocity on thermopile response, the flow of inlet 2 was reduced from 25µL min$^{-1}$ to 12µL min$^{-1}$. Results were obtained by measuring area under the curve for the thermopile signal after injection of glucose (100mg dL$^{-1}$) (**Figure 4-13**).
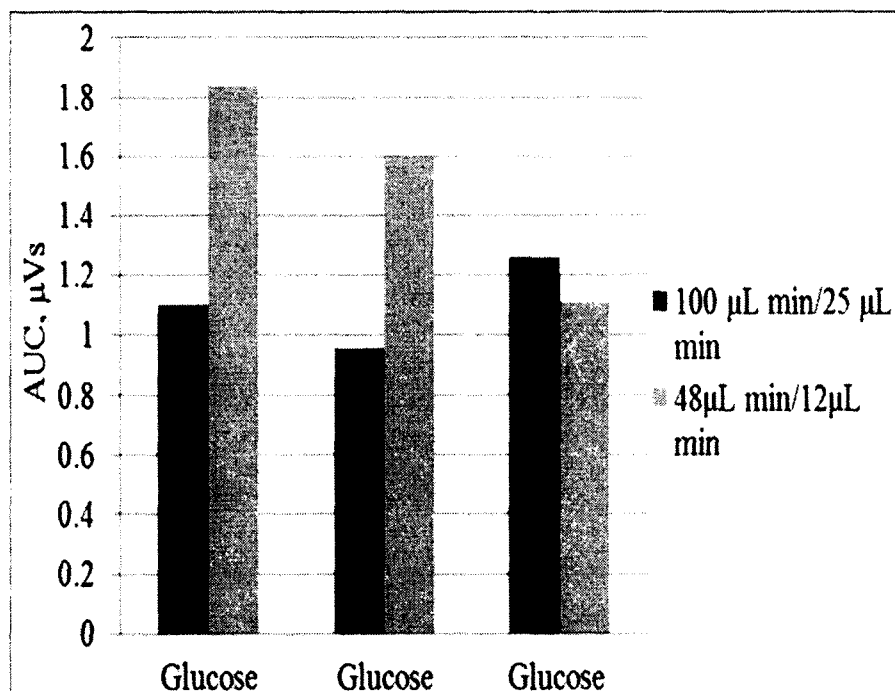
**Figure 4-13:** Peak areas after glucose (100mg dL$^{-1}$) injection when the flow rate of inlet 2 was reduced.

### 4.1.6 *Effect of Channel Geometry on Thermopile Response*

To demonstrate the effect of the microfluidic device channel geometry on the thermopile signal, several experiments were performed using hydrodynamically focused microfluidic device, single inlet channel, and three way split channel device. These experiments were performed using a microfluidic channel coated with streptavidin using the layer-by-layer method. The injection sample volume was 52µL and the concentration of glucose was 100mg dL$^{-1}$.

### 4.1.6.1 Hydrodynamically Focused Channel

The shape of the signal response was evaluated when a hydrodynamically focused microfluidic device was used to inject the substrate in the channel. The flow rates were 100µL min$^{-1}$ for inlet 1 and 25µL min$^{-1}$ for inlet 2. The response had a symmetric parabolic shape (**Figure 4-14**), which gradually increased while the substrate flowed

through the channel and gradually decreased as the heat of the chemical reaction

dissipated as the sample left the channel.
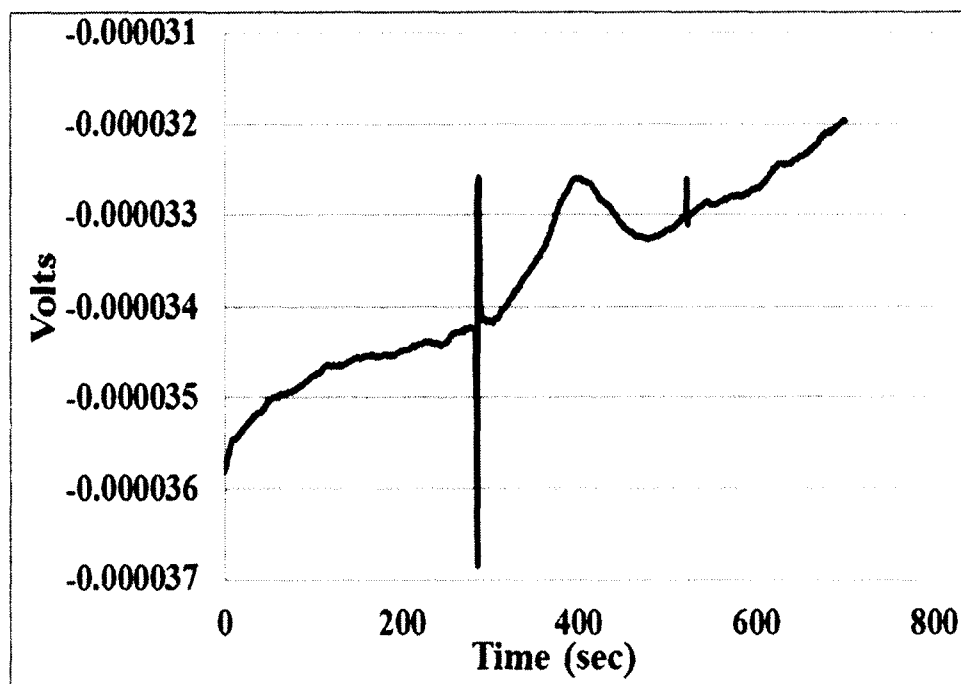


**Figure 4-14:** Signal response when glucose (100mg dL$^{-1}$) was injected in hydrodynamically focused device.

4.1.6.2    Three Split Channel Device

The three split channel device maintained the same flow rate over the measuring

and reference junctions of the thermopile (**Figure 3-8**). The response of the thermopile

was evaluated using flow rates of 25μL min$^{-1}$ in each channel. Injection of glucose into

the device using an injection valve created an artifact that affected the shape of the signal

response (**Figure 4-15**).
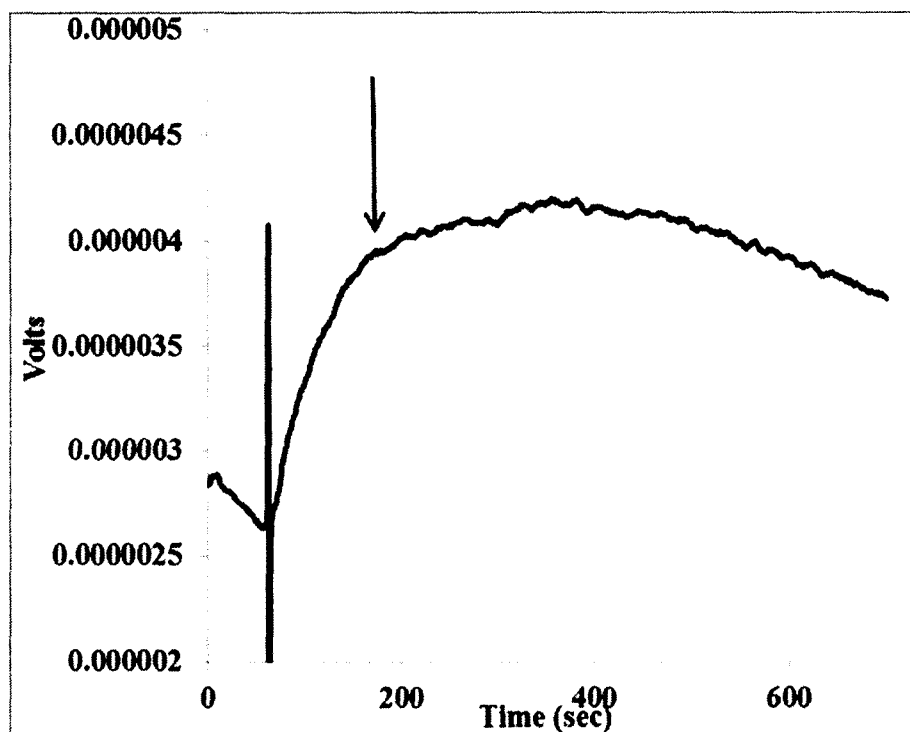
**Figure 4-15:** Signal response when glucose (100mg dL-1) was injected in three split channel device.

### 4.1.6.3    Single Inlet Device

A single inlet device was used to test the performance of the system. The flow rate over the measuring junction of the thermopile was $25\mu L$ min$^{-1}$. The reference junctions of the thermopile were positioned under the adhesive Kapton® tape and exposed to air at room temperature (**Figure 3-7**). Injection of the sample created an artifact that altered the shape of the thermopile response (**Figure 4-16**).
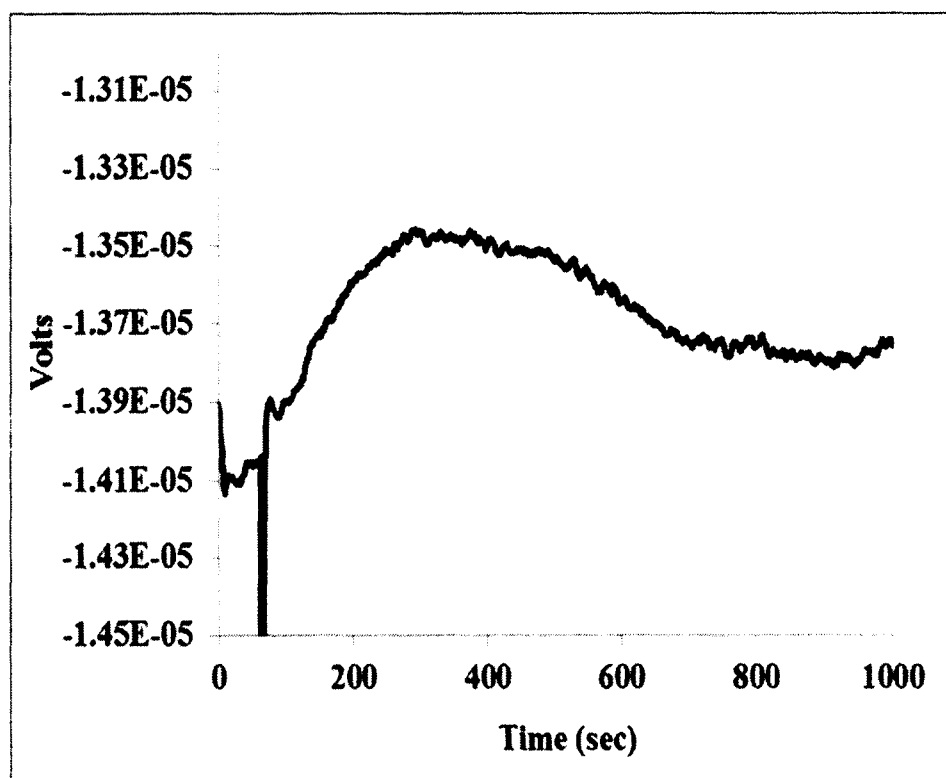
**Figure 4-16:** Signal response when glucose (100mg dL$^{-1}$) was injected in single inlet device.

4.1.7 *Effect of Aluminum Heat Sink on Thermopile Response*

The effect of a heat sink located under the reference junctions of the thermopile was evaluated in respect to the thermopile signal. An aluminum microfluidic device holder was built to form an air gap under the measuring junctions of the thermopile, while the reference junctions were in contact with the aluminum. The flow rates in these experiments were 100µL min$^{-1}$ for inlet 1 and 25µL min$^{-1}$ for inlet 2. Streptavidin was immobilized using layer-by-layer technology and the concentration of injected glucose was 100 mg dL$^{-1}$. **Figure 4-17** presents the results from the area under the curve (AUC) of the thermopile response when the reference junctions of the device were located over an aluminum heat sink and over air respectively. **Figure 4-18** shows the thermopile

response when the reference junctions of the sensor were in contact with a heat sink.

**Figure 4-19** shows the response of the sensor when the thermopile reference junctions were not in contact with a heat sink. The experiments were performed using the same microfluidic device and sensor. The results were baseline transformed using Mathlab software. The peak height when an aluminum sink was used under the junctions of the thermopile was 2.4μV. The signal was reduced to 0.65μV when the reference junctions were exposed to air.
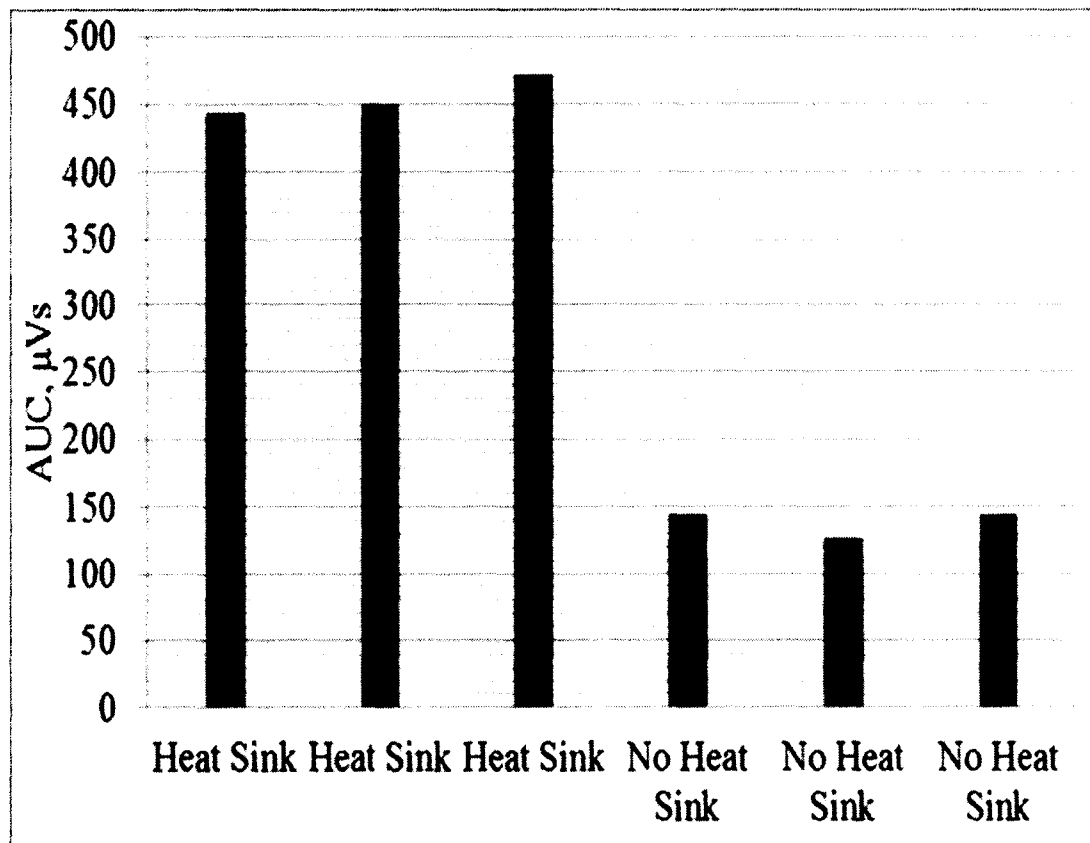


Figure 4-17: Area under the curve for thermopile response when the reference junctions were located over an aluminum heat sink and when the junctions were free standing.
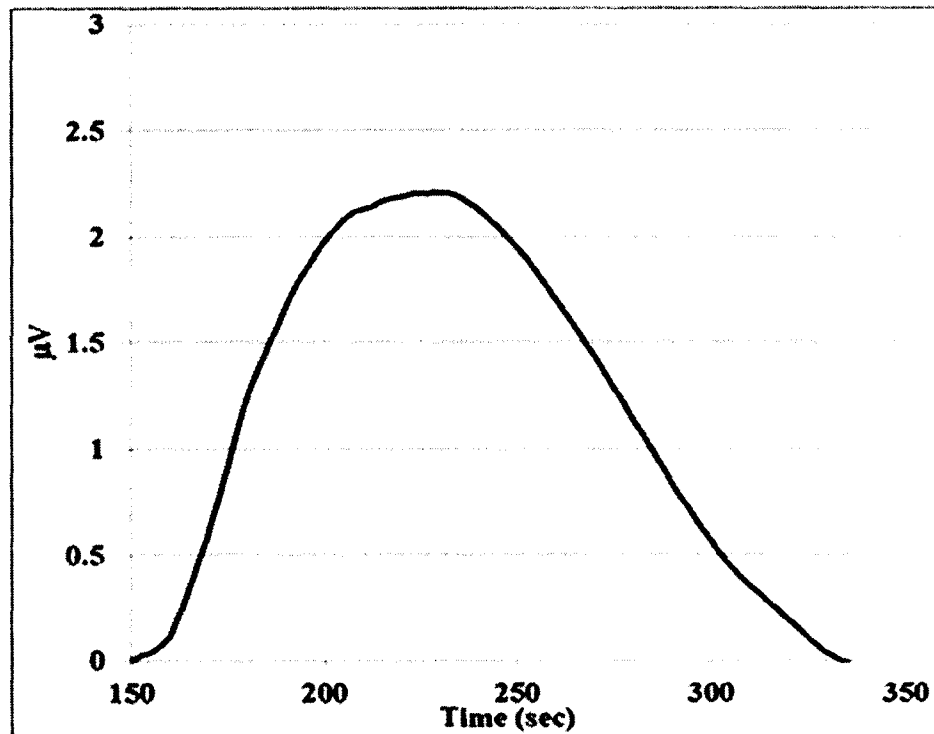
**Figure 4-18:** Thermopile response when the reference junctions were in contact with an aluminum heat sink.
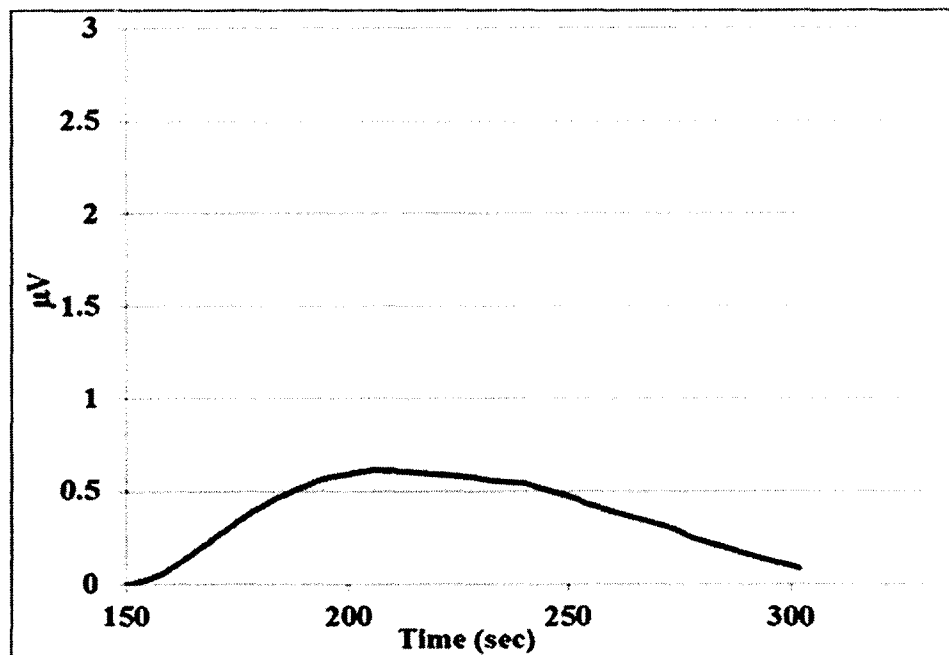


**Figure 4-19:** Thermopile response when the reference junctions were not controlled.

4.1.8     *Effect of Glucose Concentration on Thermopile Response*

Several experiments were performed to evaluate the effect of glucose

concentration on thermopile response. The concentration of the substrate was increased

from 100mg dL$^{-1}$ to 200 mg dL$^{-1}$. The flow rates in these experiments were 100μL min$^{-1}$

for inlet 1 and 25μL min$^{-1}$ for inlet 2. Streptavidin was immobilized over the lower

channel wall using layer-by-layer technology. The junctions of the thermopile were in

contact with an aluminum heat sink. Increasing the concentration of glucose from

55.5mM to 110mM did not affect thermopile response (**Figure 4-20**).
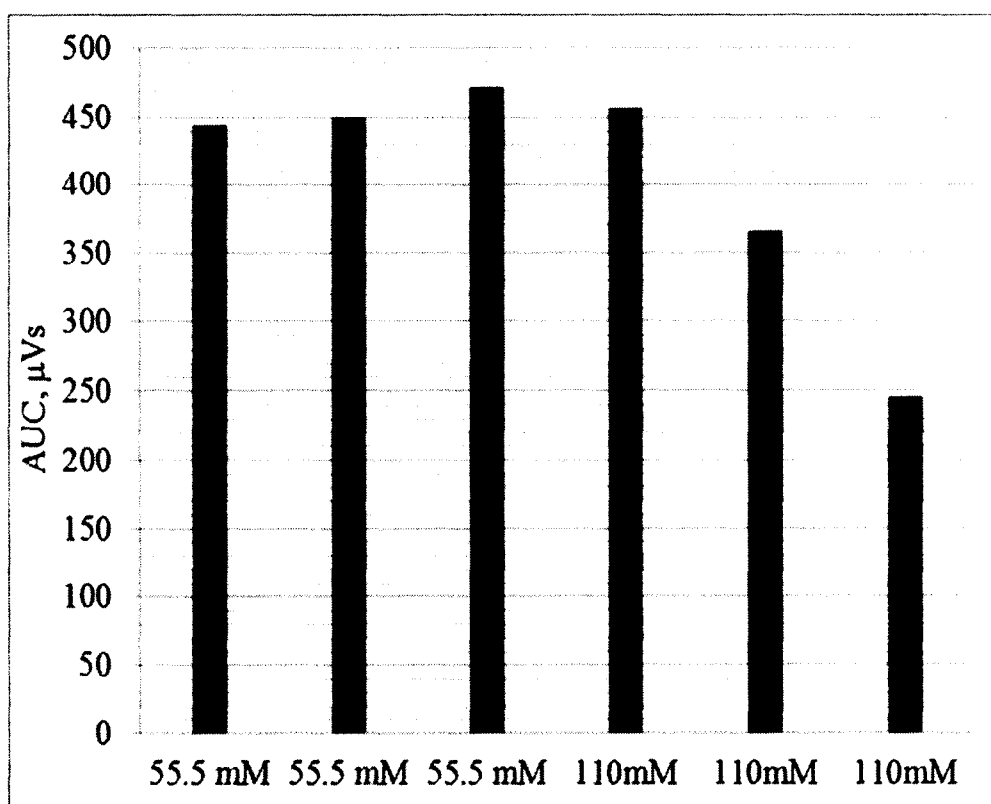


**Figure 4-20:** Area under the curve for thermopile response when 100mg dL$^{-1}$ and
200mg dL$^{-1}$ glucose concentration were used.

## 4.2    Two-dimensional Unsteady State Heat Transfer Mathematical Model

A two-dimensional unsteady state mathematical model was developed and solved

using Mathcad. The model predicts that the peak height of the thermopile response is

$2.5\mu V$ (**Figure 4-21**) and the temperature change between the measuring and the

reference junctions of the thermopile is 0.35mK (**Figure 4-22**).
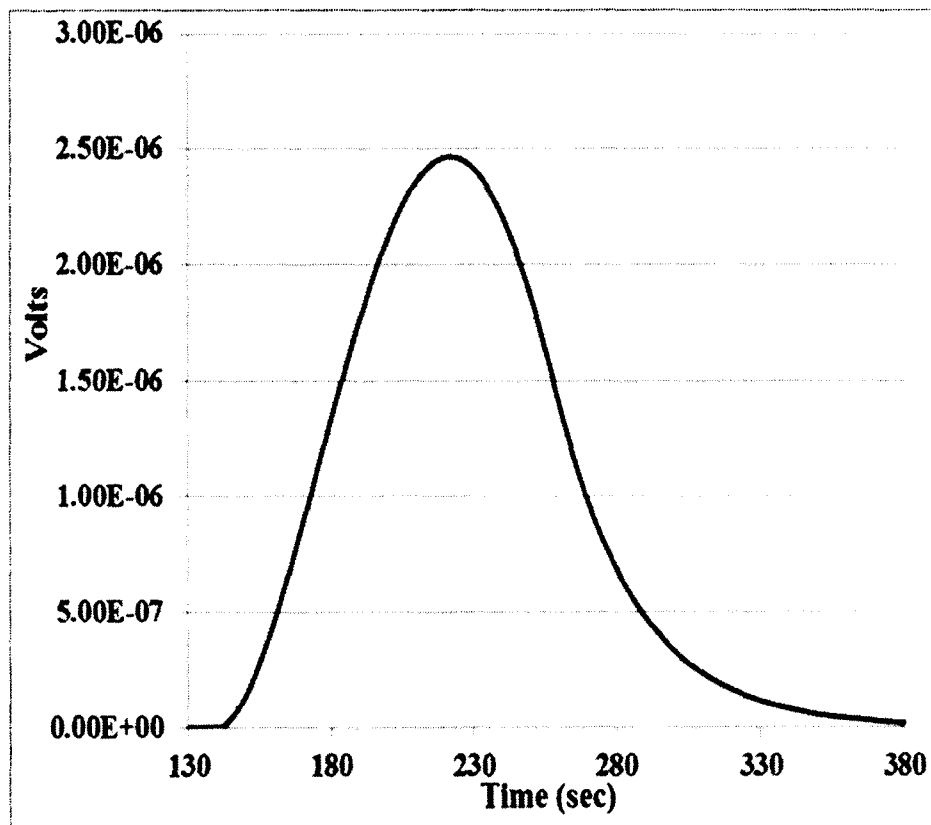


**Figure 4-21:** Predicted thermopile response.
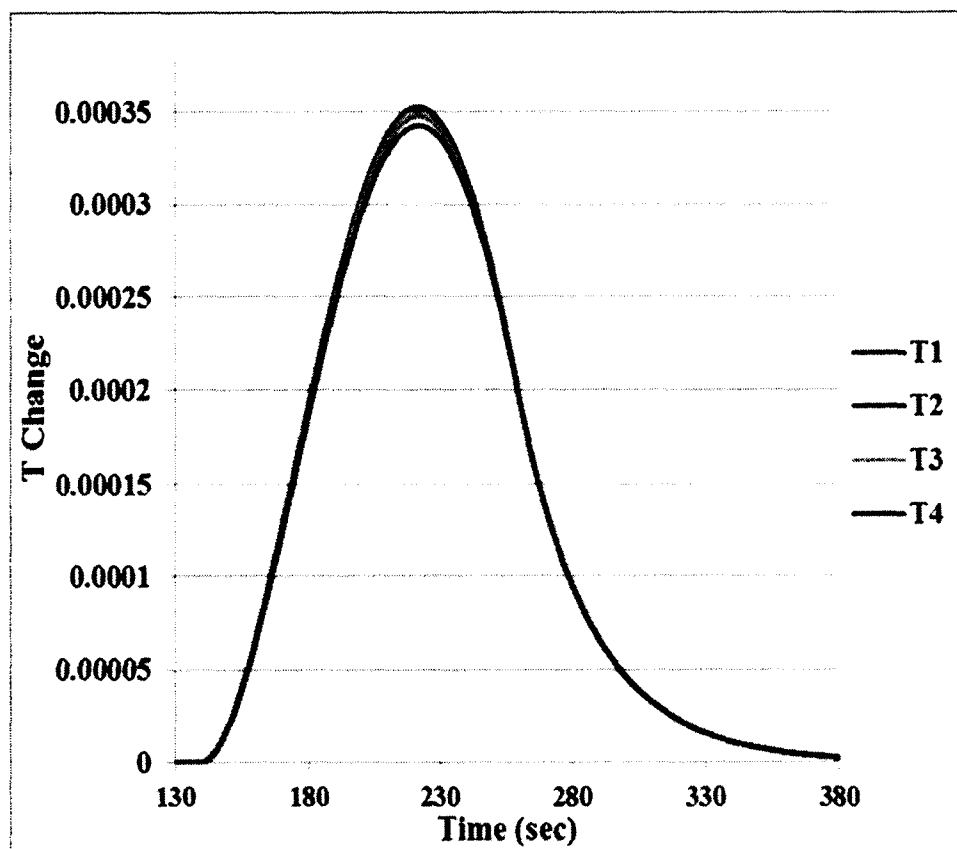
**Figure 4-22:** Temperature change for each component of the system. T1- temperature of fluid, T2-temperature of cover slip, T3-temperature of thermopile, T4-temperature of acrylic tape.

## 4.3 Solid Works Heat Transfer Simulation

Solid Works heat transfer simulations were performed to evaluate the effect of flow rate, duration of enzymatic reaction and location of the reaction zone on thermopile response.

### 4.3.1 *Location of the Reaction Zone*

Heat transfer simulations were performed where the reaction zone was located within the measuring junctions of the thermopile or along the entire length of the microfluidic device. The simulation results confirm that when the reaction occurs along

the length of the microfluidic device, the temperature of the measuring junctions of the

thermopile is increased (**Figure 4-23**, **Figure 4-24**, **Figure 4-25**, **Figure 4-26**).
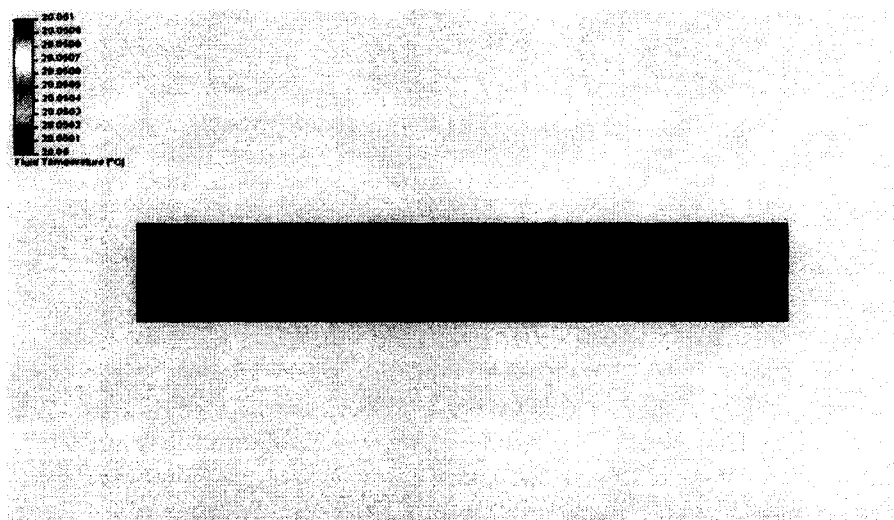


**Figure 4-23:** Fluid temperature profile top plane. Reaction zone along the length of the device.



**Figure 4-24:** Fluid temperature profile, reaction zone located within the measuring junctions of the thermopile.
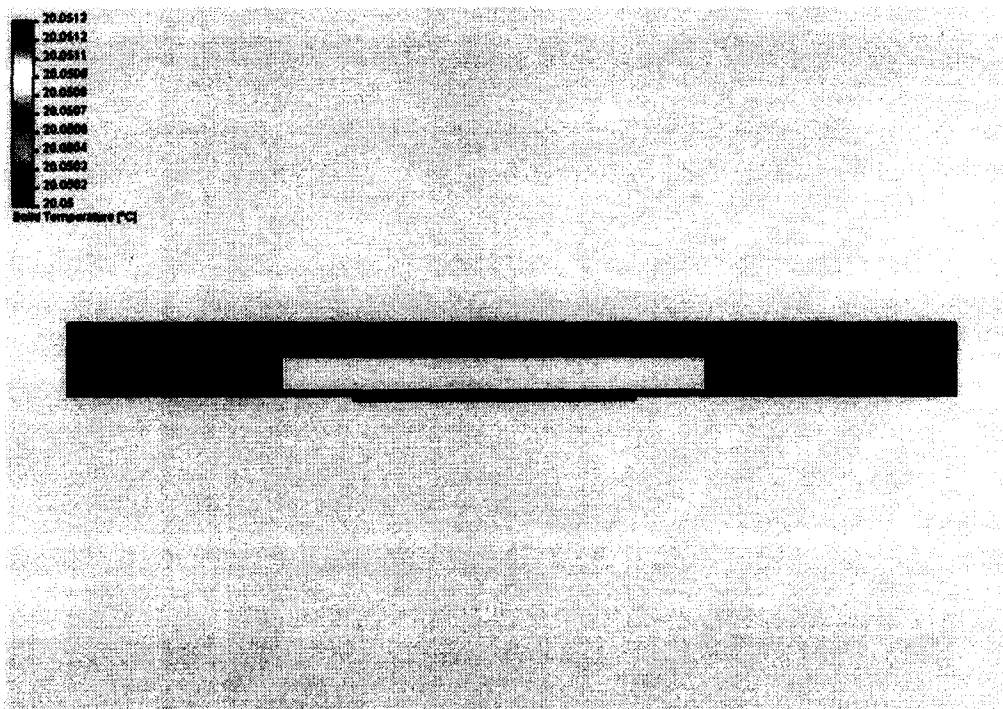
**Figure 4-25:** Temperature profile of the upper and lower channel wall, reaction zone located along the length of the channel wall.
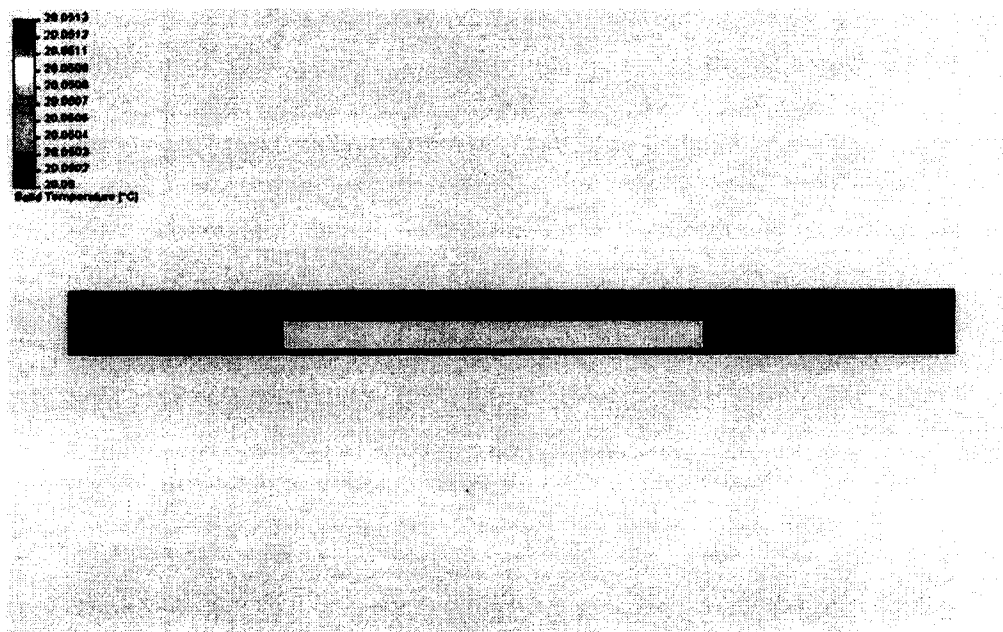


**Figure 4-26:** Temperature profile of the upper and lower channel wall, reaction zone located within the measuring junctions of the thermopile.

An XY temperature plot was constructed to display the temperature profile along

the width of the thermopile. **Figure 4-27** and **Figure 4-28** show the temperature

distribution along the thermopile in relation to the location of the heat source. When the

reaction zone was positioned within the measuring junctions of the thermopile, the

temperature difference between the reference and measuring junctions was $0.08mC°$.

When the reaction zone was located along the length of the device the temperature

difference increased to $0.11mC°$.
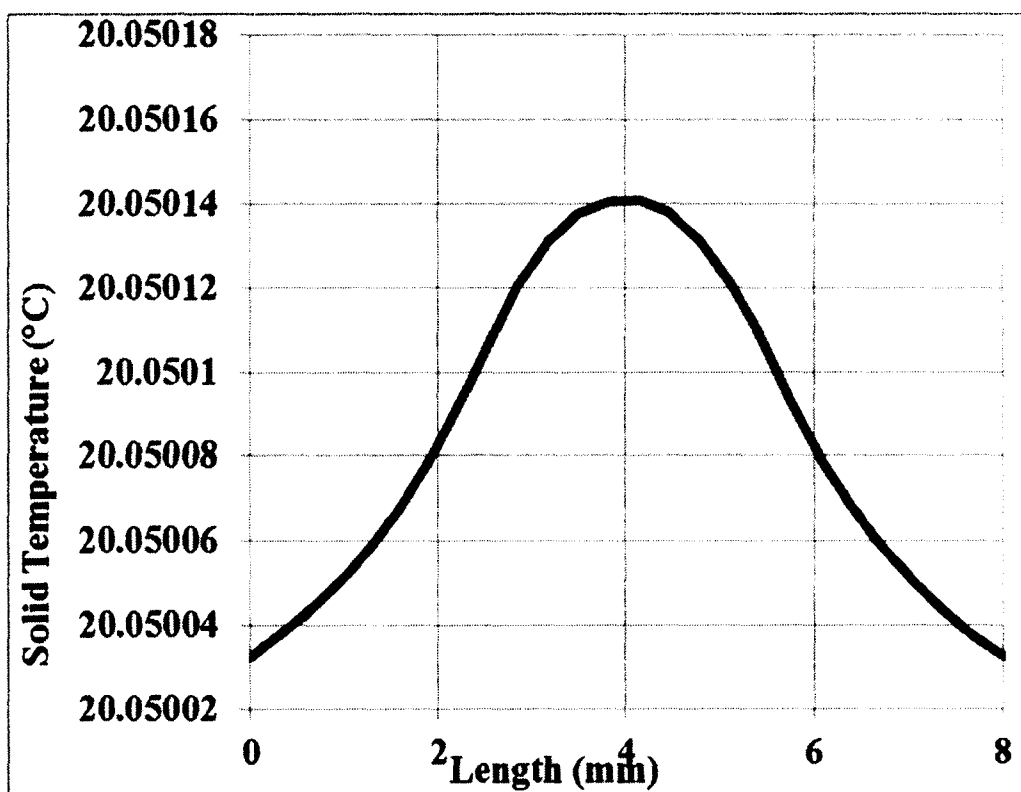


**Figure 4-27:** Temperature profile across the width of the thermopile. Reaction zone located along the length of the device.
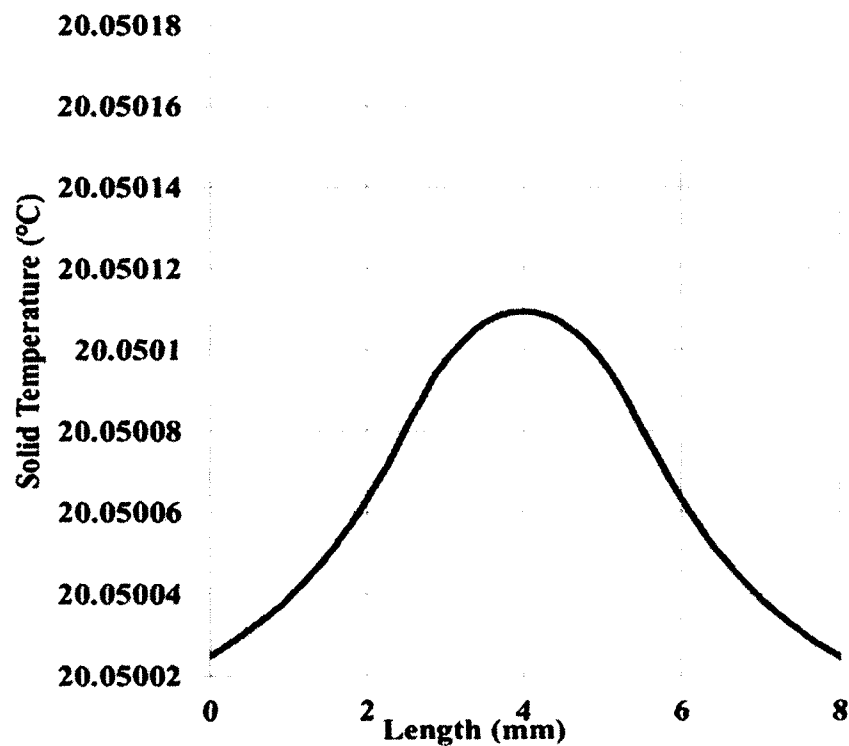
**Figure 4-28:** Temperature profile across the width of the thermopile. Reaction zone located within the measuring junctions of the thermopile.

4.3.2    *Effect of Flow Rate on Thermopile Response*

Time-dependent Solid Works simulations were performed to evaluate the effect of flow rate on thermopile response. The simulations were performed for 120 seconds of the enzymatic reaction. The flow rate of inlet 2 was maintained constant at $25\mu L$ $min^{-1}$ while the flow rate of inlet 1 was either $100\mu L$ $min^{-1}$ or $50\mu L$ $min^{-1}$. **Figure 4-29** and **Figure 4-30** show the temperature distribution in the fluid.
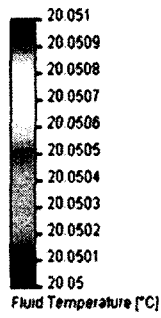
**Figure 4-29:** Fluid temperature distribution. Inlet 1 flow rate 100μL min⁻¹, inlet 2 flow rate 25μL min⁻¹.



**Figure 4-30:** Fluid temperature distribution. Inlet 1 flow rate 50μL min⁻¹, inlet 2 flow rate 25μL min⁻¹.

Figure 4-31 and Figure 4-32 show the temperature profile across the thermopile.

The temperature change between the measuring and reference junctions of the thermopile

was 0.1°mC when the flow rate of inlet 1 was 100µL min⁻¹. When the flow rate of inlet 1

was decreased to 50µL min⁻¹, the temperature difference decreased to 0.08°mC due to

increased heating of the sensor reference junctions.
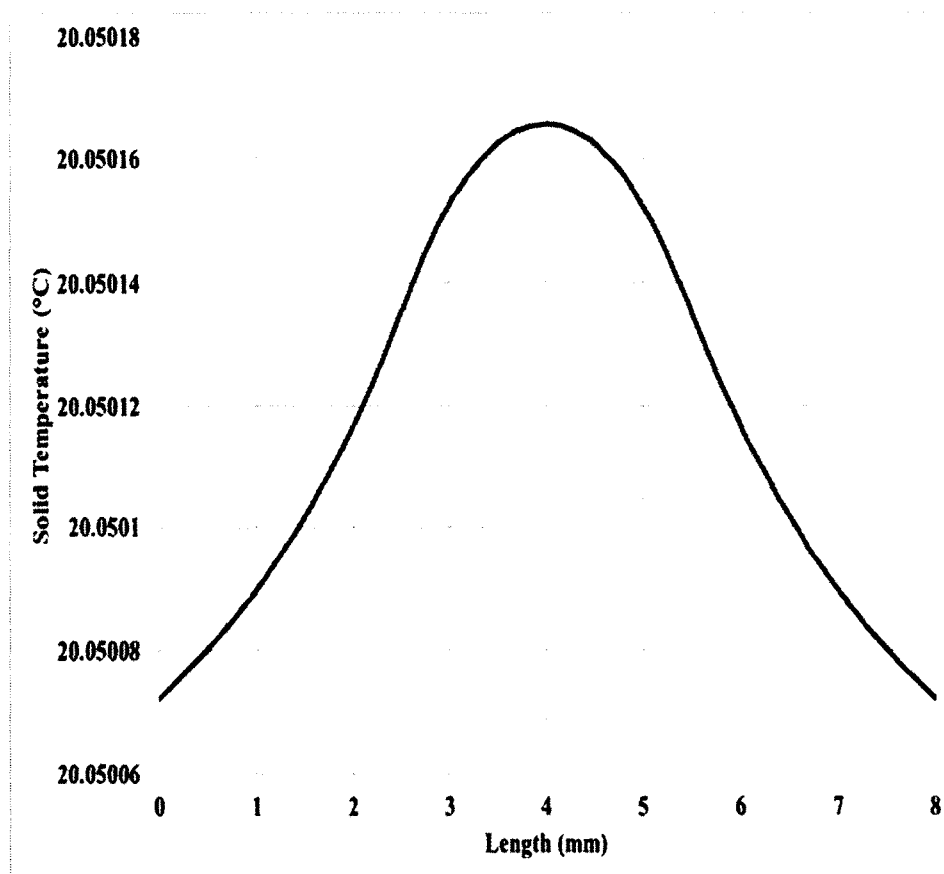


Figure 4-31: Temperature profile across the thermopile. Inlet 1 flow rate 100µL
min⁻¹, inlet 2 flow rate 25µL min-1.

**Figure 4-32:** Temperature profile across the thermopile. Inlet 1 flow rate $50\mu L$ min$^{-1}$, inlet 2 flow rate $25\mu L$ min$^{-1}$.

### 4.3.3    *Effect of Duration of Enzymatic Reaction on Thermopile Response*

Time dependent SolidWorks simulations were performed for 120 and 30 seconds durations of the enzymatic reaction. **Figure 4-33** and **Figure 4-34** show the temperature profile in the fluid. When the enzymatic reaction preceded for 30 seconds, the temperature change between the reference and measuring junctions of the thermopile was $0.08°mC$ (**Figure 4-35**).The predicted thermopile output was 576nV. The thermal difference between the junctions of the sensor increased to $0.1°mC$ when the duration of the reaction increased to 120 seconds (**Figure 4-36**). The predicted thermopile output was 720µV.
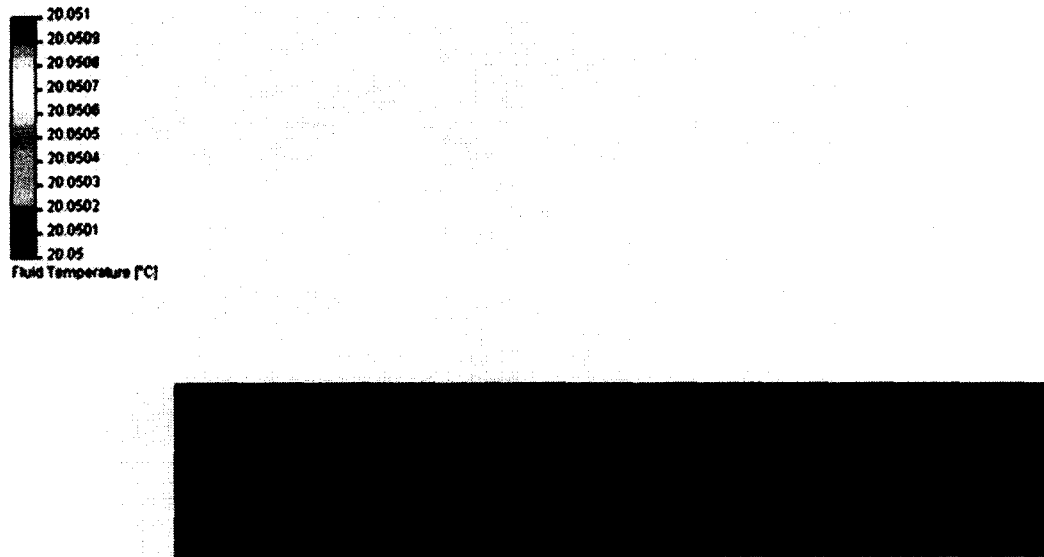
**Figure 4-33:** Temperature distribution in the fluid. Time dependent simulations for 30 seconds.



**Figure 4-34:** Temperature distribution in the fluid. Time dependent simulations for 120 seconds.
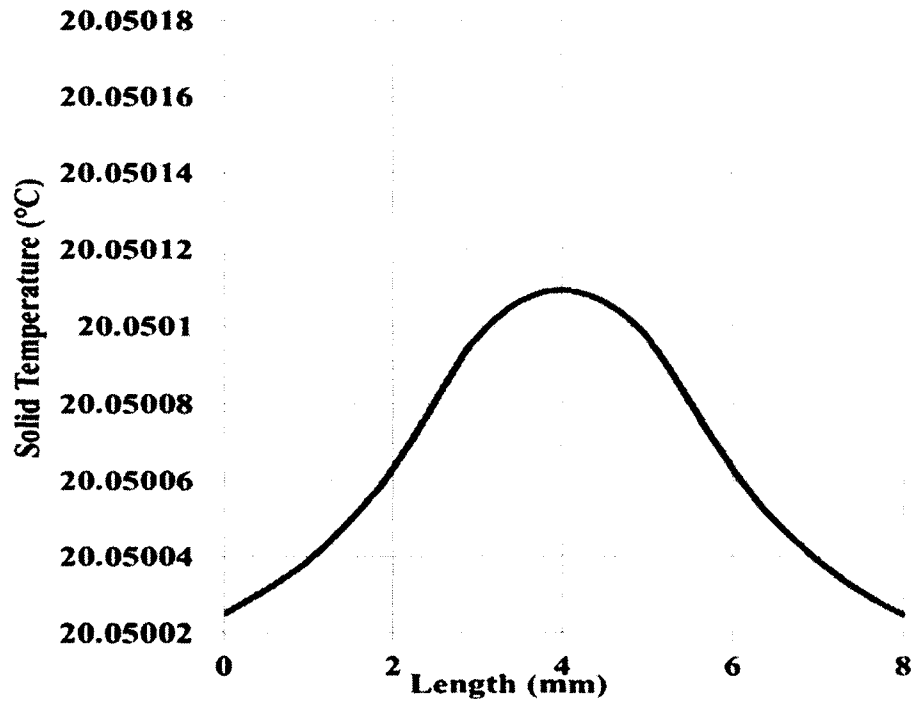
**Figure 4-35:** Thermopile temperature profile, 30 second duration of enzymatic reaction.
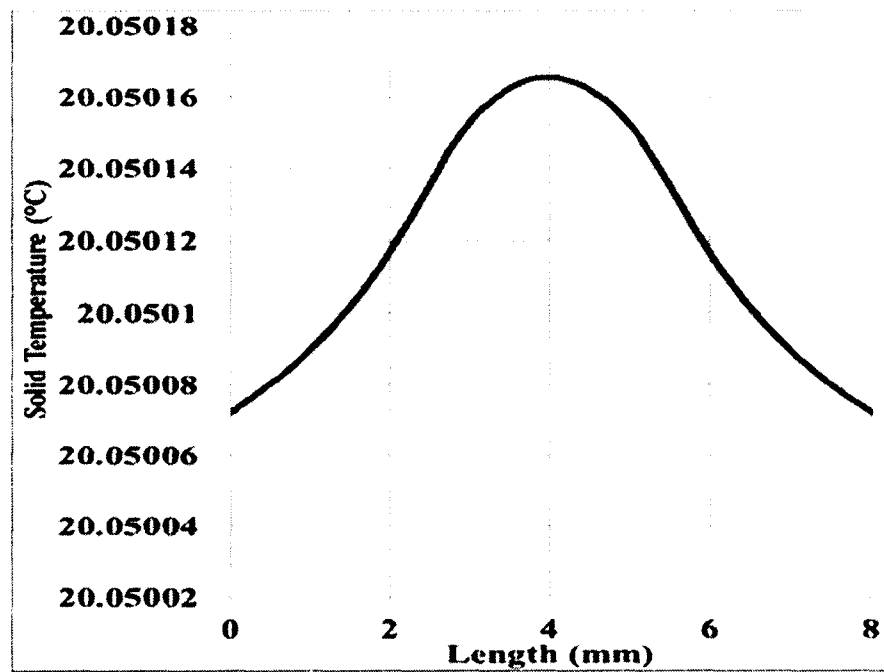


**Figure 4-36:** Thermopile temperature profile, 120 second duration of the enzymatic reaction.

## 4.4    Standard Curve

A standard calibration curve was generated for the range of 0-10µM concentration

of 8OHdG by plotting the concentration of 8OHdG versus the average area under the

curve of the thermoelectric signal corresponding to each concentration (**Figure 4-37**).

The R square value of the linear fit was 0.9148. The magnitude of the thermopile output

was inversely proportional to the concentration of 8OHdG.
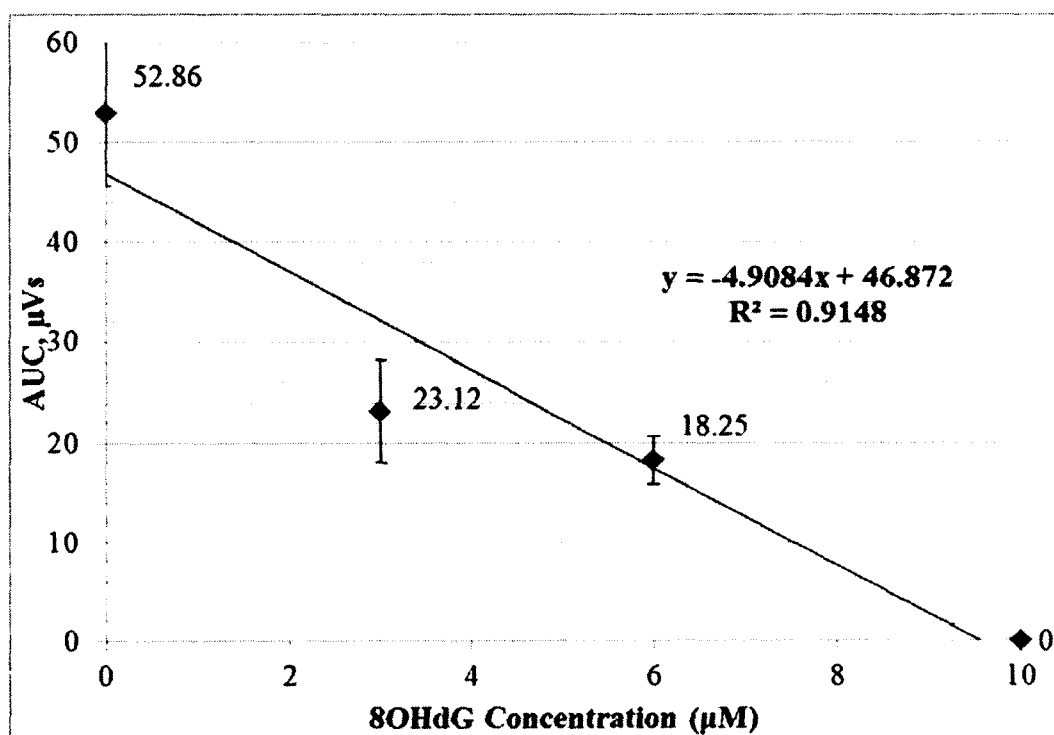


**Figure 4-37**: Standard calibration curve, 8OHdG concentration range 0-10µM.

The average area under the curve and the standard error within the experiments

for each data point are presented in **Table 4-1**.

**Table 4-1:** Area under the curve and standard error within the same device.

| Concentration 8OHdG | Average AUC | Standard Error |
|---|---|---|
| 0 μM | 64.7 μVs | 3.24 |
| 0 μM | 46.4 μVs | 14.86 |
| 0 μM | 47.5 μVs | 3.7 |
| 3 μM | 27.7 μVs | 4.8 |
| 3 μM | 28.5 μVs | 9.7 |
| 3 μM | 13.3 μVs | 1 |
| 6 μM | 15.2 μVs | 2.4 |
| 6 μM | 19.8 μVs | 1.44 |
| 6 μM | 19.75 μVs | 3.34 |
| 10 μM | 0 μVs | 0 |
| 10 μM | 0 μVs | 0 |
| 10 μM | 0 μVs | 0 |

The average of three experiments for each concentration of 8OHdG was plotted to create the standard calibration curve. The results for average area under the curve for each concentration of 8OHdG as well as the standard error between experiments are shown in **Table 4-2**. The standard error between experiments decreases as the magnitude of the signal decreases.

**Table 4-2:** Average AUC for 8OHdG calibration curve and standard error between devices.

| Concentration of 8OHdG | Average AUC | Standard Error |
|---|---|---|
| 0 μM | 52.86 μVs | 7.26 μVs |
| 3 μM | 23.12 μVs | 5.1 μVs |
| 6 μM | 18.25 μVs | 2.4 μVs |
| 10 μM | 0 μVs | 0 μVs |

## 4.5    8OHdG Detection in Mouse Urine

The concentration of 8OHdG in urine samples from three different APP

transgenic mice was measured and quantified using thermoelectric ELISA. **Figure 4-38**

shows a thermoelectric signal obtained when the concentration of 8OHdG was measured

in the biological samples. The thermoelectric signal was baseline transformed using

MATLAB for accurate measurement of the peak height. The duration of the signal was

120 seconds and the peak height of the signal was 400nV.
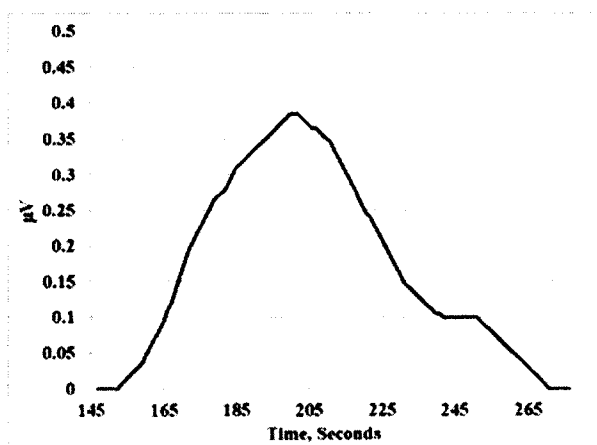


**Figure 4-38:** Thermoelectric signal when the concentration of 8OHdG was measured in mouse urine.

The concentration of 8OHdG was measured in three urine samples from different APP transgenic mice. The area under the curve for each measurement, as well as the average, standard deviation, and standard error within each experiment are presented in **Table 4-3**. The concentration of 8OHdG in each sample was respectively 2.25, 1.87, and 3.94µM. The average concentration of 8OHdG in each urine sample is shown in **Figure 4-39**.

**Table 4-3:** Concentration of 8OHdG in mouse urine samples.

|  | Urine Sample 1 | Urine Sample 2 | Urine Sample 3 |
|---|---|---|---|
| Measurement 1 | 30 µVs | 40.9 µVs | 22 µVs |
| Measurement 2 | 44.8 µVs | 56.2 µVs | 35.4 µVs |
| Measurement 3 | 32.6 µVs | 16 µVs | 25.2 µVs |
| Average AUC | 35.8 µVs | 37.7 µVs | 27.53 µVs |
| Standard Deviation | 7.9 | 20.3 | 6.99 |
| Standard Error | 4.57 | 11.73 | 4.04 |
| **Concentration of 8OHdG** | **2.25 µM** | **1.87µM** | **3.94 µM** |
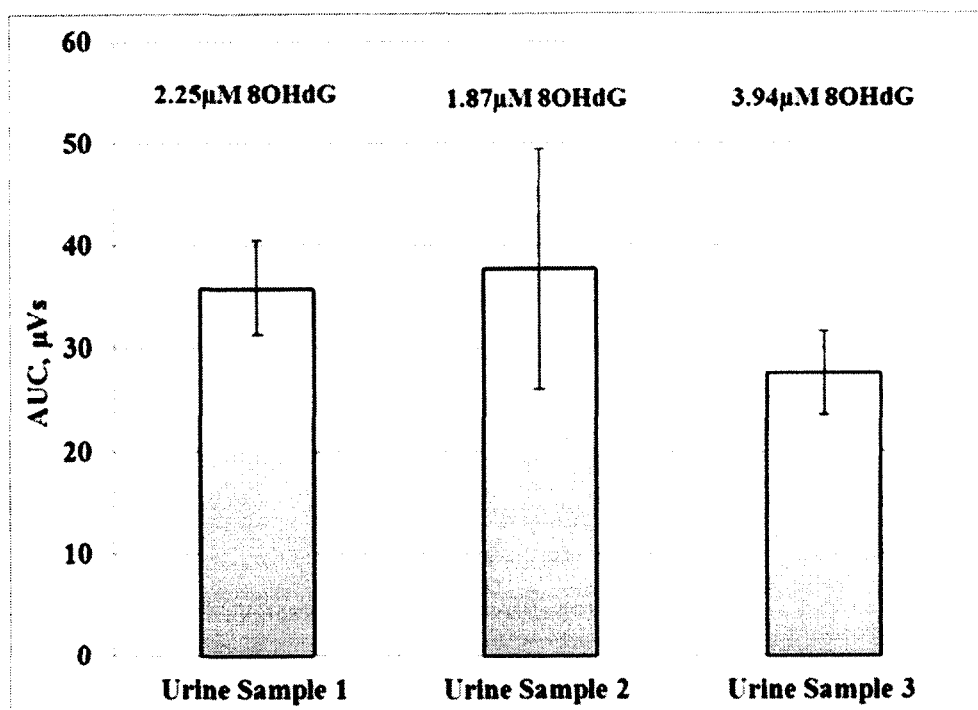
**Figure 4-39:** 8OHdG concentration in mouse urine.

# CHAPTER 5

# DISCUSSION

## 5.1    Advantages of Thermoelectric ELISA

Current methods for detection of 8OHdG include mass spectrometry, capillary

electrophoresis, ELISA, and HPLC. These technologies are limited by high cost, complex

chemistry and sample purification procedures, as well as the need for highly trained

personnel to operate the instruments.

The proposed thermoelectric method for detection and quantification of 8OHdG

simplifies the detection chemistry, and replaces expensive instruments with simple,

inexpensive voltage meters and a compact, inexpensive microfluidic chip with an

integrated thermoelectric sensor. In addition to reducing the cost and complexity of the

instrument, performing thermoelectric ELISA in a microfluidic device decreases the cost

of the reagents and the amount of sample that is used for the assay. Performing ELISA in

a microfluidic device also decreases the time for the incubation steps by increasing the

mass transfer rate of the analyte. In addition, performing the assay under flow conditions

eliminates the washing protocol between the incubation steps that is required when

performing traditional ELISA in a microwell plate.

The applications of thermoelectric ELISA are not limited to quantification and

detection of 8OHdG. Thermoelectric ELISA overcomes many of the drawbacks of other

ELISA methods by providing a simple, inexpensive way for rapid determination of the

concentration of an analyte (antigen or an antibody specific antigen) under laminar flow conditions. Current methods for performing ELISA require expensive absorbance, luminescent or florescent plate reader instruments.

ELISA tests are currently performed in a 96 microwell plate using a significant amount of precious biological sample reagents. The thermoelectric method overcomes these challenges by performing the test in a microfluidic device. In addition to reducing the cost and complexity of the instrument, performing thermoelectric ELISA in a microfluidic device decreases the cost of reagents and the amount of sample that is used for the assay.

A drawback related to the current methods for performing ELISA is the high background noise due to insufficient washing of plates or non-specific binding of enzyme-conjugated antibodies to the bottom of the plate. Because the thermoelectric method is a flow through system, the excess antibodies and /or antigens are completely removed from the microfluidic system prior to the enzymatic detection step. In addition, performing the assay under flow conditions eliminates the washing protocol between the incubation steps that is required when performing the assay in a microwell plate.

Another issue related to the colorimetric detection method for ELISA is caused by the fast reaction between the enzyme and substrate that requires reading of the sample to be performed quickly. In addition, incubation of the substrate has to be carried out in the dark. All of these obstacles are eliminated by the thermoelectric method as the reaction between the enzyme and substrate is not affected by light and timing. In addition, the substrate can be introduced multiple times after the thermoelectric signal returns to baseline level. Multiple data points for the same sample can be obtained to increase

statistical significance and minimize variation in the ELISA detection method. Multiple

data points cannot be obtained using the colorimetric method because once the color is

developed the sample cannot be read again.

Another advantage of the thermoelectric method is that it can be performed using

a number of different enzymes since the method is based on detection of the enthalpy of

the enzymatic reaction.

## 5.2    Heat Transfer Mathematical Model

The unsteady state mathematical model assumes that there is no lateral heat

dissipation towards the reference junctions of the thermopile. The predicted thermopile

signal correlates well with the experimental results obtained when the reference junctions

of the thermopile were positioned over a heat sink. Under those experimental conditions,

the heat that dissipated towards the reference junctions of the thermopile is transferred

towards the aluminum heat sink. As a result, the reference junctions of the thermopile are

under constant temperature control. The temperature difference between the reference

and the measuring junction is higher when compared to the results when the reference

junctions are not under temperature control (**Figure 4-18** and **Figure 4-19**). The

mathematical model predicted that the peak height of the thermopile response was 2.5μV

(**Figure 4-21**) while the experimental results confirm that the signal response was 2.4μV.

The duration of the predicted response was 230 seconds while the duration of the actual

response was 180 seconds. The values of the predicted and the experimental values for

the peak height of the signal are close, confirming the accuracy of the mathematical

model to simulate heat transfer and thermopile temperature change in a microfluidic

device.

## 5.3     Heat Transfer Simulation using SolidWorks

Heat transfer simulations using SolidWorks confirm that the location and size of the reaction zone, the duration of the enzymatic reaction and the velocity of the fluid have measurable effects on thermopile response.

Increasing the size of the reaction zone, by positioning it along the length of the lower channel wall increased the thermopile output. When the reaction occurred within the measuring junctions of the thermopile, the predicted temperature difference between the measuring and the reference junctions was 0.08°mC that corresponds to thermopile output of 576nV (**Figure 4-27**). When the reaction zone was positioned along the length of the lower channel wall, the temperature difference increased to 0.11°mC and the predicted thermopile output increased to 792nV (**Figure 4-28**). The increase in the temperature difference between the measuring and the reference junctions was not significant. This could be caused by loss of thermal energy upstream of the thermopile.

Changing the velocity of the fluid and the ratio of the flow rates affected the response of the thermopile. Increasing the flow rate of inlet 1 from 50μL min$^{-1}$ to 100μL min$^{-1}$ increased the magnitude of the signal detected by the thermopile. When the flow rate of inlet 1 was 100μL min$^{-1}$, the temperature difference between the junctions of the thermopile was 0.1°mC corresponding to 720nV thermopile output (**Figure 4-31**). The temperature difference decreased to 0.08°mC corresponding to 576nV thermopile signal, when the flow rate of inlet 1 was reduced to 50μL min$^{-1}$. The temperature of the measuring junction is the same under both conditions (20.05019K) confirming that increasing the flow rate of inlet 1 did not affect the amount of thermal energy that was detected by the thermopile (**Figure 4-31** and **Figure 4-32**). The difference of the

thermopile output is caused by the different amount of thermal energy that dissipated laterally to the reference junctions of the thermopile. Changing the flow rate of inlet 1 affects the width of the hydrodynamically focused reaction zone within the measuring junctions of the thermopile. Increasing the flow rate of inlet 1 decreased the width of the reaction zone an as result the transfer of thermal energy to the reference junctions of the thermopile.

Simulations were performed to evaluate the effect of the duration of the enzymatic reaction on the thermopile output. The simulation results show that the temperature difference was $0.08°mC$ when the enzymatic reaction proceeded for 30 seconds. This temperature difference corresponds to a thermopile output of 576nV. Increasing the duration of the enzymatic reaction increased the total amount of heat that was detected by the thermopile as well as the heat that dissipated laterally to the reference junctions of the sensor. The temperature difference between the measuring and the reference junctions of the thermopile increased to $0.1°mC$ corresponding to a thermopile output of 720nV.

## 5.4    Microfluidic Device Parameter Optimization

Several factors can affect the accuracy and magnitude of the thermoelectric ELISA signal. These factors include noise level, data acquisition system, flow rate, microfluidic device design, and temperature control of the reference junctions of the thermopile.

Nonspecific signals associated with introduction of glucose into the microfluidic device were detected by the thermopile. These nonspecific signals were observed when the microfluidic chip was positioned in a plastic holder. The nonspecific noise was

eliminated when the microfluidic chip was placed in an aluminum holder (**Figure 4-2**). The aluminum acts as a heat sink that is in contact with the lower microfluidic channel upstream of the area of the thermopile. The aluminum absorbed the non-specific heat that is released during the random events associated with introduction of glucose in the microfluidic device, completely eliminated the nonspecific noise and improved the accuracy of the measurement system. The nonspecific heat could be caused by mixing glucose with the buffers or a non-specific interaction between glucose and the walls of the microfluidic chip when the sample enters the device.

The performance of the thermoelectric system was evaluated according to the data acquisition system that was used to collect and record that signal from the thermopile. The average noise level when the experiments were performed using an Agilent nanovolt meter was up to 10nV. The amplifier increased the electrical noise in the system up to 300nV. The increase in the noise level in the system is caused by the higher sampling rate of the amplifier. The sampling rate of the nanovolt meter was 1 point per second, while the amplifier collected data of 100 points per second. Different sampling rates had an effect on the shape of the response.

The total amount of heat detected by the thermopile was higher when commercially prepared streptavidin coverslips were used instead of coverslips coated with streptavidin using layer-by-layer technology (**Figure 4-7**). In addition, peak height of the signal response also decreased when the streptavidin was immobilized using the layer-by-layer method (**Figure 4-8** and **Figure 4-9**). The amount of heat that was generated during a glucose oxidation event is proportional to the amount of glucose enzyme immobilized over the measuring junctions of the thermopile. The higher amount

of heat that is detected by the thermopile when commercially supplied coverslips were used implies that layer-by-layer technology yields lower loading capacity for streptavidin when compared to the technology that Xenopore Corp., uses to immobilize streptavidin. However, the signal decrease is not significant enough to affect the quality and feasibility of the test. In addition, the cost of preparing in-house streptavidin coated coverslips is lower when compared to obtaining them from an outside vendor. The magnitude of the signal can be increased by adding more layers of polyelectrolytes to provide more reaction sites for streptavidin immobilization.

Increasing the sample injection volume from 13 $\mu$L to 52 $\mu$L increases the total amount of heat that is generated by the reaction, the duration of the thermopile response and the magnitude of the thermopile response peak height (**Figure 4-10**). Increasing the sample volume increases the reaction time, resulting in more substrate available for oxidation that leads to an increase in reaction heat. Because more heat is generated, it takes longer for the generated heat to dissipate. As a result, the duration of the thermopile response increases from an average of 90 seconds to an average of 180 seconds. The rate of heat dissipation can be increased by increasing flow rate, but at the expense of signal strength.

The fluid velocity and the ratio of inlet 1/inlet 2 flow rates had a significant effect on the thermopile signal. The flow rate ratio affects the width of the hydrodynamically focused area within the measuring junctions of the thermopile. Changing the ratio of the flow rates from 1:2 to 1:4 decreases the width of the hydrodynamically focused fluid stream and the amount of heat that dissipates towards the reference junctions of the thermopile. The lateral heat dissipation affects the temperature difference between the

measuring and reference junctions of the thermopile. When the ratio of the flow rates of inlet 1: inlet 2 is 1:4, the difference in the temperature between measuring and reference junction of the thermopile is higher and results in faster thermopile response. Reducing the flow rate of inlet 2, while keeping the flow rates ratio to 1:4, increases the magnitude of the signal detected by the thermopile. This is caused by a combination of two factors. Lower flow rate allows for longer time of diffusion of the substrate to the lower channel wall and as a result more glucose molecules react with the enzyme. In addition, reducing the flow rate increased the duration of the signal that results in a larger area under the curve response of the thermopile (**Figure 4-13**).

The channel geometry of the microfluidic device had a significant effect on thermopile response. When a hydrodynamically focused microfluidic chip was used to measure the heat of the enzymatic reaction between glucose and glucose oxidase, the signal response was parabolic and symmetric (**Figure 4-14**). When a split three channel device was used, a significant artifact associated with the injection was observed. This was caused by a significant pressure drop associated with the injection of sample. The change in the pressure was higher since the dimension of the channel over the thermopile is narrower when compared to the hydrodynamically focused device (**Figure 4-15**). The same injection artifact was observed when a single inlet device was used, confirming the correlation between these artifacts and the dimensions of the channel (**Figure 4-16**). The reference junctions of the thermopile in the single inlet design were exposed to air and fluctuations in the ambient temperature, and as result there was more instability and variation in the baseline and the thermopile output. The reference junctions of the three

channel split design and the hydrodynamically focused device were exposed to both air and fluid and as a result the temperature fluctuations were reduced.

Positioning of the reference junctions of the thermopile over a heat sink had a significant impact on the magnitude of the signal output. An aluminum heat sink absorbs the heat that dissipates towards the reference junctions of the thermopile and provides constant control of the reference junctions. In addition, the start and end points of the signal response were easily detected, improving the accuracy in determining the duration and magnitude of the signal. Since the reference junctions are maintained at a constant temperature, the temperature difference depends only on the temperature increase of the measuring junction. When the reference junctions are not positioned over a heat sink, some of the reaction heat dissipates towards the reference junctions reducing the temperature difference between both junctions and the thermoelectric output. The signal obtained using the same device under the same experimental conditions affected the thermoelectric signal. The signal response was $2.4\mu V$ when the junctions of the thermopile were positioned over a heat sink and decreased to $650nV$ when the reference junctions were in contact with the air.

Changing glucose concentration from 100mg dL$^{-1}$ to 200mg dL$^{-1}$ did not have an effect on thermopile output (**Figure 4-20**) for concentrations below 100mM. The decrease at higher concentrations is probably due to oxygen limiting the enzymatic reaction. Since oxygen is one of the reactants that would limit the reaction, increasing the concentration of the reactants would not have an effect on the output of the thermopile since the other co-reactant oxygen is not increased. Another factor that could explain this observation is diffusion limitations. When the amount of glucose that is oxidized by the

enzyme at the surface of the device is limited by diffusion, increasing the concentration of the substrate will not change the amount that would reach the surface.

The reproducibility of thermoelectric ELISA depends on several other factors. These factors include: the amount of enzyme attached to the surface of the microfluidic device, the efficiency of the antibody/antigen binding and the Seebeck coefficient of the thermopile

## 5.5    Thermoelectric ELISA Standard Curve Generation

The magnitude of the thermoelectric response was inversely proportional to the concentration of 8OHdG in the mouse urine samples. The $r^2$ value for the standard calibration curve was 0.9148, indicating a good fit of the data points of the graphs to a straight line. The equation that describes the linear response shows that the upper limit of the thermopile signal was 46.87$\mu$V. This value for the AUC corresponds to a concentration of 10$\mu$M of 8OHdG in a biological sample.

The AUC of the thermoelectric response decreases as the concentration of the analyte increases. There are two possible mechanisms that can explain the reduction of the thermoelectric response. Increased levels of 8OHdG affect the efficiency of binding between the primary and the secondary antibody. As a result the concentration of the surface immobilized enzyme is reduced (**Figure 5-1**).
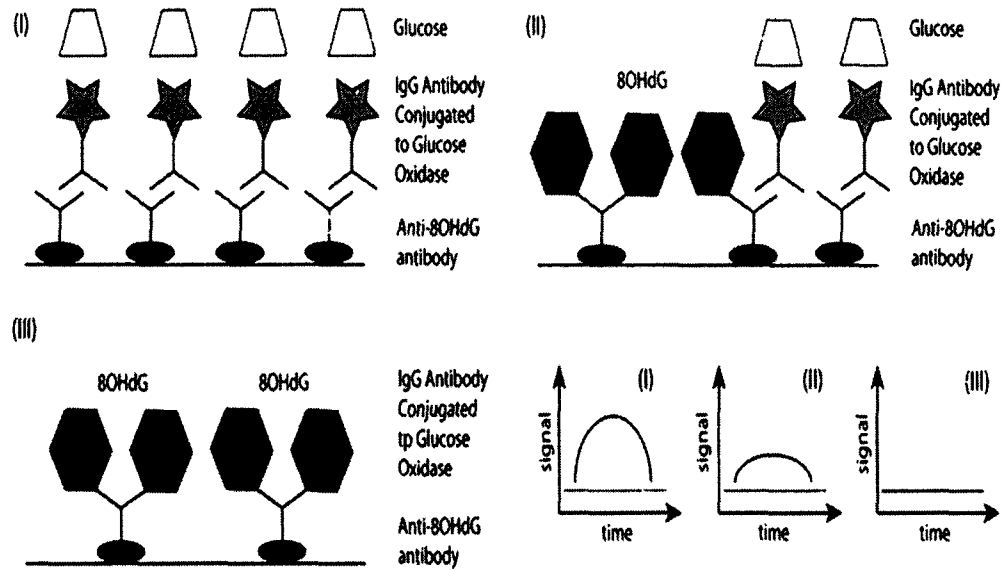
**Figure 5-1:** Molecular mechanism of thermoelectric ELISA. The concentration of surface immobilized enzyme is decreased as the levels of 8OHdG increase.

Another possible mechanism involves decreased efficiency of the enzymatic reaction as the concentration of the analyte increases. Higher levels of the analyte could interfere with the rate of the enzymatic reaction by physically obstructing the active sites of glucose oxidase (**Figure 5-2**).
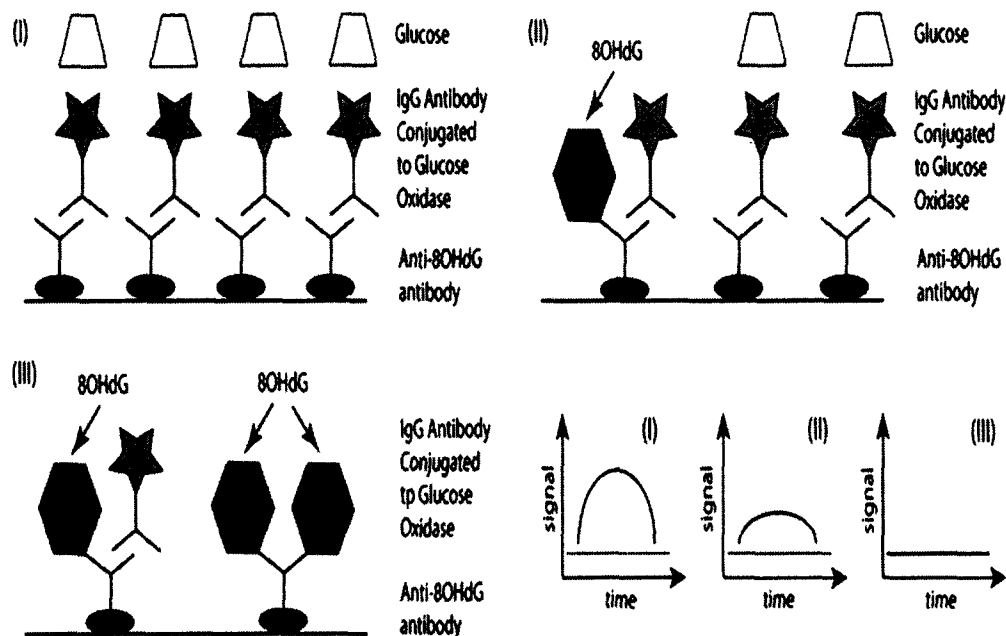
**Figure 5-2:** Molecular mechanism of thermoelectric ELISA. Reduced efficiency of enzymatic reaction when the concentration of 8OHdG is increased.

The standard error between and within experiments decreased as the size of the thermoelectric response decreased (**Table 4-2**). The increased variation of the signal could be a result of thermal fluctuations that have a more pronounced effect as the size of the signal increased. The thermal stability of the system can be improved by positioning the reference junction of the thermopile over a heat sink.

## 5.6    Detection of 8OHdG in Mouse Urine Samples

The reported value for 8OHdG concentration in APP mouse urine sample was 1.82μM. The value was estimated using CE-LIF (Zhang, *et al.* 2013). The concentration of 8OHdG in mouse urine has also been measured using ELISA. The reported concentration was 0.53μM (Kawakatsu, *et al.* 2013).

In this study, the measured values for 8OHdG concentration in three different urine samples from APP transgenic mice were 2.25μM, 1.87μM, and 3.94μM. These

results were obtained using the thermoelectric ELISA method. The values for 8OHdG obtained using CE-LIF and thermoelectric ELISA were within the same range confirming the accuracy of the thermoelectric method. Variation in the concentration of samples depends on the overall level of oxidative stress in the organism. The overall level of oxidative stress in APP transgenic mice is higher compared to normal mice due to the mutation in the APP gene. The quantification of 8OHdG using CE-LIF was performed on a single sample and does not reflect the variability in a sample population.

The quantification of 8OHdG using the thermoelectric ELISA technology is performed using a polyclonal anti-8OHdG antibody, while the CE-LIF was performed using a monoclonal one. The polyclonal antibody may have lower specificity for the modified guanine and it may cross react with other products of the oxidative stress repair pathway, such as the modified base or the modified 8-hydroxyguanosine that is the product of the RNA repair. Future work will focus on development of a method for conjugation of biotin or other linker moieties to a monoclonal antibody and evaluating performance of the system.

# CHAPTER 6

# CONCLUSIONS AND FUTURE WORK

## 6.1 Conclusions

The feasibility of a thermoelectric ELISA was successfully demonstrated by measuring the concentration of 8OHdG in a microfluidic device. The values of 8OHdG in a mouse urine sample obtained using thermoelectric ELISA were close to the values obtained using CE-LIF instrument.

The thermoelectric ELISA method for detection of antigens, analytes, or antibodies has multiple applications. The method can be used for quantification of the concentration of antigens or antibodies in biological samples such as blood, plasma, serum, urine, CFS fluids, saliva, etc. The method can be used to measure cytokine levels or other inflammatory markers or as a screening method for detection of early-stage cancers (Scholler *et al.*, 2006).

The technology can be applied in a variety of viral tests to measure the viral antibody concentration in biological samples. It can enable rapid detection and characterization of food-borne pathogens and toxins, as well as water-borne materials, including allergens, pollutants, heavy metals, and antigens in biological samples such as blood and body fluids. Another application is in the field of toxicology for rapid screening for certain classes of drugs.

## 6.2    Future Work

Future work will be focused on increasing the sensitivity and decreasing the response time of the system. This will include modifying the design and the materials that are used for fabrication of the microfluidic device. The design of the thermopile could be modified to allow integration in the new system. In addition, the sensor can be positioned inside the microfluidic device. This work will be extended to include applications of the thermoelectric ELISA method for pathogen detection as well as detection of a variety of analytes and biomarkers.

# APPENDIX A

# SIGNAL EXPRESS RESULTS FOR DEVICE PARAMETERS OPTIMIZATION

## A.1 Thermopile Output when Plastic Holder was Used



**Figure A-1:** Thermoelectric signal when plastic holder was used.



**Figure A-2:** Repeat of glucose (100mg dL$^{-1}$) injection when plastic holder was used.

## A.2    Thermopile Output when Aluminum Holder was Used
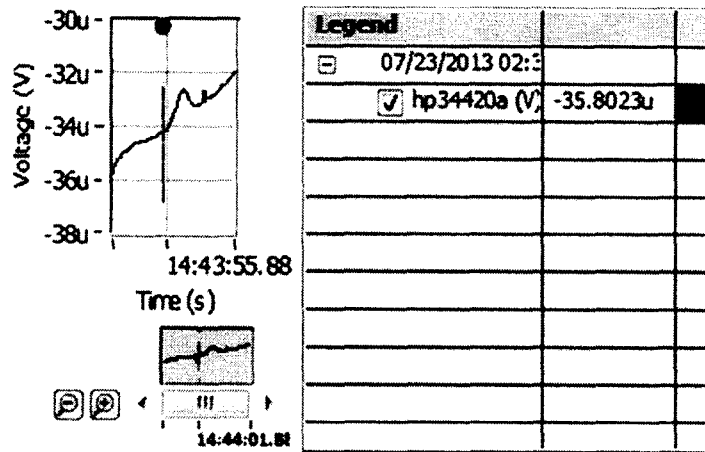


**Figure A-3:** Thermoelectric signal when aluminum holder was used.
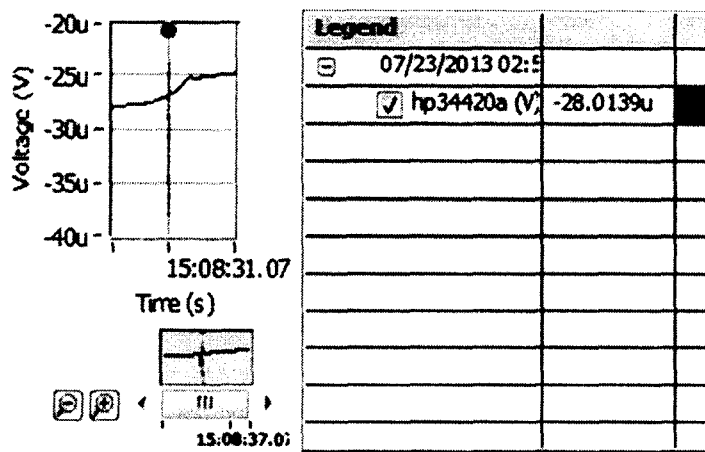


**Figure A-4:** Repeat of glucose (100mg dL$^{-1}$) injection when aluminum holder was used.

## A.3 Thermopile Output when Amplifier was Used
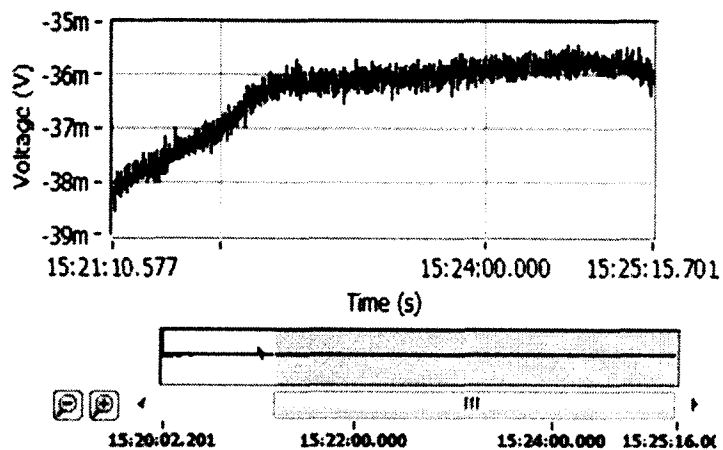


**Figure A-5:** Thermoelectric signal when amplifier was used.
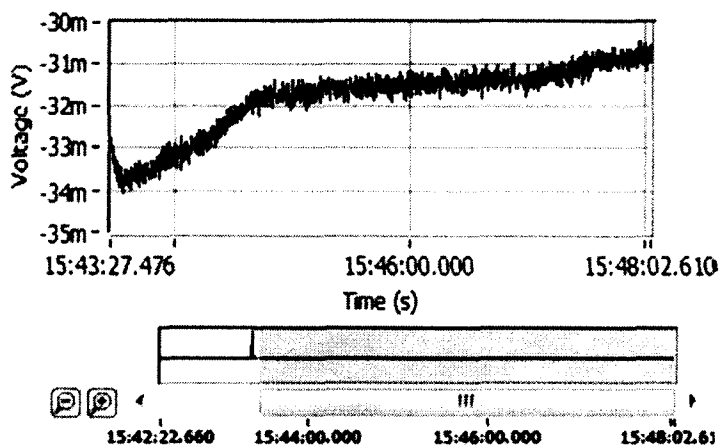


**Figure A-6:** Repeat of glucose (100mg dL$^{-1}$) injection when amplifier was used.

## A.4    Thermopile Output when Layer-by-layer was Used



**Figure A-7:** Thermoelectric signal when layer-by-layer method was used to immobilize streptavidin.



**Figure A-8:** Repeat of glucose (100mg dL$^{-1}$) injection when layer-by-layer method was used to immobilize streptavidin.

## A.5 Thermopile Output when the Flow Rate of Inlet 2 was 12μL min⁻¹



**Figure A-9:** Glucose (100mg dL⁻¹) injection when inlet 1 flow rate was 48μL min⁻¹ and inlet 2 flow rate was 12μL min⁻¹.



**Figure A-10:** Repeat of glucose (100mg dL⁻¹) injection when inlet 1 flow rate was 48μL min⁻¹ and inlet 2 flow rate was 12μL min⁻¹.

### A.6    Thermopile Output using Different Flow Rate Ratio of Inlet 1 and Inlet 2



**Figure A-11:** Glucose (100mg dL$^{-1}$) injection when inlet 1 flow rate was 100µL min$^{-1}$ and inlet 2 flow rate was 25µL min$^{-1}$.



**Figure A-12:** Glucose (100mg dL$^{-1}$) injection when inlet 1 flow rate was 50µL min$^{-1}$ and inlet 2 flow rate was 25µL min$^{-1}$.

## A.7 Thermopile Output when Three Split Channel Device was Used
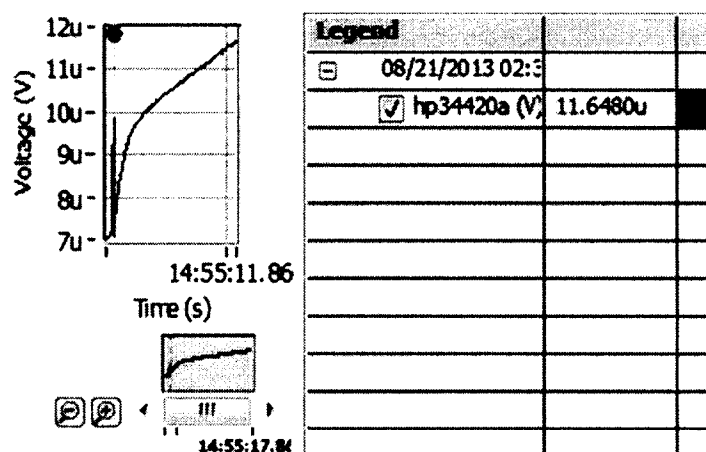


**Figure A-13:** Glucose injection (100mg dL$^{-1}$) using flow rate of 25µL min$^{-1}$ in each channel.
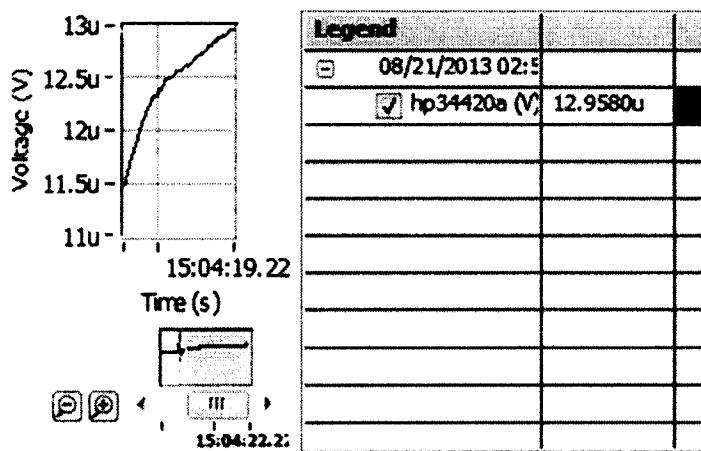


**Figure A-14:** Repeat of glucose injection (100mg dL$^{-1}$) using flow rate of 25µL min$^{-1}$ in each channel.

## A.8 Thermopile Output when Single Inlet Device was Used
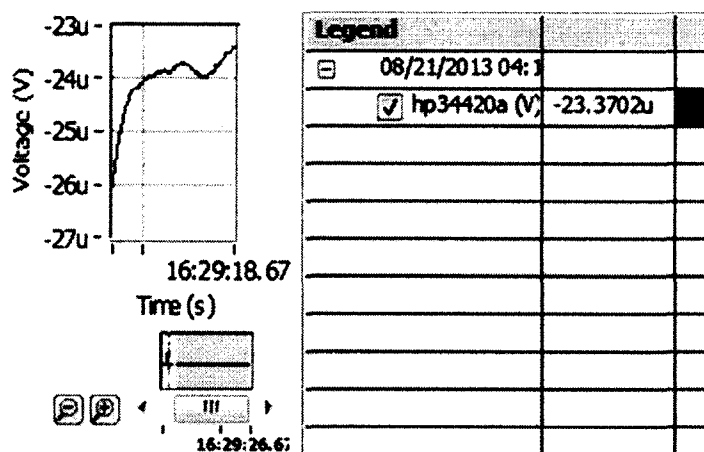


**Figure A-15:** Glucose injection (100mg $dL^{-1}$) , flow rate of 25µL $min^{-1}$.
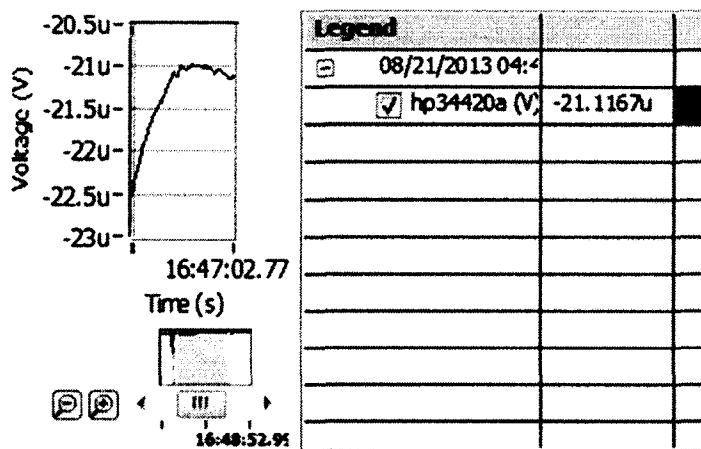


**Figure A-16:** Glucose injection (100mg $dL^{-1}$), flow rate of 25µL $min^{-1}$.

## A.9 Thermopile Output when the Concentration of Glucose was 200mg dL-1
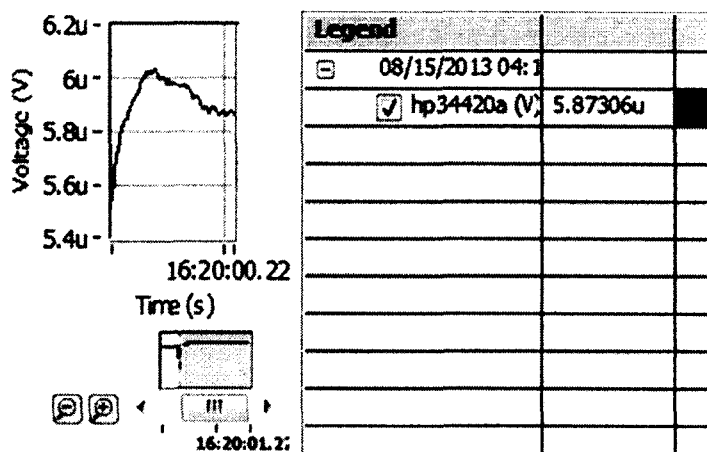


**Figure A-17:** Glucose injection (200mg dL$^{-1}$).
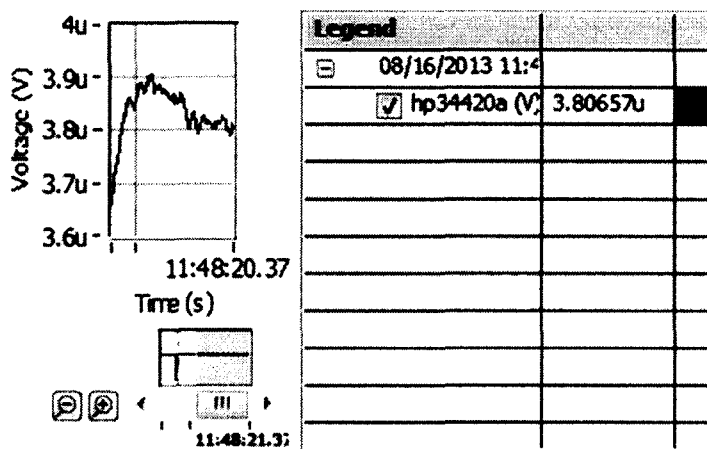


**Figure A-18:** Glucose injection (200mg dL$^{-1}$).

## A.10 Thermopile Output when Aluminum Heat Sink was Used



**Figure A-19:** Glucose injection (100mg dL$^{-1}$), thermopile reference junctions positioned over an aluminum heat sink.



**Figure A-20:** Repeat of glucose injection (100mg dL$^{-1}$), thermopile reference junctions positioned over an aluminum heat sink.

# APPENDIX B

# SIGNAL EXPRESS RESULTS FOR STANDARD CURVE AND LEVELS OF 8-HYDROXYDEOXYGUANOSINE

## B.1    Thermopile Output for Standard Calibration Curve Generation
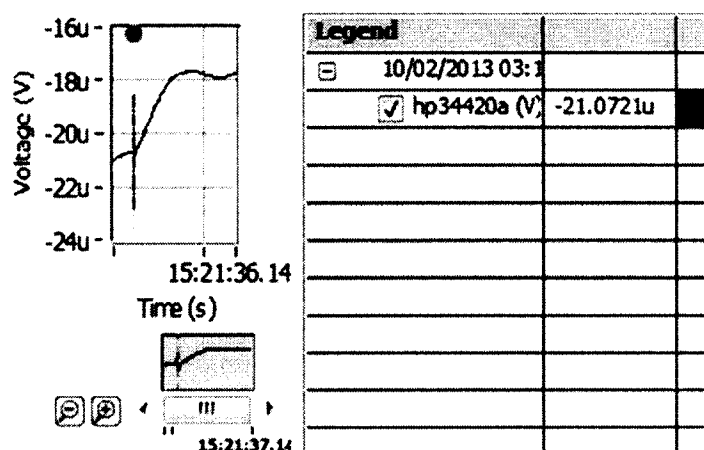


**Figure B-21:** Thermopile response when 0μM 8OHdG was used.
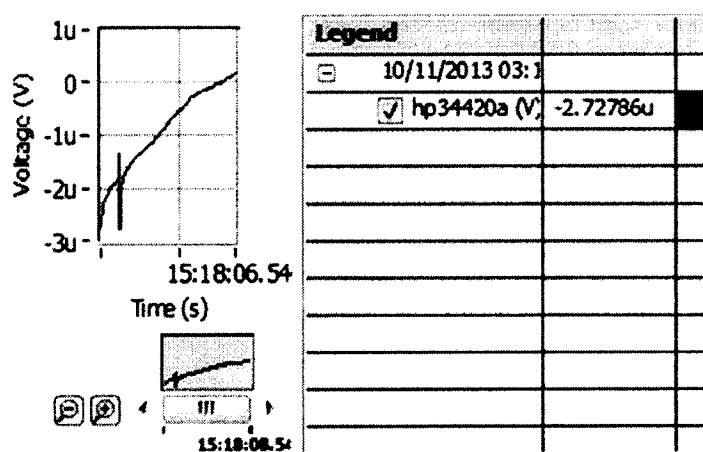


**Figure B-22:** Thermopile response when 10μM 8OHdG was used.

**Figure B-23:** Thermopile response when 6μM 8OHdG was used.



**Figure B-24:** Thermopile response when 3μM 8OHdG was used.

## B.2 Thermopile Output for 8OHdG Quantification in Mouse Urine Samples
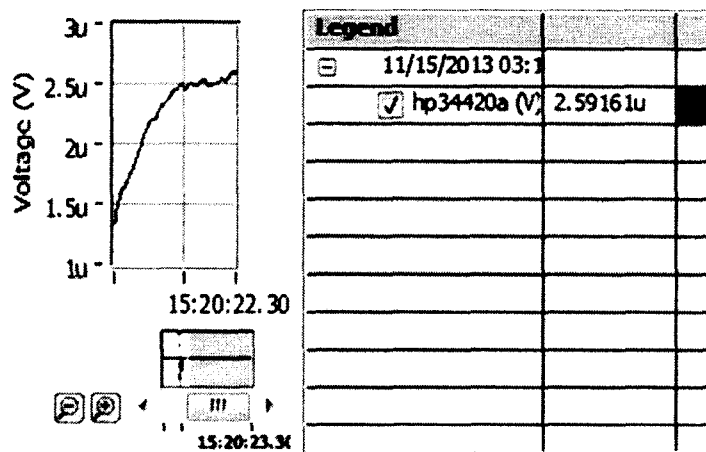


**Figure B-25:** Thermopile signal when urine sample was used. The concentration of 8OHdG was estimated to be 2.25$\mu$M.
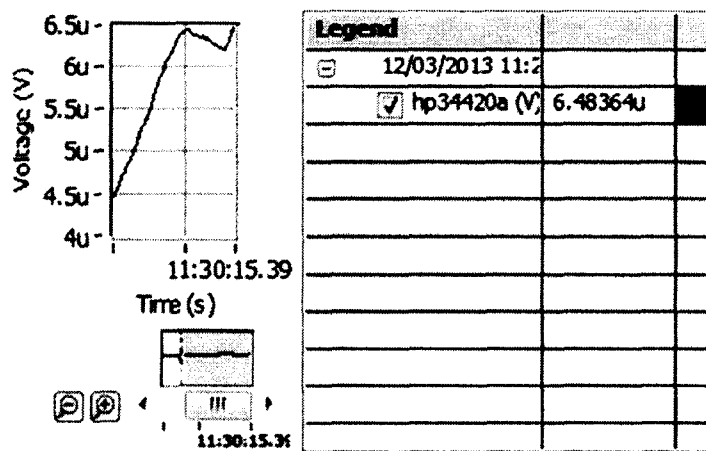


**Figure B-26:** Thermopile signal when urine sample was used. The concentration of 8OHdG was estimated to be 1.87$\mu$M.

**Figure B-27:** Thermopile signal when urine sample was used. The concentration of 8OHdG was estimated to be 3.94μM.

# APPENDIX C

# STREPTAVIDIN IMMOBILIZATION BY LAYER-BY-LAYER
# SELF-ASSEMBLY

## C.1 Preparation of Polyelectrolytes

### C.1.1 PEI Preparation

100 μl PEI (50% w/v in water) was added to 25 ml of distilled water (DI) and

the pH was adjusted to 8 by the addition of 10M HCl using a pH electrode.

### C.1.2 PAcr Preparation

142.85 μl PAcr (35% w/v) was dissolved in 25 ml of DI water and 25 μl of 5M

Nacl (Amresco) and the pH was adjusted to 8 by the addition of 10M NaOH.

## C.2 Preparation of Stock Solutions

### C.2.1 Preparation of 2% Micro-90 Solution

0.74 ml of Micro-90 was dissolved in 37.85 ml of water.

2% Micro-90 solution was then prepared by adding 0.8 ml of the above solution

to 100 ml of water.

### C.2.2 Preparation of EDC Solution

EZ link (Thermo Fisher, Scientific) contains

EDC (1-[3-(Dimethyl-amino) propyl]-3-ethylcarbodiimide hydrochloride),

MESb (2-[N- Morpholino] ethane sulfonic acid buffer) and

Amine-PEG$_2$-Biotin.

Dissolve all the pouch ingredients of MESb in 500 ml of milli-Q water to obtain a

0.1M solution.

From the above solution, 4 ml was dissolved in 36 ml of milli-Q water to obtain a

10mM solution of MESb. The pH was then adjusted to 5.5 by the addition of HCl

Thirty-eight mg of EDC solution (5gm, Molecular weight, 191.7) was dissolved

in 1 ml of 10mM MESb to obtain a 200 mM solution. This is the stock EDC solution.

C.2.3     Preparation of Biotin Solution

Fifty mg of Amine-PEG$_2$-Biotin (50 mg, 374.51gm/mole) was dissolved in 667

µL of 10 mMMESb to obtain a 200 mM solution.

Seven hundred and 50 µL of 10 mM MESb was added to 250 µL of the above

solution to obtain one ml of 50 mM Biotin solution.

Add 750 µL of 10 mM MESb to 250 µL of the stock EDC solution to obtain One

ml of 50mM EDC.

Add 50 mM of 1 ml Biotin solution and 50 mM of 1 ml EDC solution to obtain 2

ml of 25 mM each (Biotin and EDC).

Add 8 ml of water to the above mixture to obtain 10 ml of 5 mM (Biotin and

EDC). This is the stock biotin solution.

C.2.4     Preparation of Streptavidin Solution

One mg of Streptavidin (Prozyme, Hayward, CA) was dissolved in 10 ml of 10

mM Trisb, PH 7.5 (Amresco). This is the stock streptavidin solution.

# APPENDIX D

# VALUES OF PARAMETERS USED FOR MATHEMATICAL MODEL

**Table D-1:** Values of parameters in the computation.

| Symbols | Parameters | Values | Units |
|---|---|---|---|
| *Glass Slide* | *Glass* | | |
| $\rho_0$ | Glass density | 2.6 | $gm\ cm^{-3}$ |
| $C_0$ | Glass heat capacity | 0.2 | $cal\ gm^{-1}\ K^{-1}$ |
| $K_0$ | Glass thermal conductivity | 0.96 | $W\ m^{-1}\ K^{-1}$ |
| $h_0$ | Glass slide thickness | $1 \times 10^{-3}$ | m |
| T0(0) | Initial glass slide temperature | 298 | K |
| *Fluid* | *Water* | | |
| $\rho_3$ | Water density | 1.0 | $gm\ cm^{-3}$ |
| $C_3$ | Water heat capacity | 1.0 | $cal\ gm^{-1}\ K^{-1}$ |
| $K_3$ | Water thermal conductivity | 0.58 | $W\ m^{-1}\ K^{-1}$ |
| Tin | Inlet water temperature | 298 | K |
| T1(0) | Initial water temperature | 298 | K |

| H1 | Water convection coefficient | 22590 | $W\ m^{-2}\ K^{-1}$ |
|---|---|---|---|
| $h_1$ | Channel Height | $1 \times 10^{-6}$ | m |
| **Glass Coverslip** | **Glass** | | |
| $\rho_0$ | Glass density | 2.6 | $gm\ cm^{-3}$ |
| $C_0$ | Glass heat capacity | 0.2 | $cal\ gm^{-1}\ K^{-1}$ |
| $K_0$ | Glass thermal conductivity | 0.96 | $W\ m^{-1}\ K^{-1}$ |
| $h_0$ | Glass coverslip thickness | $175 \times 10^{-6}$ | m |
| T2(0) | Initial glass coverslip temperature | 298 | K |
| **Thermopile** | **Kapton Tape** | | |
| $\rho_2$ | Kapton density | 1.42 | $gm\ cm^{-3}$ |
| $C_2$ | Kapton heat capacity | 0.26 | $cal\ gm^{-1}\ K^{-1}$ |
| $K_2$ | Kapton thermal conductivity | 0.155 | $W\ m^{-1}\ K^{-1}$ |
| $h_3$ | Kapton thickness | $125 \times 10^{-6}$ | m |
| T3(0) | Kapton initial | 298 | K |

| | temperature | | |
|---|---|---|---|
| **Protective tape** | **Acrylic tape** | | |
| $\rho_4$ | Acrylic density | 1.2 | $gm\ cm^{-3}$ |
| $C_4$ | Acrylic heat capacity | 0.35 | $cal\ gm^{-1}\ K^{-1}$ |
| $K_4$ | Acrylic thermal conductivity | 0.2 | $W\ m^{-1}\ K^{-1}$ |
| $h_4$ | Acrylic thickness | $109 \times 10^{-6}$ | m |
| T4(0) | Acrylic Initial temperature | 298 | K |
| **Air** | **Air** | | |
| $\rho_1$ | Air density | $1.29 \times 10^{-3}$ | $gm\ cm^{-3}$ |
| $C_1$ | Air heat capacity | 0.239 | $cal\ gm^{-1}\ K^{-1}$ |
| $K_1$ | Air thermal conductivity | 0.0227 | $W\ m^{-1}\ K^{-1}$ |
| H0 | Air convection coefficient | 25 | $W\ m^{-2}\ K^{-1}$ |
| T inf | Air temperature | 298 | K |
| Q | Flow rate | 25 | $\mu L\ min^{-1}$ |
| As | Area of reaction zone | $24 \times 10^{-6}$ | $mm^{-2}$ |
| Rx_heat | Power of reaction | $1.22 \times 10^{-6}$ | $J\ sec^{-1}$ |

| S coef | Seebeck coefficient | 7.2 | $\mu V \ mK^{-1}$ |
|--------|---------------------|-----|-------------------|
| t | Duration of the reaction | 120 | sec |

# BIBLIOGRAPHY

Bankar, S, M Bule, and R Singhal, "Glucose Oxidase-An Overview." *Biotechnology Advances*, 2009: 489-501.

Bartholomeusz, DA, RW Boutte, and J.D. Andrade. "Xurography: rapid prototyping of microstructures using a cutting plotter." *Journal of Micromechanical Systems*, 2005: 1364-74.

Bruus, Henrik. Theoretical microfluidics. Technical University of Denmark, 2006.

Cadet,J ,T Douki, J Ravant, and P Mascio. "Sensitized formation of oxidatevly generated damage to celluar DNA by UVA radiation." *Photochemical and photobiolofical sciences*, 2009: 903-911.

Chioua, C, P Changb, E Chana, T Wub, K Tsaob, and J Wu. "Urinary 8-hydroxydeoxyguanosine and its analogues as DNA marker of oxidative stress: development of ELISA and measurement in both bladder and prostate cancers." *Clinica Chimica Acta*, 2003: 87-94.

Crowther, J. The ELISA Guidebook. Humana Press, 2000.

Erholaa, M, *et al*. "Biomarker evidence of DNA oxidation in lung cancer patients: association of urinary 8-hydroxy-2'-deoxyguanosine excretion with radiotherapy, chemotherapy, and response to treatment." *FEBS Letters*, 1997: 287-291.

Feinstein, S, Y Akov, BE Lachmi, S Lehrer, L Rannon, and D Katz. "Determination of human IgG and IgM class antibodies to West Nile virus by enzyme linked immunosorbent assay (ELISA)." *Journal of Medical Virology*, 1985: 63-72.

Guilbeau, EJ, BC Towe, and M Muehlbauer. "A potentially implantable thermoelectric sensor for measurement of glucose." *ASAIO Journal*, 1987: 329-35.

Halliwell, B. "Biochemistry of oxidative stress." *Biochemical Society Transactions*, 2007: 1147-50.

Incropera, F. and D Dewitt. Fundamentals of heat and mass transfer. John Wiley and Sons, 2008.

124

Lerchner, J, AWolf, GWolf, V Baier, E Kessler, M Nietzsch, and M Krügel. "A new micro-fluid chip calorimeter for biochemical applications." *Thermochimica Acta* , 2006:144-50.

Joshi, UM, R Roy, AR Sheth, and HP Shah. "A simple and sensitive color test for the detection of human chorionic gonadotropin." *Obstetrics and Gynecology*, 1981: 252-4.

Kartalov, EP, MA Unger, and SR Quake. "Polyelectrolyte surface interface for single-molecule fluorescence studies of DNA polymerase." *Biotechniques*, 2003: 505-10.

Kasai, H., Crain, C., Kuchine, Y., Nishimura, N., Otsyama, A., Tanooka, H. "Formation of 8-hydroxyguanosine moiety in celluart DNA and evidence for its repair." *Carcenogenesis*, 1986: 1849-1851.

Kasai, H. "A new automated method to analyze urinary 8-hydroxydeoxyguanosine by a high-performance liquid chromatography-electrochemical detector system." *Journal of Radiation Research*, 2003: 185-89.

Kasai, H, K Kawai, and Yun-shan L. "Analysis of 8OHdG and 8-OH-Gua as biomarkers of oxidative stress." *Genes and Enviroment*, 2008: 33-40.

Kawakatsu, M, *et al.* "Nicaraven attenuates radiation-inducediInjury in hematopoietic stem/progenitor cells in mice." *PLoS One*, 2013: e60023.

Klungland, A, *et al.* "Accumulation of premutagenic DNA lesions in mice defective in removal of oxidative base damage." *PNAS*, 1999: 13300-05.

Kopparthy, V, S Tangutooru, G Nestorova, and E Guilbeau. "Thermoelectric microfluidic sensor for bio-chemical applications." *Sensors and Actuators: Chemical*, 2012: 608-15.

Kvasnicováa, V, E Samcováa, A Jursováb, and I Jelínekb. "Determination of 8-hydroxy-2'-deoxyguanosine in untreated urine by capillary electrophoresis with UV detection." *Journal of Chromatography* A, 2003: 513-17.

Lee, D, C Chang, S Huang, and R: Yang. "The hydrodynamic focusing effect inside rectangular microchannels." *Journal of Micromechnanic and Microengineering*, 2006: 1024-32.

Lin, H, A Jenner, C Ong, S: Whiteman,M Huang, and B Halliwell. "A high-throughput and sensitive methodology for the quantification of urinary 8-hydroxy-2'-deoxyguanosine: measurement with gas chromatography-mass spectrometry after single solid-phase extraction." *Biochemical Journal*, 2004: 541-48.

Loft, S, *et al.* "Prospective study of 8-oxo-7,8-dihydo-2-deoxyguanosine excretion and the risk for lung cancer." *Carcinogenesis*, 2006: 1245-50.

Loft, S, H Danielsen, L Mikkelsen, L Risom, L Forchhammer, and P. Møller. "Biomarkers of oxidative damage to DNA and repair." *Biochemical Society Transactions*, 2008: 1071-76.

Lovell, M, and W Markesbery. "Ratio of 8-Hydroxyguanine in intact DNA to free 8-hydroxyguanine is increased in Alzheimer Disease ventricular cerebrospinal fluid." *JAMA Neurology*, 2001: 392-96.

Lovell, MA, and WA Markersbery. "Oxidative DNA damage in mild cognitive impairment and late-stage Alzheimer's disease." *Nucleic Acid Research*, 2007: 7497-507.

Lvov, Y, and H Möhwald. Protein architecture: interfacing molecular assemblies and immobilization in biotechnology. Marcel Deekker, 2000.

Lvov, Y, K Ariga, I Ichinose, and T Kunitake. "Assembly of multicomponent protein films by means of electrostatic layer-by-layer adsorption." *Journal of the American Chemical Society*, 1995: 6117-23.

Lvov, Y, K Ariga, M Ondaa, I Ichinoseb, and T Kunitake. "A careful examination of the adsorption step in the alternate layer-by-layer assembly of linear polyanion and polycation." *Colloids and Surfaces A: Physicochemical and Engineering Aspects*, 1999: 337-46.

Mattiasson, B. "A general enzyme thermistor based on specific reversible immobilization using the antigen--antibody interaction. Assay of hydrogen peroxide, penicillin, sucrose, glucose, phenol and tyrosine." *FEBS Letters*, 1977: 107-10.

Mattiasson, B, C Borrebaeck, B Sanfridson, and K Mosbach. "Thermometric enzyme linked immunosorbent assay: TELISA." *Biochemica et Biophysica Acta*, 1977: 221-7.

Mei, S, Q Yao, L Cai, J Xing, G Xu, and C Wu. "Capillary electrophoresis with end-column amperometric detection of urinary 8-hydroxy-2'-deoxyguanosine." *Electrophoresis*, 2003: 1411-15.

Moreira, P, et al. "Nucleic acid oxidation in Alzheimer disease." *Free Radical Biology and Medicine*, 2008: 1493-05.

Muehlbauer, M, E Guilbeau, B Towe, and T Brandon. "Thermoelectric enzyme sensor for measuring blood glucose." *Biosensors and Bioelectronics*, 1990: 1-12.

Pan, H, D Chang, L Feng, F Xu, H Kunag, and M Lu. "Oxidative damage to DNA and its relationship with diabetic complications." *Biomedical and Enviromental Sciences*, 2007: 160-163.

Pollock, D D. "Thermoelectricity: theory, thermometry, tool." ASTM Special Technical Publications.1985.

Rica, R, M.Stevens. "Plasmonic ELISA for the detection of analytes at ultralow concentrations with the naked eye." *Nature Protocols*, 2013: 1759-1764.

Ravant, J. "Measuring oxidized DNA lesions as biomarkers of oxidative stress: an analytical challenge." *FABAD Journal of Pharmaceutical Sciences*, 2005: 100-13.

Rebelo, I., J Piedade, and A Oliveira-Brett. "Development of an HPLC method with electrochemical detection of femtomoles of 8-oxo-7,8-dihydroguanine and 8-oxo-7,8-dihydro-2'-deoxyguanosine in the presence of uric acid." *Talanta*, 2004: 323-31.

Robinson JE,D Holton,J Liu,H McMurdo,A Murciano, and R Gohd. "A novel enzyme-linked immunosorbent assay (ELISA) for the detection of antibodies to HIV-1 envelope glycoproteins based on immobilization of viral glycoproteins in microtiter wells coated with concanavalin A." *Journal of Immunological Methods*, 1990: 63-71.

Shimoi K,H Kasai, N Yokota, S Toyokuni, and N Kinae. "Comparison between high-performance liquid chromatography and enzyme-linked immunosorbent assay for the determination of 8-hydroxy-2'-deoxyguanosine in human urine." *Cancer Epidemology, Biomarkers , and Prevention*, 2002: 767.

Scholler, N, M Crawford, A Sato, C W Drescher, and K O'Briant. "Bead based ELISA for validation of ovarian caner early detection markers." *Clinical Cancer Research*, 2006: 12(7), 2117-24.

Songa, M, *et al*. "Urea, the most abundant component in urine, cross-reacts with a commercial 8-OH-dG ELISA kit and contributes to overestimation of urinary 8-OHdG." *Free Radical Bilogy and Medicine*, 2009: 41-46.

Stephan, O, and S Vieths. "Development of a real-time PCR and a sandwich ELISA for detection of potentially allergenic trace amounts of peanut (*Arachis hypogaea*) in processed foods." *Journal of Agricultural and Food Chemistry*, 2004: 3754-60.

Tangutooru, SM, VL Kopparthy, GG Nestorova, and EJ Guilbeau. "Dynamic thermoelectric glucose sensing with layer-by-layer glucose oxidase immobilization." *Sensors and Actuators B: Chemical*, 2012: 637-41.

Toyokuni, S, T Tanaka, et al. "Quantitative immunohistochemical determination of 8-hydroxy-2'-deoxyguanosine by a monoclonal antibody N45.1: its application to ferric nitrilotriacetate-induced renal carcinogenesis model." *Journal of Technical Methods and Pathology*, 1997: 365-74.

Weimann, A, D Belling, and H Poulsen. "Quantification of 8-oxo-guanine and guanine as the nucleobase, nucleoside and deoxynucleoside forms in human urine by high-performance liquid chromatography–electrospray tandem mass spectrometry." *Nucleic Acid Research*, 2002: e7.

Weiss, D, and C Lunte. "Detection of a urinary biomarker for oxidative DNA damage 8-hydroxydeoxyguanosine by capillary electrophoresis with electrochemical detection." *Electrophoresis*, 2000: 2080-85.

Wu, L, C Chiou, P Chang, and J Wu. "Urinary 8OHdG: a marker of oxidative stress to *DNA* and a risk factor for cancer , atherosclerosis, and diabetes." *Clinica Chimica Acta*, 2004: 1-9.

Xie, B, M Mecklenburg, B Danielsson, O Öhmanb, and F Winquist. "Microbiosensor based on an integrated thermopile." *Analytica Chimica Acta*, 1994: 165-70.

Yin, B, R Whyatt, F Perera, M Randall, T Cooper, and R Santella. "Determination of 8-Hydroxydeoxyguanosine by an immunoaffinity chromatography-monoclonal antibody based ELISA." *Free Radical Biology and Medicine*, 1995: 1023-32.

Zhang, C, G Nestorova, RA Rissman, and J Feng. "Detection and quantification of 8-hydroxy-2'-deoxyguanosine in Alzheimer's transgenic mouse urine using capillary electrophoresis." *Electrophoresis*, 2013: 2268-74.

Zhang, Y, and S Tadigadapa. "Calorimetric biosensors with integrated microfluidic channels." *Biosensors and Bioelectronics*, 2004: 1733-43.